

TOWARDS A REAL-TIME DYNAMIC WILDFIRE SIMULATOR FOR BELGIUM

A REVIEW AND SENSITIVITY ANALYSIS

Aantal woorden: 20518

Lander De Visscher

Studentennummer: 01202352

Promotor: prof. dr. Bernard De Baets

Copromotor: dr. ir. Jan Baetens

Masterproef voorgelegd voor het behalen van de graad: master in de richting

Bio-ingenieurswetenschappen: milieutechnologie.

Academiejaar: 2016 - 2017

Deze pagina is niet beschikbaar omdat ze persoonsgegevens bevat.
Universiteitsbibliotheek Gent, 2021.

This page is not available because it contains personal information.
Ghent University, Library, 2021.

Dankwoord

Zie zo, hier zit ik dan, op dezelfde stoel waar ik meer dan een jaar geleden begon aan mijn thesis. En kijk, na veel bloed, zweet en tranen – maar toch vooral sloten koffie – kan ik me verheugen om binnen een dik uur het afgewerkte resultaat af te printen en in te dienen. Hoewel ik graag had kunnen zeggen dat ik dit volledig alleen heb verwezenlijkt, is dat verre van de realiteit. Bij deze maak ik dus nog even tijd om de nodige mensen te bedanken.

Ten eerste wil ik mijn promotor/tutor, Dr. Jan Baetens, van harte bedanken voor de voortreffelijke begeleiding bij het maken van dit proefstuk. Zijn inbreng bood me telkens nieuwe perspectieven en zo ook nieuwe moed, wanneer ik weer eens in de knoop zat. Daarnaast bedank ik ook graag mijn tweede promotor, Prof. Bernard De Baets, voor zijn kritische revisies die de *finishing touch* gaven aan hetgeen ik in de volgende 100 pagina's zal tentoon spreiden. Bij uitbreiding wil ik, naast mijn mede-thesisstudenten, iedereen aan de vakgroepen KERMIT en BIOMATH bedanken. Om het met een (licht aangepast) filmcitaat te zeggen: *Ladies and gentlemen, it has been a privilege working with you this year.*

Daarnaast wil ik nog even wat mensen van buiten de faculteitsmuren in de bloemetjes zetten. Eerst en vooral heel de (Belgisch-Britse) ska/punk scene, en in het bijzonder alles en iedereen in en rond Koala Commission, Chrandesyx en El Topo Bookings, want *music is love, music is life*. Vervolgens bedank ik al mijn *geeky* vriendjes om samen *dank memes* uit te wisselen, fossielen te gaan zoeken en ons te verliezen in eindeloze D&D sessies. Ook iedereen die op regelmatige basis mijn klaagzangen heeft mogen/moeten aanhoren, zij het op kot, in de frietketel of eender waar, mag ik niet vergeten te vermelden.

Ten slotte wil ik mijn familie en vooral mijn ouders, Koen en Linde, bedanken. Naast het feit dat jullie de (enige) reden zijn dat ik hier in de eerste plaats rondloop, staan jullie al heel mijn leven met woord en daad voor me klaar. Hier kan ik niet dankbaar genoeg voor zijn.

And now for something completely different...

Summary

Wildfires pose, despite their seemingly minor importance in Belgium, a serious threat to our few remaining nature reserves and the residential areas in their proximity. Hence, the need for an effective management and suppression arises. Wildfire models—and more specifically wildfire spread models—could be useful tools for the latter, as they try to simulate the spread of a wildfire. During the past decades, a multitude of said models has been developed, yet none of them have been evaluated in a Belgian context.

In this dissertation three wildfire spread models are selected from the available models and these are evaluated in a Belgian context. For this purpose, a dataset is used containing seven documented wildfires in Belgium and the Netherlands. The goal is to assess whether or not these models are readily applicable in a Belgian context, and this for the sake of operational purposes. The evaluation is subdivided in two main parts. Firstly, we evaluated two publicly available simulators, namely FARSITE and ForeFire. Secondly, we tested the model proposed by Depicker et al. (2016)—which is a cellular automaton—through model calibration, simulations and a sensitivity analysis with the available data.

It was ascertained that none of the simulations obtained with these models could provide any information which would be relevant in an operational setting. This was mainly attributed to the poor quality of the data available. Furthermore, the lack of a (detailed) documentation of the progression of the wildfires hampered both the calibration of the CA-based model and the thorough analysis and mutual comparison of the models in general.

Samenvatting

Natuurbranden vormen, ondanks hun eerder beperkt voorkomen in België, een ernstige bedreiging voor enkele van onze weinige natuurgebieden en de hieraan grenzende woongebieden. Bijgevolg steekt de nood aan doeltreffende beheer- en bestrijdingsmaatregelen de kop op. Natuurbrandmodellen – en meer specifiek brandverspreidingsmodellen – kunnen bij dit laatste een belangrijk hulpmiddel zijn, aangezien ze het verloop van een natuurbrand pogen te voorspellen. Gedurende de voorbije decennia werden ettelijke van deze modellen opgesteld, echter geen werd reeds getest voor natuurbranden in België.

In deze thesis werden, uit de hele schare aan bestaande modellen, drie brandverspreidingsmodellen geselecteerd en beoordeeld in een Belgische context. Hierbij werd gebruik gemaakt van een dataset bestaande uit zeven gedocumenteerde natuurbranden in België en Nederland. Het doel hiervan is om na te gaan of deze modellen voldoende ontwikkeld zijn om operationeel toegepast te worden in onze contreien. De evaluatie is opgedeeld in twee onderdelen. In eerste instantie hebben we twee modellen uit de literatuur getest, met name FARSITE en ForeFire. In tweede instantie evalueerden we het model voorgesteld door Depicker et al. (2016) – een cellulaire automaat – aan de hand van een kalibratie, gevoeligheidsanalyse en simulaties met de beschikbare dataset.

Hierbij hebben we vastgesteld dat de simulaties die bekomen werden met deze modellen, ons geen informatie konden verschaffen die bruikbaar zou zijn voor operationele doeleinden. Dit werd voornamelijk toegeschreven aan de lage kwaliteit van de beschikbare data. Bovendien werd, naast de kalibratie van het CA-gebaseerde model, een grondige analyse en onderlinge vergelijking van de drie modellen belemmerd door het ontbreken van een (gedetailleerde) beschrijving van het verloop van de natuurbranden.

Contents

Dankwoord	i
Summary	iii
Nederlandse samenvatting	v
Contents	ix
List of Symbols	xi
List of Abbreviations	xv
List of Figures	xvii
List of Tables	xix
1 Introduction	1
2 Wildfires: a brief description	3
2.1 General description	3
2.1.1 Definition and scales	3
2.1.2 Spread mechanism	4
2.1.3 Fuels	6
2.1.4 Combustion reactions	10
2.1.5 Heat transfer	11
2.1.6 Phenomenology	12
2.1.7 Remaining questions	13
2.2 Prevalence and impact	14
2.2.1 Global	14
2.2.2 Europe and Belgium	15
2.3 Wildfire management	17

3	Wildfire modelling	19
3.1	General considerations	19
3.1.1	Wildfire model usage	19
3.1.2	Hurdles in wildfire modelling	20
3.2	Wildfire models	21
3.2.1	History	21
3.2.2	Classification	22
3.3	Physically based models	22
3.4	(Quasi-)empirical models	25
3.5	Simulation and analogue models	28
3.5.1	Landscape level simulations	28
3.5.2	Wind-slope correction	28
3.5.3	Simulation models	29
3.5.4	Coupled fire-atmosphere models	35
3.5.5	Analogue models	36
3.6	Uncertainty in wildfire modelling and simulation	38
3.7	Wildfire modelling in Belgium	38
4	Study areas and model description	41
4.1	Case description	41
4.1.1	Overview	41
4.1.2	Wildfire perimeter	42
4.1.3	Fuel complex	44
4.1.4	Topography and street maps	46
4.1.5	Weather	47
4.1.6	Wildfire ignition and progress	48
4.2	Model description and settings	50
4.2.1	FARSITE	50
4.2.2	ForeFire	52
4.2.3	CA-based model	56
5	A evaluation of FARSITE and ForeFire	73
5.1	Model evaluation	73
5.2	Benchmark simulations	74
5.2.1	FARSITE	74
5.2.2	ForeFire	78
5.3	Incorporation of detailed terrain information	81
5.3.1	Case 1	81
5.3.2	Case 2	83

5.4	General discussion and conclusion	85
5.4.1	Simulation results	85
5.4.2	Usability	86
6	Calibration and evaluation of the CA-based model	87
6.1	Evaluation of pre-calibrated parameters	87
6.2	Case-dependent calibration	88
6.2.1	Method	88
6.2.2	CA1	90
6.2.3	CA2	93
6.3	Overall calibration	95
6.4	Sensitivity analysis	98
6.4.1	Method	98
6.4.2	Results and discussion	100
6.5	Conclusions	102
7	Conclusions and perspectives	103
	Bibliography	105
A	Fuel classifications	119

List of Symbols

α	correction factor of component of the ignition probability, determined by the cell's vegetation
B	Stefan-Boltzmann constant
β	packing ratio
β_d	radiation dumping ratio
χ	fraction of the combustion energy emitted as radiation
c_i	cell i of the grid
$c_{p,f}$	heat capacity of the fuel
δ_θ	adjustment term of the wind direction
δ_U	adjustment factor of the wind speed
Δt	temporal resolution
Δx	spatial resolution
d_{fb}	fuelbed depth
d_p	particle diameter
ϵ	effective heating number
ε	random number between [0,1]
ϵ_f	fuel emissivity
f_i	burn frequency
γ	tilt angle of the fire front towards the unburnt fuel
γ_a	topographic aspect

γ_s	slope angle
h	heat content
h_w	latent heat
I	fire line intensity
I_r	reaction intensity
κ	local front curvature
λ	local front depth
M	fuel moisture content
N_i	neighbourhood of cell i
n_{burn}	number of time steps during which a cell is burning
n_{steps}	number of simulated time steps
n_{cells}	number of grid cells
O	observed burnt area
Ω	objective function
p_i	ignition probability during 1 time step
p_j	probability that the wildfire will spread from the neighbouring cell c_j during the next time step
p_{veg}	component of the ignition probability, determined by the cell's vegetation
p'_{veg}	adjusted component of the ignition probability, determined by the cell's vegetation
Γ	closed contour, defining the zero level set of a level set function
φ	level set function
ϕ_s	additive slope correction factor
ϕ_w	additive wind correction factor
ψ	parameter in wind and slope functions
Q_{ig}	pre-ignition heat

R	rate of spread
R_0	no-wind no-slope rate of spread
R_w	wind-induced rate of spread
ρ_a	density of air
ρ_b	oven-dry bulk density
ρ_p	oven-dry particle density
S	rate of spread, normal to the fire front
S_h	area of the hull enclosing the observed and simulated burnt area
S_i	first order sensitivity index of parameter i
σ	surface-area-to-volume ratio
$\dot{\sigma}$	mass exchange rate due to pyrolysis
Σ_s	multiplicative slope correction matrix
σ_s	multiplicative slope correction factor
T_a	air temperature
T_i	ignition temperature
θ_w	wind direction
U	wind speed
\mathbf{U}_{ws}	equivalent wind vector
$\hat{\mathbf{v}}$	unit vector in the direction of the fire spread
W	fuel loading; dry weight mass of the fuelbed per unit area
\mathbf{w}	wind vector
\dot{W}	fuel mass consumed per unit area
x	categorical predictor of a logistic regression
ξ	propagating flux ratio
\mathbf{y}_M	model outputs, obtained with the input values in matrix M

List of Abbreviations

CA	cellular automata
CBH	canopy base height
CFD	computational fluid dynamics
EC	European Commission
ECMWF	European Centre for Medium-Range Weather Forecasts
EFFIS	European Forest Fire Information System
FBP	Canadian Forest Fire Behavior Prediction System
FMC	fuel moisture content
GIS	geographical information systems
GSA	global sensitivity analysis
GUI	graphical user interface
JRC	Joint Research Centre
LC	land cover
MODIS	Moderate Resolution Imaging Spectroradiometer
NFFL	USDA National Forest Fire Laboratory
PCC	products of complete combustion
PICC	products of incomplete combustion

RH	relative humidity
ROS	rate of spread
SI	sensitivity index
WFDS	WUI Fire Dynamics Simulator
WUI	wildland urban interface

List of Figures

2.1	Spatio-temporal scales of fire	5
2.2	Schematic representation of diffusion flames	6
2.3	Representation of a typical fuelbed	9
2.4	Example of a surface fire, crown fire, and fire whirl	13
2.5	Average annual burnt area	14
2.6	Wildfire prevalence in Europe	16
2.7	Wildfire prevalence in Belgium	16
3.1	One-dimensional, steady fire line spread hypothesis	23
3.2	Example of the visualised output of WFDSs	24
3.3	Schematic overview of the three main fire perimeter representations	30
3.4	Schematic representation of Huygen’s fire perimeter propagation	31
3.5	An example of fire perimeters obtained with FARSITE	31
3.6	An example of fire perimeters obtained with Forefire	32
3.7	Two main approaches of perimeter propagation based on near-neighbour proximity	33
3.8	An example of fire perimeters obtained by the cell contact model	34
3.9	A schematic representation of the level set method	35
3.10	An example of fire perimeters obtained with MESO-NH/ForeFire	36
3.11	An example of fire perimeters obtained with a cellular automata (CA)-based model	37
3.12	A wildfire risk map for Belgium, based on logistic regression (Depicker et al., 2016).	39
4.1	Locations of the wildfires	42
4.2	Three recorded perimeters of Case 1.	43
4.3	Comparison of the wildfire perimeters registered by European Forest Fire Information System (EFFIS) and those in the fire reports of Cases 1 and 2	44

4.4	Overview of fuel classes according to the Joint Research Centre (JRC) FUELMAP and USDA National Forest Fire Laboratory (NFFL) classification	45
4.5	Landscape of the Kalmthout Heath (Case 2)	46
4.6	Average wind speed and standard deviations during the wildfires versus the burnt area	47
4.7	Fire perimeters and approximate ignition locations for the selected wildfires	49
4.8	Soil texture and p_{veg} maps of Cases 1–4	58
4.9	Geographical data of wildfire Case 1.	59
4.10	Geographical data of wildfire Case 2.	60
4.11	Geographical data of wildfire Case 3.	61
4.12	Geographical data of wildfire Case 4.	62
4.13	Geographical data of wildfire Case 5.	63
4.14	Geographical data of wildfire Case 6.	64
4.15	Geographical data of wildfire Case 7.	65
4.16	Overview of the weather data for Case 1	66
4.17	Overview of the weather data for Case 2	67
4.18	Overview of the weather data for Case 3	68
4.19	Overview of the weather data for Case 4	69
4.20	Overview of the weather data for Case 5	70
4.21	Overview of the weather data for Case 6	71
4.22	Overview of the weather data for Case 7	72
5.1	Results of FARSITE simulations for Cases 1–4.	75
5.2	Results of FARSITE simulations for Cases 5–7.	77
5.3	Results of ForeFire simulations for Cases 1–4.	79
5.4	Results of ForeFire simulations for Cases 5–7.	80
5.5	Results of FARSITE and ForeFire simulations for Case 1 with adjusted fuels.	82
5.6	Results of FARSITE and ForeFire simulations for Case 2 with adjusted fuels.	84
6.1	Burn frequency map of Case 1 with pre-calibrated parameters	89
6.2	Variability of the values of Ω	89
6.3	Evolution of Ω in the case-dependent calibration of CA1	91
6.4	Burn frequency maps obtained with the case-dependent calibrated parameter set of CA1 for Cases 1–4.	92
6.5	Burn frequency maps obtained with the case-dependent calibrated parameter set of CA2 for Cases 1–4.	94
6.6	Value of the objective function Ω (OF) versus the number of evaluations by the Nelder-Mead algorithm in the case-dependent calibration of CA1 for Cases 1–4, using the remaining three cases as calibration data.	96

6.7	Burn frequency maps obtained with the overall calibrated parameter set of CA1 for Cases 1–4.	97
6.8	Mean wind direction (a) and speed (b) data during the entire wildfire duration of Case 2, from ten weather stations (station 1 is closest to the observed perimeter, 10 is the furthest). Minimal and maximal values are marked with dashed lines.	99
6.9	Burn frequency map and burn frequency variance map (a) and the sensitivity maps (b) of Case 2. S1 and S2 are the estimated first-order sensitivities of the wind direction and wind speed, respectively.	101

List of Tables

2.1	Spatio-temporal scales of wildfires	4
3.1	Comparison of individual wildfire events and wildfire regimes	20
3.2	General framework for wind-slope correction Sharples (2008).	29
3.3	Main advantages and disadvantages of wildfire of different simulation methods.	37
4.1	Overview of the wildfire dataset.	42
4.2	Comparison of the wildfire perimeters registered by EFFIS and those in the fire reports of Cases 1 and 2	44
4.3	Overview of the fire dataset, provided by the JRC.	49
4.4	Overview of the evaluated wildfire simulators.	50
4.5	Overview of the input data, needed in a FARSITE project.	52
4.6	CORINE land cover (LC) classes with the corresponding JRC fuel classes and ForeFire parameters.	55
4.7	ForeFire parameters that are constant for all present fuel classes.	55
4.8	Possible values for p_{veg} , according to Eq. (4.5a).	57
5.1	Burnt areas simulated with FARSITE and corresponding wildfire durations for Cases 1–4	74
5.2	Accuracy measures of FARSITE simulations for Cases 1–4	75
5.3	Burnt areas simulated with FARSITE and corresponding wildfire durations for Cases 5–7	77
5.4	Accuracy measures of FARSITE simulations for Cases 5–7	77
5.5	Burnt areas simulated with ForeFire and corresponding wildfire durations for Cases 1–4	78
5.6	Accuracy measures of ForeFire simulations for Cases 1–4	79
5.7	Burnt areas simulated with ForeFire and corresponding wildfire durations for Cases 5–7	80
5.8	Accuracy measures of ForeFire simulations for Cases 5–7	80

5.9	Burnt areas simulated with FARSITE and ForeFire and corresponding wildfire durations for Case 1 with adjusted fuels	81
5.10	Accuracy measures of FARSITE and ForeFire simulations for Case 1 with adjusted fuels	82
5.11	Burnt areas simulated with FARSITE and ForeFire and corresponding wildfire durations for Case 2 with adjusted fuels	83
5.12	Accuracy measures of FARSITE and ForeFire simulations for Case 2 with adjusted fuels	84
6.1	Optimal parameter sets for the case-dependent calibration of CA1.	91
6.2	Accuracy measures and burnt areas obtained with the case-dependent calibrated parameter set of CA1	92
6.3	Optimal parameter sets for the case-dependent calibration of CA2.	93
6.4	Accuracy measures and burnt areas of the simulations obtained with the case-dependent calibrated parameter set of the CA2 for Cases 1–4.	94
6.5	Optimal parameter sets for the overall calibration of CA1.	95
6.6	Accuracy measures and burnt areas of the simulations obtained with the overall calibrated parameter set of CA1 for Cases 1–4.	97
A.1	JRC fuel classification and corresponding NFFL classes.	119

CHAPTER 1

Introduction

Even though wildfires are key natural processes that shape ecosystems and influence natural cycles, they are mostly associated with their devastating impacts on both humans and their environment. In the past year, two major wildfire events occurred in both Chile and Portugal, which caused the death of 75 people, while laying in ashes homes and several thousands hectares of natural land. Belgium, too, has had its own catastrophic year in 2011, when several wildfires swept through more than 2000 ha of nature reserves—luckily without the loss of human lives. Yet, it was a close call, as a fire truck was lost in the fire on the Kalmthout Heath and its passengers had to flee the flames on foot. Furthermore, some residential areas are located in the near proximity of these heathlands. Hence, (slightly) different weather conditions might have meant the loss of homes and, again, lives. In order to effectively guard ourselves and our surroundings against such disasters, a key aspect is to understand and predict a wildfire's behaviour. In this respect, mathematical wildfire models could be effective tools, as they try to capture the mechanics behind this phenomenon and provide predictions that can serve as a basis for decision making. This dissertation will revolve around such models, and more specifically those that simulate the wildfire dynamics in real-time.

Chapter 2 will give a brief general description of wildfires, with a focus on the main drivers and key processes behind, and the impacts and prevalence of these fires. Next, an overview of the different types and aspects of wildfire modelling is presented in Chapter 3. The core of this thesis encompasses on the one hand a review of two renowned wildfire simulators, namely FARSITE and ForeFire (Chapter 5), and on the other hand, the calibration, evaluation and sensitivity analysis of a CA-based model (Chapter 6). This is done on the basis of a dataset comprising seven wildfires in Belgium and the Netherlands, of which an overview is given in Chapter 4, alongside a description of the evaluated models. The main goal of all this is to assess whether or not these models are readily applicable in a Belgian context, and this for the sake of operational purposes (i.e. the faster than real-time prediction of wildfire spread after ignition).

CHAPTER 2

Wildfires: a brief description

Wildfire is a global natural phenomenon that has influenced biogeochemical cycles and ecosystem patterns throughout the history of terrestrial life (Bowman et al., 2009; McKenzie and Perera, 2015). Ever since the appearance of the first terrestrial plants—about 420 million years ago—the Earth’s biosphere has been intrinsically flammable. This is due to the combination of combustible vegetation, a high atmospheric oxygen level (right in the so-called “fire window” of 13-26%), periodically dry seasons, and a high frequency of ignition causes (e.g. lightning) (Scott and Glasspool, 2006; Bowman et al., 2009). Despite its frequent occurrence and ecological and socio-economic impacts, there is still a big gap in our knowledge of wildfire behaviour. Nevertheless, the extensive research on the topic during the last century has revealed some of the underlying mechanisms. A general description of the concept and its key processes will be provided in Section 2.1. Sections 2.2 and 2.3 will briefly discuss the impact and occurrence of wildfires and the strategies for wildfire management, respectively, since these subjects were already covered in a previous dissertation (Depicker et al., 2016).

2.1 General description

2.1.1 Definition and scales

The definition of wildfire depends on the perspective of its user. From a fire management point of view, wildland fire is defined as: “any non-structure fire that occurs in vegetation or natural fuels, which includes prescribed fire and wildfire” (The National Wildfire Coordinating Group, 2015). The distinction between these last two lies in whether the fire is intentionally ignited and used as a management tool (as is the case in the former) or unwanted and beyond any human control (as is the case in the latter). Throughout the remainder of this dissertation this distinction will not be made, since the processes which control the fire dynamics stay the same. Hence, wildfire will be used as a synonym for wildland fire.

Sullivan (2009a) defines a wildfire more mechanistically as: “the complicated combination of energy released (in the form of heat) due to the chemical reactions (broadly categorised as oxidation reactions) in the process of combustion and the transport of that energy to surrounding unburnt fuel, and the subsequent ignition of that fuel”. This definition reveals the two broad categories in which the processes governing wildfire can be subdivided, namely: chemical combustion on the one hand and physical heat transfer and fluid mechanics on the other hand. Note that these processes occur at different spatio-temporal scales, ranging from millimetres and milliseconds to kilometres and hours (Table 2.1). This already hints to a major difficulty in the study of wildfire behaviour. Furthermore, wildfires can be described at different levels, ranging from flames to fire regimes (Figure 2.1).

Table 2.1: Indicative spatio-temporal scales of the main processes and components in wildfires, adapted from Sullivan (2009a).

Type	Time scale (s)	Vertical scale (m)	Horizontal scale (m)
Combustion reactions	0.0001 – 0.01	0.0001 – 0.01	0.0001 – 0.01
Fuel particles	–	0.001 – 0.01	0.001 – 0.01
Fuel complex	–	1 – 20	1 – 100
Flames	0.1 – 30	0.1 – 10	0.1 – 2
Radiation	0.1 – 30	0.1 – 10	0.1 – 50
Conduction	0.01 – 10	0.01 – 0.1	0.01 – 0.1
Convection	1 – 100	0.1 – 100	0.1 – 10
Turbulence	0.1 – 1000	1 – 1000	1 – 1000
Spotting	1 – 100	1 – 3000	1 – 10000
Plume	1 – 10000	1 – 10000	1 – 100

2.1.2 Spread mechanism

Unlike fire in human-made structures, where the flames spread over solid surfaces, the fuels of wildfires consist of discrete particles separated by air spaces (Williams, 1977). Thus, since the early beginnings, wildfire spread is described as a succession of sustained ignitions of fuel particles (Fons, 1946). The subsequent combustion can occur with or without flames, the latter being referred to as *smouldering* (see Section 2.1.4). The flame propagation over the wildland surface occurs via so-called diffusion flames, characterized by the following positive feedback loop (Saito, 2001; Ward, 2001):

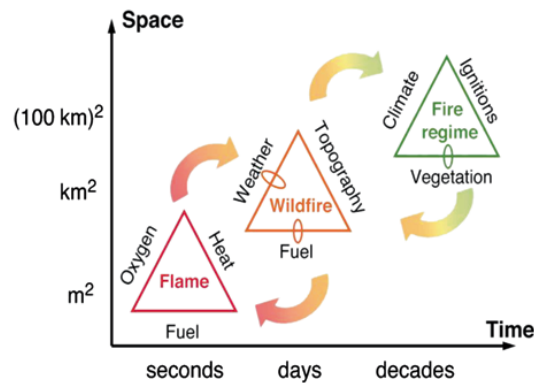


Figure 2.1: Spatio-temporal scales of fire, from Moritz et al. (2005) (Keane, 2015)

1. pre-ignition (preheating, dehydration, and volatilisation of organics) and thermal decomposition (pyrolysis) of unburnt condensed phase fuel with the production of highly flammable, volatile components (pyrolysates);
2. evaporation of pyrolysates and subsequent diffusion into the high-temperature flame;
3. combustion of the inflammable gases, resulting in combustion products and heat;
4. transfer of (part of) the heat to unburnt solid fuel.

If the heat transfer from step 3 is sufficiently high, the loop restarts and becomes self-supporting. A schematic representation of these processes is shown in Figure 2.2.

The dynamics resulting from this feedback loop can be described using some important characteristics (the cited definitions are adapted from the glossary of The National Wildfire Coordinating Group (2015)). The *rate of spread (ROS)* is the rate at which new fuel begins to burn (Williams, 1982), generally characterised by an initial acceleration and subsequent transition to a quasi-steady state (Rothermel, 1972). It thus marks the forward spread of the *fire front*—the part of a fire within which continuous flaming combustion is taking place. The *fire intensity* is the energy output from the fire. This can be expressed by metrics such as fireline intensity, reaction intensity, temperature, radiant energy, or residence time (Keeley, 2009). The *fireline intensity* is defined as the rate of heat release per unit time per unit length of fire front, while the *reaction intensity* is the rate of heat release, per unit area of the flaming fire front. The *residence time* is the total length of time that the flaming front of the fire occupies one point.

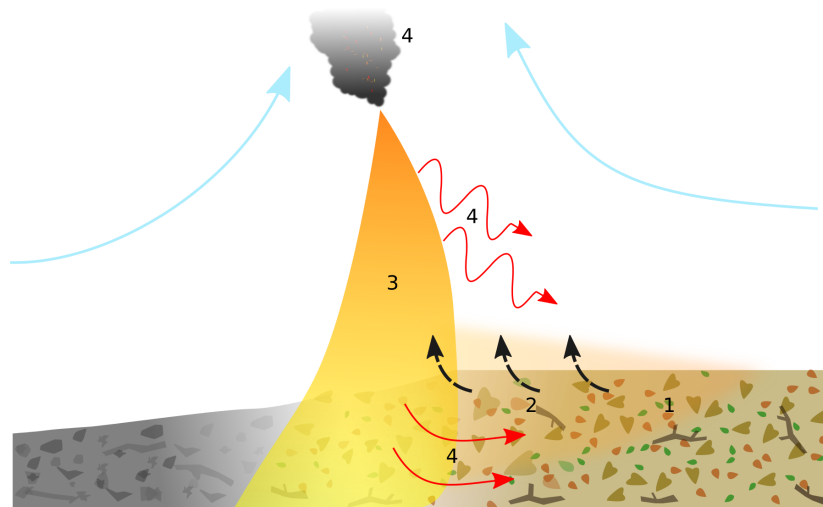


Figure 2.2: Schematic representation of the different steps in the feedback loop of diffusion flames spreading through a heterogeneous fuelbed, adapted from Morvan and Dupuy (2001): step 1: pre-ignition and pyrolysis; step 2: evaporation and diffusion of pyrolysates; step 3: combustion; step 4: heat transfer (due to radiation, convection and embers in the smoke plume). The blue arrows indicate the convective movement of surrounding air.

Due to the release of hot, buoyant gases and particles during the combustion processes, atmosphere, biosphere, and hydrosphere are all connected at the flame front (Bowman et al., 2009). Therefore, the dynamic fire behaviour simultaneously depends on and influences a vast amount of highly variable environmental processes and parameters. This leads to a high degree of unpredictability and forms a source of uncertainty (Cruz and Alexander, 2013; Thompson and Calkin, 2011). Consequently, two fire events will rarely be the same; in fact, when studying *fire regimes* (i.e. the fire behaviour at landscape level over a time-span of several years or decades), every observed wildfire could be considered as a single realisation of a stochastic process (McKenzie et al., 2011).

2.1.3 Fuels

One of the three basic requirements for fire – next to oxygen and a heat source – is fuel, so, unsurprisingly, this parameter has a major impact on fire behaviour. In a wildfire context, the fuel consists of live and dead biomass (mostly vegetation). A detailed description of different wildland fuels is provided by Keane (2015), which forms the basis of this section.

Since wildland fuels again comprise a wide spatial scale range (Table 2.1), they can be described at different levels, each characterised by a set of physico-chemical properties. The smallest fuel element is an individual fuel particle (e.g. a leaf or log), which can be classified into different fuel components and types (such as litter or woody biomass). The coarsest scale

of fuel description is the so-called *fuelbed*, which is defined by Keane (2015) as the complex array of biomass types for a given area. The higher levels are characterised by bulk properties, which are mostly statistical summaries of those of individual particles. There are numerous particle and bulk characteristics, and they often have a dynamic nature. Most of them influence wildfire behaviour in some way or another through complex interactions that are often still poorly understood (Nelson, 2001; Finney et al., 2013). Therefore, only some properties that are generally considered to be (the most) crucial will be discussed here.

Particle properties

At the particle scale, wildland fuels have the widest range of properties, which can be of a chemical or physical nature. Relevant chemical properties are the chemical composition (and foremost the fuel moisture content) and heat content. Since most wildland fuels are live or dead plant biomass, the organic constituents are (in descending order of abundance) cellulose, hemicellulose, and lignine next to some extractives (such as oils and proteins), while the inorganic comprise minerals (ash) and water. The relative proportions of these components depend on numerous biochemical processes and vary between species, plant parts, live and dead fuels, and seasons (Keane, 2015; Finney et al., 2013). Due to its disproportional importance, the influence of water will be discussed separately. The other components can affect the fire behaviour by changing the heat content (h), expressed as the heat of combustion released per mass unit of burned fuel [kJ kg^{-1}], or by altering the combustion reactions (see Section 2.1.4). So-called ether extractives (such as oils and resins) may, for example, increase the heat content (Philpot, 1969), while the silica-free inorganic fraction can influence pyrolysis reactions, acting as inhibitor (or catalyst) (Philpot, 1970; Di Blasi, 1998; Williams, 1982).

In addition to the chemical properties of a fuel particle, also its physical characteristics play a profound role in wildfire dynamics. These include thermal properties (e.g. heat capacity and conductivity), geometric properties, such as the surface-area-to-volume ratio (σ) and particle diameter (d_p), and particle density (ρ_p). In short, the physical properties will mostly affect the heat transfer between the fire front and the surrounding fuel and the dynamic behaviour of the moisture content. More particularly, the geometry and density determine whether a given fuel mainly promotes a fast fire spread (fine fuels, with short residence times and a rapid ignition) or intense fires (coarse, dense fuels, with long residence times).

Spatial structure and bulk properties

As mentioned earlier, the properties at a higher level of fuel description are derived from those of the particles that make up this level, and if applicable, account for its spatial structure. In a fuelbed, this spatial structure involves a vertical and horizontal dimension (Simeoni, 2016). Vertically it is generally stratified into three fuel layers: ground, surface and canopy or crown fuels (Figure 2.3). A related metric is the *canopy base height (CBH)* that can be defined as the lowest height above the ground at which there is sufficient canopy fuel to propagate fire vertically through the canopy (Scott and Reinhardt, 2001). The definition of the boundaries between these layers is largely arbitrary and therefore variable in literature (Keane, 2015). Moreover, in reality these layers can overlap, forming a so-called *fuel ladder*, which can transport fire from the surface to the crown layer, resulting in intense fires. The horizontal fuel distribution, on the contrary, strongly influences the fire spread since it represents the fuel density and the connectivity between different fuel patches.

Some important bulk properties include the *fuel loading* (W), which is the dry weight mass of the fuelbed or fuel component per unit area [kg m^{-2}], the bulk density ρ_b , fuelbed depth (d_{fb}) and *packing ratio* (β). The latter is defined as the ratio $\frac{\rho_b}{\rho_p}$ and represents the compactness of the fuelbed (Rothermel, 1972).

Fuel moisture

The fuel moisture content (FMC) is perhaps the most critical fuel characteristic for wildfires, since it influences most fire processes in some way (Finney et al., 2013; Nelson, 2001; Simard, 1968). First of all, it increases the heat of pre-ignition and thus the preheating time of the fuel due to the latent heat that has to be provided for the endothermic evaporation of water. Next to that, the high thermal conductivity of water hampers the ignition of high moisture fuels by an increased conduction of supplied heat through and away from the fuel particles. Furthermore, the released water vapour dilutes the air oxygen, thus limiting combustion and lowering the flame temperature. The combined result of these interactions is the limitation of ignition and combustion, favouring of smouldering over flame reactions, and a decreased fuel consumption.

The FMC is highly dynamic due to its link with other environmental processes. Moreover, it is necessary to make a distinction between live and dead fuels, since their moisture dynamics are fundamentally different (Saito, 2001; Simeoni, 2016). The live FMC is governed by ecophysiological processes with diurnal and seasonal variations. Dead fuel moisture content, on the contrary, is mostly governed by evaporation. Hence, it relies on short-term changes in weather conditions (temperature and humidity) that alter the equilibrium moisture content. To ease the description of these dead fuel moisture dynamics, the *time-lag* concept was introduced. It is defined as the time needed (under specified environmental conditions) for a fuel

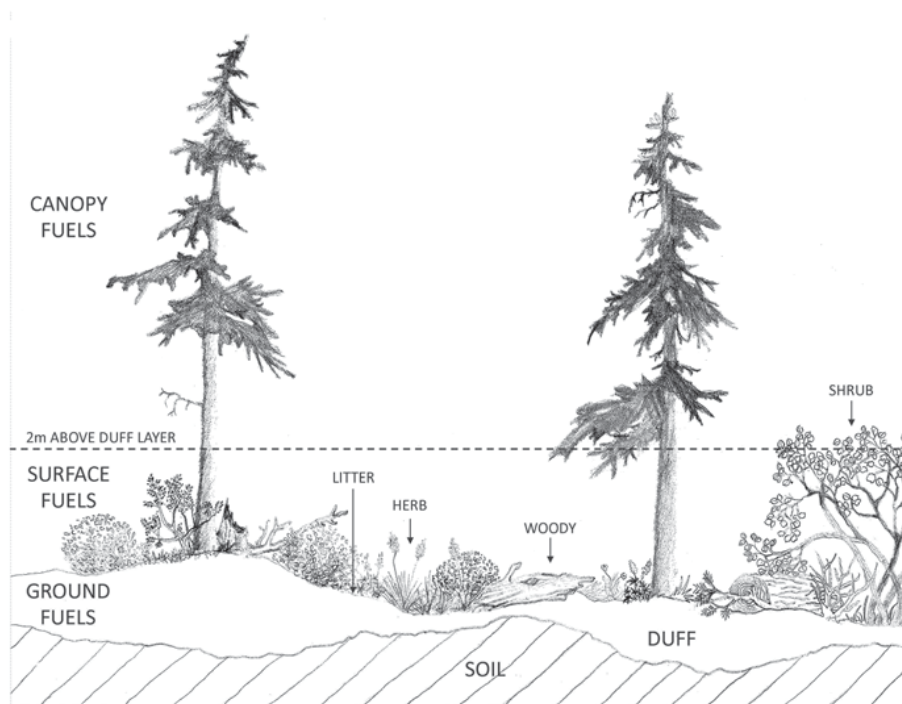


Figure 2.3: Representation of a typical fuelbed (Keane, 2015). This fuelbed is vertically stratified into three layers: ground, surface, and canopy or crown layer, which are all composed of different fuel types (such as herbs, shrubs, litter and woody biomass in the case of the surface layer).

particle to lose 63% of the difference between its initial moisture content and its equilibrium moisture content, while assuming an exponential drying function (Keane, 2015). For woody fuel particles the time-lag increases logarithmically with the particle density, while it depends on many biophysical factors (e.g. stage of decomposition) for litter and duff.

Fuel condition and flammability

The combined influence of the fuel characteristics is often expressed as the *fuel condition*. This is the relative flammability of the fuel based on type and environmental conditions, in which the *flammability* is the relative ease at which the fuels burn regardless of the amount (The National Wildfire Coordinating Group, 2015). To correctly quantify and interpret these concepts, one has to take the whole spatio-temporal context of the fuels into account, which can rarely be done in standardized tests. Moreover, Keane (2015) notes that these concepts are vaguely defined and consequently interpreted differently all over the world, so they should be used as qualitative rather than quantitative fuel descriptions.

2.1.4 Combustion reactions

In Section 2.1.2, the basic feedback loop of diffusion flames was discussed (Figure 2.2), in which the main reaction phases were identified as pre-ignition, pyrolysis and combustion. During *pre-ignition* the condensed fuel is heated causing the release of volatile organics and water (dehydration). The *pyrolysis* phase starts when enough heat is added to induce thermal degradation of the fuel components. The corresponding reaction schemes are very complex—with over a hundred reactions and fifty species for the pyrolysis of cellulose alone (Zhou and Mahalingam, 2001)—due to the diversity in fuels and reaction conditions. Cellulose, the main constituent of wildland fuels (see Section 2.1.3), is characterised by two competing pyrolysis mechanisms (Williams, 1982; Di Blasi, 1998; Drysdale, 2011):

1. *dehydration*, with the formation of char;
2. *depolymerisation*, which produces tar (primarily levoglucosan) that subsequently forms volatile, combustible pyrolysates.

These pathways are controlled by physico-chemical feedbacks in which the first pathway is favoured in moist conditions and at relatively low heating rates, while the second occurs at dry conditions and—due to its higher activation energy—high heating rates (Sullivan, 2009a). The dominating pathway subsequently determines the type of combustion. During *combustion* fuel is combined with an oxidiser (i.e. oxygen of the surrounding air) in an exothermic reaction to produce the so-called *products of complete combustion (PCC)* and *products of incomplete combustion (PICC)* (Saito, 2001):



where the released heat (Q) can support further pyrolysis. PICC are formed when the reaction is terminated before complete combustion has occurred. This happens frequently in wildfires, especially during fast and turbulent combustion (Saito, 2001). These components will then condense to form the smoke particles (Drysdale, 2011). If char formation is favoured during pyrolysis, the solid char will be the fuel of *smouldering combustion*. In this type of combustion char is oxidized at its surface without the emission of flames. If, on the other hand, depolymerisation is favoured, combustion will take place in the gas phase, resulting in *flaming combustion* (cfr. the diffusion flames discussed in Section 2.1.2). The transition from pre-ignition to self-sustained combustion is called *ignition*. It is often (approximately) quantified by a critical temperature that the condensed fuel surface has to reach before burning starts (Williams, 1982). This ignition temperature is assumed to be fuel specific.

2.1.5 Heat transfer

Williams (1982) identifies nine possible heat transfer mechanisms in a fire, that are reclassified by Sullivan (2009a) into four classes:

1. Diffusion at the molecular level (diffusion of radiacals and heat conduction through gas and condensed materials);
2. Convection (heat transfer through the motion of gases);
3. Radiation (from flames and burning fuels surfaces);
4. Solid fuel transport (which accounts for fuel deformation and *firebrand* transport, i.e. glowing particles capable of igniting unburnt fuel)

Assessing the contribution of these different heat transfer mechanisms is, however, far from straightforward, since they are mutually dependent, which can be illustrated by the following observation. Combustion of fuel produces hot gases that start to rise due to their increased buoyancy, which creates a turbulence. This turbulence can mix the hot gases with unburnt fuel (class 2), but can as well carry these gases away and thus cool the vegetation. Moreover, the upward motion can transport firebrands downwind of the fire front (class 4). If the firebrands are still burning upon landing on unburnt, flammable vegetation, they can ignite new fire fronts. This phenomenon is called *spotting*.

Generally speaking, radiation and convection are considered to be the dominant heat transfer mechanisms in wildfires (Sullivan, 2009a). Radiative heat transfer is mainly controlled by temperature, emissivity, absorptivity and geometric effects (quantified by the view factor) (Williams, 1982). Convection is governed by fluid dynamics—which on their turn depend on local weather conditions, fuel particle geometry, drag forces inside the fuelbed and the fire behaviour itself (Sullivan, 2009a; Williams, 1982).

Both mechanisms are heavily affected by wind and topography. The main effect of wind is often attributed to the tilting of the flames which results in a closer contact with the unburnt fuels (Baines, 1990; Beer, 1991; Simeoni, 2016). Moreover, wind alters the relative importance of the main heat transfer mechanisms, resulting in two spread regimes (Morandini and Silvani, 2010; Morvan, 2011; Rothermel, 1991). Under low or no-wind conditions the fire is *plume-dominated*. This is associated with a vertical, buoyant convection column (caused by the fire itself) and with a radiation-dominated fire spread. At stronger lateral wind speeds, the fire is *wind-driven* and controlled by radiation and convection. Topography (and more specifically, slope) has a similar effect as wind, in that it brings fuel closer to the flames, resulting in a faster spread uphill (Baines, 1990; Sharples, 2008; Simeoni, 2016). Moreover, topography also influences local wind patterns. It should be stressed, however, that these are all simplified descriptions of a complex reality, which is not yet well understood and much under debate (Baines, 1990; Finney et al., 2013).

In fact, most of the previously discussed mechanisms were derived from the study of *surface fires*, since most wildfires will spread in the surface layer (Keane, 2015). However, other types of wildfire can be distinguished.

2.1.6 Phenomenology

Depending on the fuel layers that are burning, wildfires are generally classified into ground, surface and crown fires. *Ground fires* burn in the duff layer (see Figure 2.3), which is characterised by a higher density, moisture content and mineral fraction than surface fuels, due to the higher state of decomposition. Consequently, these fires are associated with smouldering combustion and slow spreading rates. This, however, does not make them less dangerous, since they can burn for much longer and possibly reignite surface fires (Rein, 2009). Moreover, they consume (and heat up) the (in)organic soil to a far greater extent than surface fires, which causes severe damage to the soil biota (Hartford and Frandsen, 1992).

When the conditions are right, a surface fire can ignite the canopy layer in a forest fuelbed. This phenomenon is called a *torching* and results in a *crown fire* (Figure 2.4). This type of wildfire is associated with high intensities, large flame heights and an increased firebrand production which can cause spotting. Crown fires can be classified following the theory proposed by Van Wagner (1977):

1. *Passive crown fires* rely fully on the heat generated by the surface fire, resulting in an ROS equal to that of the surface fire;
2. *Active crown fires* generate a substantial extra heat feedback from crown to surface (but still depend on the heat of the surface fire), resulting in a higher surface (and crown) ROS;
3. *Independent crown fires* are fully self-sustained and spread faster than the surface fire.

The last category is very rare and unstable, since its required conditions (such as a very low canopy FMC) are hard to attain in practice. Finally, some extreme fire behaviours can be observed under specific conditions (Simeoni, 2016). *Eruptive* or *blow up fires* occur mainly in canyons and are characterized by a sudden, sharp acceleration (Viegas and Simeoni, 2011). *Fire whirls* (Figure 2.4) and even *fire tornadoes* can emerge in plume-dominated fires due to the strong buoyant convection (Morvan, 2011; McRae et al., 2013). These can generate larger firebrands than usual, having a higher spotting potential.

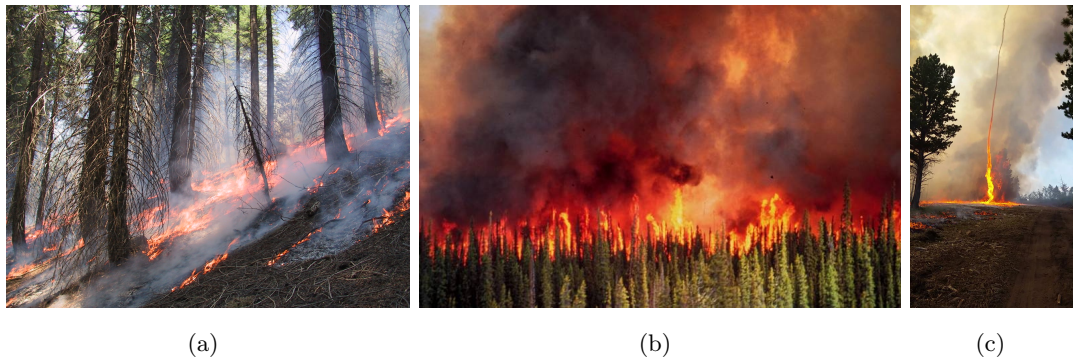


Figure 2.4: Example of a surface fire (a), crown fire (b) and fire whirl (c), by Knapp (2002), Forest Service Northern Region (2011) and Willingham (2016).

2.1.7 Remaining questions

As was mentioned several times throughout this chapter, some key questions related to wild-fire dynamics still remain unanswered. Finney et al. (2013) point out that because of this knowledge gap, a fundamental, generally accepted theory on the subject is lacking. In their critical review, they put forward a non-exhaustive list of some areas in wildfire spread that are still under debate, mainly concerning the ignition of fine fuel particles. Firstly, they challenge a widespread assumption that radiation is often the dominant heat transfer process in wildfire spread (Sullivan, 2009a; Williams, 1982), based on critical voices coming from the forest science community (Anderson, 1969; Byram et al., 1964; Beer, 1991; McCarter and Broido, 1965; Rothermel, 1972; Van Wagner, 1977). Moreover, they put forward the analysis by Baines (1990) of the experimental work of de Mestre et al. (1989), in which he suggests that the radiant heating of the fine-sized fuel particles is balanced by convective cooling, making it insufficient to cause ignition. This behaviour was confirmed by Finney et al. (2015), who additionally observed that ignition occurs due to non-steady flame convection, produced by the interaction of buoyancy and inertia in the flame zone. Nevertheless, it should be noted that these experiments all included wind and that the role of convection in wind-driven fires was already recognised (see Section 2.1.5). Secondly, Finney et al. (2013) reject the use of a critical ignition temperature (see Section 2.1.4) and a total heat balance to describe fuel ignition, stating that these are physically inconsistent. Last but not least, they conclude that although there is a substantial difference in burning characteristics between living and dead fuels—as was already pointed out in Section 2.1.3—a physical understanding of live fuel ignition processes is currently still missing.

2.2 Prevalence and impact

2.2.1 Global

Based on data from the Moderate Resolution Imaging Spectroradiometer (MODIS) aboard the Terra and Aqua satellites, Randerson et al. (2012) estimate that on average 4.64 million km²/yr were burnt between 2001 and 2010, corresponding to approximately 4% of the global land area. These authors do not discriminate between wildfires and intentional fires (e.g. used for pastoral activities in rural areas). The spatial distribution of these fires is shown in Figure 2.5. From this figure it is clear that there are significant differences in fire prevalence across the globe resulting from different human practices (e.g. slash and burn) and fire regimes.

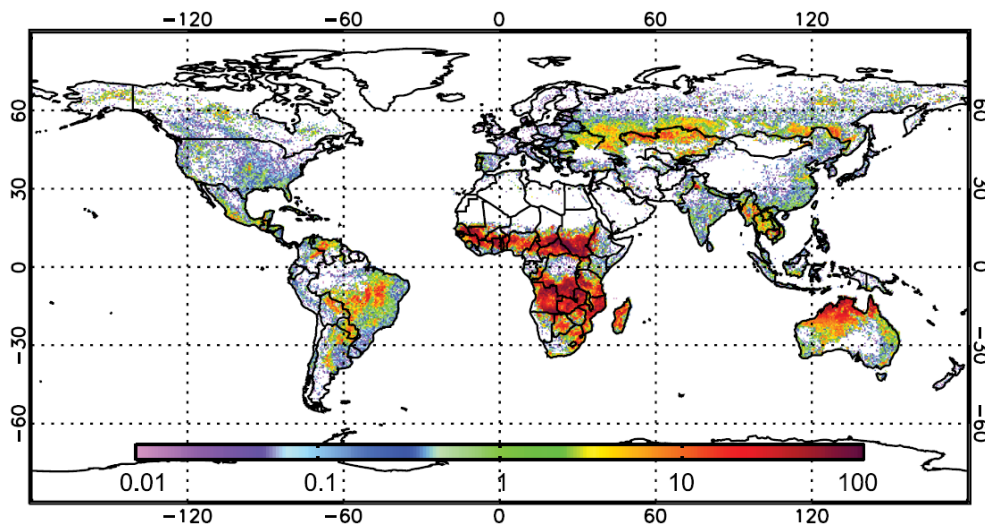


Figure 2.5: Average annual burnt area between 2001-2010 for each 0.25 degree grid cell, expressed as percentage (Randerson et al., 2012).

Many articles report expected changes in fire regimes due to climate change. Flannigan et al. (2013) predict, for instance, a significant increase in fire season length based on simulation results of three General Circulation Models and three emission scenarios for the 21st century. However, the effects on other fire regime characteristics (such as burnt area and fire frequency), are expected to vary greatly between different regions in the world (Flannigan et al., 2009; Krawchuk et al., 2009; Pechony and Shindell, 2010). Furthermore, to reliably predict the impacts of climate change, the fire-climate feedbacks will also have to be accounted for, which is not a trivial task (Bowman et al., 2009). Current data do not indicate a global increase in burnt area (Doerr and Santín, 2016). On the contrary, Giglio et al. (2013) even report a decreasing trend between 2000 and 2012. Moreover, due to missing or inaccurate global data and/or insufficient knowledge, characteristics such as fire frequency, intensity and

severity cannot be reliably assessed at the moment (Doerr and Santín, 2016; Flannigan et al., 2009). Consequently, global trends and future wildfire impacts remain uncertain.

Humans have always coexisted with wildfires, but the sometimes devastating consequences (such as large economic losses, health issues and even losses of human lives) have gained the phenomenon a bad reputation. Doerr and Santín (2016) conclude, however, that this negative perception is not caused by an increase in direct losses, but rather by an increased public attention to these effects (e.g. due to mass media). Besides, in many parts of the world the traditional Western European mentality is upheld—with its main goal being the active repression of wildfires (Pyne, 2016; Raftoyannis et al., 2014). The latter results in an unsustainable management of fire-prone areas (Donovan and Brown, 2007; North et al., 2015), as will be discussed in Section 2.3. What is already an emerging problem, however, is the spread of the wildland urban interface (WUI) and the increasing number of people living in fire-prone areas, leading to higher fire hazards (Doerr and Santín, 2016; Moritz et al., 2014; Morvan, 2011).

2.2.2 Europe and Belgium

Since the 1970s, several European countries have been collecting data on wildfires independently, but since 2000 the European Forest Fire Information System (EFFIS) has been providing harmonized information on this phenomenon (San-Miguel-Ayanz et al., 2012). Between 2000 and 2015 on average 73000 wildfire incidents per year were reported, burning approximately 430000 ha (San-Miguel-Ayanz et al., 2016). As shown in Figure 2.6 most of these fires (about 70%) occurred in five Mediterranean countries (i.e. Portugal, Spain, France, Italy and Greece). Moreover, the burnt area in these countries accounted for 88% of the total. The other European countries mentioned are Austria, Bulgaria, Croatia, Cyprus, Czech Republic, Estonia, Finland, Macedonia, Germany, Hungary, Latvia, Lithuania, Norway, Poland, Romania, Slovakia, Slovenia, Sweden and Switzerland.

For what concerns Belgium, Depicker et al. (2016) assessed the prevalence of wildfires, based on data in digital archives of Belgian newspapers and data provided by the Directorate-General of the Federal Public Internal Service Affairs. This resulted in a map of 261 reported ignitions between 1995 and 2015 and a frequency distribution of 744 wildfire ignitions, reported between 1911-1950 and 1995-2015 (Figure 2.7). An additional 113 ignitions were registered between 1995 and 2015 without geographical coordinates. The Belgian fire season falls within the standard of Europe (i.e. between March and October (Schmuck et al., 2015)), with a peak at the beginning of spring and an increased occurrence at the end of summer (Figure 2.7(b)).

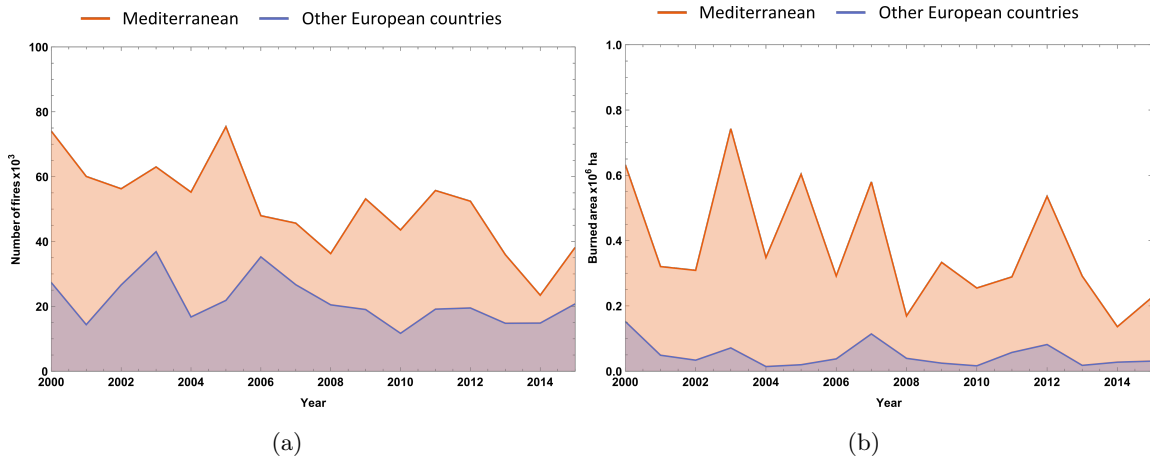


Figure 2.6: Annual reported number of wildfires (a) and burnt area (b) in Europe between 2000 and 2015, adapted from the European Fire Database.

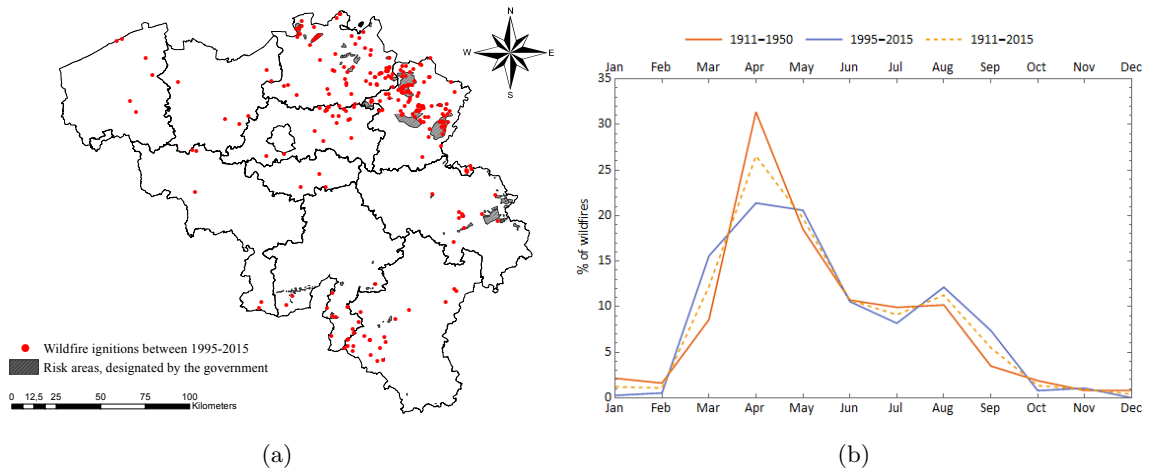


Figure 2.7: Wildfire prevalence in Belgium (a) and relative frequency of the 744 wildfire ignitions between 1911-1950 and 1995-2015 (b), adapted from Depicker et al. (2016).

2.3 Wildfire management

Since the prevalence and impact of wildfires vary strongly between regions, also management differs. In general, fire suppression policies can be categorized in preventive measures and operational interventions (Simeoni, 2016). The aim of wildfire prevention is the reduction of fire hazard and risk, mainly via fuel treatment to reduce the ignition probability or the intensity and ROS in case of a fire incident. This also comprises strategic measures, such as the efficient organization of available resources. Operational interventions, on the other hand, take place in case of a fire outbreak by means of active fire fighting and evacuating areas at risk. Fire fighting absorbs the bulk of the financial and human resources for wildfire management in most countries (Rigolot et al., 2009). However, Simeoni (2016) points out that there is always a threshold in ROS and intensity, above which fire fighters are overwhelmed by the fire, leading to very dangerous situations.

As was pointed out in Section 2.2, our social perceptions of fire are Western biased, which resulted in aggressive fire suppression policies in many regions, aiming at total fire exclusion (Doerr and Santín, 2016; Rigolot et al., 2009). This led, however, to fuel accumulation in fire-prone areas, giving rise to more catastrophic, large-intensity fires. In combination with the increasing WUI, this stresses the importance of a transition towards sustainable fire management (Doerr and Santín, 2016; Moritz et al., 2014).

CHAPTER 3

Wildfire modelling

From the general description of a wildfire in Chapter 2 it should be clear that it is an extremely complex phenomenon. Unsurprisingly, wildfire management is challenged by many issues and uncertainties. Nevertheless, Sections 2.2–2.3 highlighted the increasing importance of an effective, sustainable fire management. Wildfire models can be an important quantitative tool for aiding fire managers. This chapter will provide the reader with an introduction to wildfire modelling, starting with some general modelling considerations (Sections 3.1). Then, Sections 3.2–3.6 will give an overview of the currently available wildfire models, and Section 3.7 will briefly discuss wildfire modelling in the Belgian context.

3.1 General considerations

3.1.1 Wildfire model usage

A clear definition of the intended use of a model is a very important—if not the most important—step in its development, since it largely determines the scope and the required degree of complexity. This is not different for wildfire models. These can be of a purely theoretical nature or of a more practical one, namely the development of tools for wildfire managers that aid them in executing an effective fire suppression policy (Pastor et al., 2003). Finney et al. (2013) make a clear distinction between both model types. While a theoretical model tries to describe the underlying mechanisms of wildfires by comparing its outcomes to experiments of the actual phenomenon, an operational model just needs to make useful predictions, based on a set of relevant input data.

As explained in Section 2.3, fire management can be divided into two broad categories, being prevention policies and operational interventions. In both cases wildfire behaviour models can be used as support, but since they act on different levels, the model use will differ considerably. Preventive policies require information on fire regimes, while people conducting

operational interventions (i.e. fire fighters) require insight into the spatio-temporal dynamics of individual fires. Table 3.1 compares the properties of fire regimes and individual fire events. Fire regimes are typically described by static or dynamic models working over large temporal scales (i.e. years) and resulting in risk maps or predictions of long-term effects of land management strategies. Fire events, on the contrary, use dynamic models that cover shorter temporal scales (i.e. from minutes to weeks). This work will focus on the latter.

Table 3.1: Comparison of individual wildfire events and wildfire regimes (Falk et al., 2007; McKenzie and Perera, 2015).

	Fire event	Fire regime
Material	Fuel properties	Vegetation properties
Atmosphere	Weather conditions	Climate conditions
Process	Fire behaviour and effects	Fire-ecology interactions
Spatial extent	Burnt area, fire perimeter	Fire size distribution, annual burnt area
Temporal extent	Fire date(s), burning duration	Fire frequency, fire season

The aim of fire event models is to predict the spread of a wildfire across the landscape under specific environmental conditions. They can be used in real-time decision support systems or as training tools for fire fighters (Gollner et al., 2015; Sullivan, 2009c). Some land management tools also make use of simple wildfire-spread submodels, with the goal of creating a range of hypothetical individual fire events *in silico* that are subsequently used to simulate fire regimes and predict their impact on landscapes and ecosystems. An example thereof is the LANDSUM submodel in Fire-BGCv2 by Keane et al. (2011).

3.1.2 Hurdles in wildfire modelling

A model that is intended to be used in operational tools has to fulfil a number of requirements. Firstly, it has to be validated with experimental data, which can be collected from field or laboratory experiments. The former have the advantage of including all the interactions between the different compartments (i.e. fire, fuel, atmosphere and topography), but are costly and hard to control (Sullivan, 2009a,b). The latter, on the contrary, can be relatively cheap and easy to control, but may exclude relevant processes (e.g. fire-atmosphere interactions), which hampers the upscaling of these data (Sullivan, 2009b). Secondly, the model input data should be easily accessible to the end user. Thirdly, the resources of the end user should be able to cope with the computational cost of solving the model equations within a practical time frame. Last but not least, the spatio-temporal domain and boundary conditions of the

model should match those of the end user. For example, a model describing the fire spread over a fuel patch of one by one meter during a few seconds is useless for a fire manager who requires information on the fire behaviour at landscape level.

As stated in Chapter 2, fire behaviour is governed by a vast number of coupled processes that act across a wide range of spatio-temporal scales, and which depend on many highly variable environmental conditions. These three aspects make wildfire modelling a very challenging task (Simeoni, 2016). The incorporation of many physical processes, interacting at different scales, results in extremely complex and computationally demanding models. Simpler models, on the other hand, tend to oversimplify the intrinsically complex behaviour of wildfires. Moreover, collecting data for calibration and validation is also a hurdle, due to the practical problems in measuring the involved variables at the required detail during field experiments and the limited upscaling potential of laboratory data (Papadopoulos and Pavlidou, 2011; Sullivan, 2009b). Therefore, wildfire models can be extremely hard or even impossible to calibrate and validate, which limits the trust of the end user in their predictions.

3.2 Wildfire models

3.2.1 History

The study and modelling of wildfire behaviour and spread was initiated in the beginning of the previous century by foresters and other land managers, in order to protect their lands (Sullivan, 2009a). Ever since, the scientific community has become more and more interested in this study area. Initially, research focused on defining the main processes and variables that influence wildfires, and implementing them into models. These studies were mainly conducted by forestry agencies of (western) countries with vast fire-prone areas, such as the US, Australia and Canada (Sullivan, 2009b). These first modelling attempts resulted in physically-based models on the one hand—starting with the one of Fons (1946)—and in (quasi-)empirical models on the other hand, intended for direct usage in (simple) operational tools—such as the rotating discs based on the work of McArthur in the 1960s (Pastor et al., 2003). Generally, these first models aimed at predicting the ROS in the direction of the head fire (i.e. that portion of the wildfire with rapid spread and higher intensity, mostly aligned with the wind and/or slope direction (The National Wildfire Coordinating Group, 2015)).

The uprise of computer science and technology in the 1980s and of remote sensing and geographical information systems (GIS) in the 1990s opened new horizons. Catalysed by the increasing computational power and easy access to geographical data, the one-dimensional models could be extended to predict fire spread across (two-dimensional) landscapes. This led to the development of fire spread simulation software, such as FARSITE (Finney, 2004). Moreover, the development of computational fluid dynamics (CFD) made it possible to include more (detailed) physics into the models (Morvan, 2011).

All these developments have resulted in a large number of wildfire models, which comprise a broad spectrum of model structures.

3.2.2 Classification

Over the years, several reviews on wildfire modelling have been conducted—most notably the ones by Sullivan (2009a,b,c) and Pastor et al. (2003), that will form the basis of following sections. Wildfire models can be classified based on different aspects, such as the nature of the equations, the predicted variables, and the modelled phenomenology (Pastor et al., 2003). Here, we opt for a classification following the one proposed by Sullivan (2009a,b,c). It subdivides the whole range of models into five classes:

1. *Physically based models*: attempt to mechanistically represent the physics (and chemistry) of fire spread;
2. *Empirical models*: have no physical basis and are generally only of a statistical nature;
3. *Quasi-empirical models*: use some form of physical framework upon which to base the chosen statistical modelling;
4. *Simulation models*: implement (one or more of) the preceding types of models in order to simulate the spread of wildfires across a landscape;
5. *Analogue models*: use other models to simulate the spread of wildfires across a landscape.

From these definitions a clear distinction follows between classes 1 to 3 and classes 4 and 5. While the former try to predict one or more fire characteristics (mostly the ROS and fire line intensity I) from a given set of conditions, the latter try to simulate how the fire spreads across a landscape. The remainder of this chapter will detail these different modelling approaches and provide some examples. It should be noted that the majority of these models were developed for surface fires, as these are the most abundant and thus well studied (see Section 2.1).

3.3 Physically based models

The first general modelling approach boils down to the mathematical representation of the underlying physico-chemical processes of wildfire dynamics (Section 2.1) and subsequently combining the resulting equations into a system of (partial) differential equations. The solution of this system, for a set of initial and boundary conditions, yields a quantitative prediction of (some of) the fire spread variables, most notably the ROS and I . As the mechanics behind wildfires are universal, the physically based models rely on the same basic theoretical principles, such as the conservation of mass, momentum, and energy (Pastor et al., 2003; Sullivan, 2009a). Still, they can differ considerably.

A first distinction is based on whether or not the chemical combustion reactions are explicitly included, referred to as physical and quasi-physical models, respectively (Sullivan, 2009a). The latter rely on higher-level (empirical) submodels to determine the amount of energy released and the flame characteristics (Pastor et al., 2003; Sullivan, 2009a). Secondly, the physically based models vary in the considered processes, their implementation, their assumptions, and the used (numerical) solution methods (Finney et al., 2013; Pastor et al., 2003; Sullivan, 2009a). This results again in a multitude of models with a varying degree of complexity.

Model complexity

All physically based models start from an idealisation of the fuel and flame front. The simplest one is the so-called one-dimensional, steady fire line spread hypothesis (Pastor et al., 2003). It assumes a combustion interface and an inclined, flat, isothermal flame front to be moving through a homogeneous fuel bed, characterised by some bulk properties (Section 2.1.3), at a stationary (constant) ROS (Figure 3.1). It is clear that this greatly reduces the system complexity, and relies on strong assumptions. The resulting models generally do not calculate the (local) air flow and thus rely on submodels to determine the wind fields and flame characteristics (Simeoni, 2016). Moreover, radiant heat transfer is mostly assumed to be the controlling spread mechanism, as opposed to convection, which is often treated ambiguously or even completely ignored (Finney et al., 2013; Pastor et al., 2003).

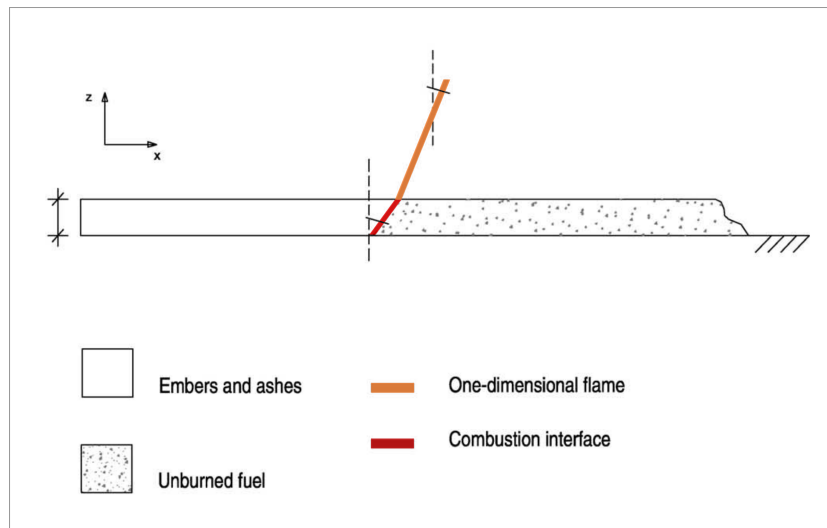


Figure 3.1: Schematic representation of the one-dimensional, steady fire line spread hypothesis (Pastor et al., 2003).

The last three decades, there is a trend to include more physics and complexity into wildfire models, in order to make them more generally applicable (Morvan, 2011). The foundations hereof were laid by Grishin (1997). He treats the fuel bed as a heterogeneous, multi-phased and multi-storied medium (thus also accounting for canopy layers) in three dimensions. Detailed models generally calculate the turbulent flow fields by means of CFD (Morvan, 2011; Simeoni, 2016). Furthermore, some authors include fire-atmosphere interactions by coupling models for wildfire spread and atmospheric flows. Examples hereof are FIRETEC (Linn, 1997) and WUI Fire Dynamics Simulator (WFDS) (Mell et al., 2007) (Figure 3.2).

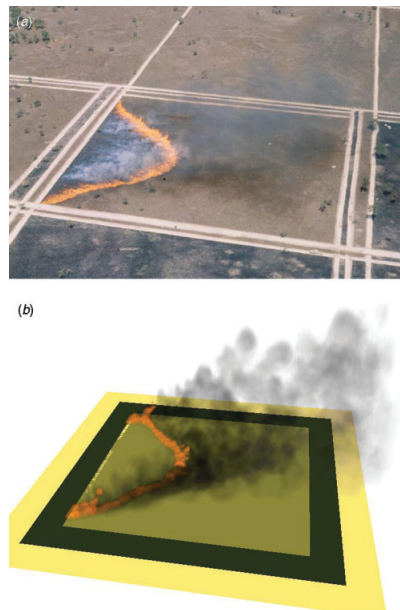


Figure 3.2: Example of the visualised output of WFDS (b), compared to an aerial photo of the modelled experimental fire (a) at the same time after ignition (Mell et al., 2007).

Performance

The varying complexity of physically based models influences their performance. In particular, detailed models are generally built to give high-resolution, (two- or) three-dimensional descriptions of all variables. This comes, however, at the cost of high computational demands and/or small working ranges, which makes them of no use for operational tools (Sullivan, 2009a). Moreover, Simeoni (2016) and Sullivan (2009a) note that the validation, calibration and generation of input data (e.g. initial and boundary conditions) are extremely difficult. Hence, the detailed models are often simplified to make them operationally usable. An example hereof is the one-dimensional model of Balbi et al. (2009), which is derived from an earlier three-dimensional model (Balbi et al., 2007).

Although simpler models can be less computationally demanding and easier to operate, the underlying assumptions make them less general, thus limiting the trust of end users in their results (Simeoni, 2016; Sullivan, 2009a). The lack of a general wildfire theory as a basis for these assumptions forms another major issue (see Section 2.1.7). Finney et al. (2013) argue that many of the assumptions (of simplified, but also of detailed models) are made without any experimental basis. The dominant role of radiation in many of these models and the ignition process of fuel particles (e.g. via a critical temperature) are examples thereof.

3.4 (Quasi-)empirical models

(Quasi-)empirical models are derived from experimental data, using statistical methods. These models emerged from the need of wildfire managers to quickly determine the fire behaviour, which could not be fulfilled by the (first) physically-based models (Keane, 2015; Sullivan, 2009b). The purpose of the (quasi-)empirical models is to provide the key characteristics of an advancing or head fire. Hence, these models are traditionally one-dimensional (Sullivan, 2009b). The fire characteristics of interest are mostly the ROS R [m s^{-1}] and the fire line intensity I [kW m^{-1}], due to their imposed danger on the fire fighters. They are related by (Byram, 1959):

$$I = h\dot{W}R, \quad (3.1)$$

with h [kJ kg^{-1}] the fuel's heat content and \dot{W} [kg m^{-2}] the fuel mass consumed per unit area. The formulation of (quasi-)empirical models is a two-step process. Firstly, the environmental variables with the most influence on fire behaviour have to be identified. Secondly, the statistical relation between the key environmental and fire properties has to be established. Concerning the first step, there is a consensus that the dominant variables are primarily wind and slope, and to a lesser extent the FMC of the fine fuels (see also Section 2.1). The formulation of the statistical models—with often complex, non-linear dependencies on these and other variables—is, however, much less uniform.

Model structures

Most (quasi-)empirical models assume a steady ROS, so that one set of environmental conditions results in a unique ROS value. Due to the lack of a general experimental methodology, comparing these models is not trivial. First of all, a distinction can be made between the empirical models, that are of a purely statistical nature, and quasi-empirical models, that utilise some sort of physical framework. Sullivan (2009b) compares some of these models by their functional relationships between the ROS and two main variables, namely the wind and FMC. The wind conditions varied greatly among the considered models in this paper (with the majority of the wind speeds being rather low), as did the wind measurements (e.g. at 2 m or 10 m above the ground). Nevertheless, all of them used either a power law or an

exponential function to relate the wind speed to the ROS. Sullivan (2009b) concludes that the choice of this function depends on the wind speed range and on whether zero wind speed was included. In the latter case, the model assumes the same fire behaviour mechanisms irrespective of the wind speed. This is not physically consistent, because different heat transfer processes dominate at high (wind-driven) as compared to low (plume dominated) wind speeds (see Section 2.1.5). Sullivan (2009b) argues that the use of a threshold wind speed includes physical knowledge in the model, making it quasi-empirical. This threshold wind speed is defined by Cheney et al. (1998) as the wind speed at which fires spread forward consistently, and is estimated to be 1.39 m s^{-1} (10 m above ground) for open grasslands. Moreover, model fitting at low wind speeds can result in predicted ROS values that increase more rapidly than when assuming a linear relationship between the wind speed and ROS. In wind-driven fires this behaviour would be not physical (Beer, 1991). It is interesting to note that the models reviewed by Sullivan (2009b), with experimental wind speed ranges above the proposed threshold of Cheney et al. (1998), result in a near-linear wind speed function, confirming the linear relationship found by physically-based models (Sullivan, 2009a).

The functional forms which relate the FMC to the ROS vary substantially between the models. Sullivan (2009b) concludes that this could result from the different modelling approaches of the wind function, but could also—and maybe more likely—reflect differences between fuel types. Finally, it should be noted that most of the models combine the wind and FMC functions via multiplication.

Performance

An advantage of the (quasi-)empirical models is that they give statistical predictions of fire behaviour for a certain set of environmental conditions (Simeoni, 2016). This also points out their major limitation, i.e. the limited range of conditions under which they can operate as they cannot be reliably extrapolated beyond it. Hence, their performance is highly dependent on the experimental data. These data can be collected from experimental fires or well-documented wildfires (Simeoni, 2016). The former, for which has been opted most frequently (Sullivan, 2009b), can be conducted in either laboratory or field conditions. Lab-scale experiments are cheaper and easier to carry out but they are limited to small scales and controlled environments. Hence, the assumption that their findings can be upscaled to large-scale environmental conditions is questionable (see e.g. the work of Cheney et al. (1993)). Nevertheless, due to their simplicity and ease of use, (quasi-)empirical models have been used in most operational wildfire management tools for calculating the forward ROS of wildfires, especially in regions with relatively homogeneous environmental conditions. Some examples include the empirical Fire Danger Rating Systems and the Red Book in Australia (McArthur, 1965, 1967; Noble et al., 1980; Sneeuwjagt and Peet, 1985)—though the former are now obsolete as they have been replaced by more accurate models (Cruz et al., 2015)—and the Canadian Forest Fire Behavior Prediction System (FBP) (Forestry Canada Fire Danger

Group, 1992). The quasi-empirical model of Rothermel (1972), developed in the USA, has been by far the most influential, as it is included in the widely used fire behaviour calculation system BEHAVE (Andrews, 1986). Moreover, it is used in many simulation models (Section 3.5), including FARSITE, which is generally considered to be the most complete and accurate wildfire simulator (Papadopoulos and Pavlidou, 2011; Pastor et al., 2003; Sullivan, 2009c).

Rothermel's model

In the quasi-empirical wildfire model proposed by Rothermel (1972), the forward ROS R [m min^{-1}] of a surface fire is expressed as the ratio of the heat flux received by the unburnt fuel to the heat required for sustained fire spread. This ratio is based on the equations derived from a thermal balance by Frandsen (1971), and has been modified over the years (e.g. by Albini (1976)). It is given by:

$$R = \frac{I_r \xi (1 + \phi_w + \phi_s)}{\rho_b \epsilon Q_{ig}} \quad (3.2)$$

where I_r [$\text{kJ m}^{-2} \text{min}^{-1}$] is the reaction intensity, ξ [-] is the propagating flux ratio (i.e. the fraction of the heat of combustion reaching the surrounding fuel under no-wind, no-slope conditions), ϕ_w [-] and ϕ_s [-] are the wind and slope correction factors, respectively, ρ_b [kg m^{-3}] is the fuel bulk density, ϵ [-] is the effective heating number defining the amount of fuel which is available to sustain fire spread, and Q_{ig} [kJ kg^{-1}] is the heat needed to bring the fuel to ignition. The reaction intensity I_r depends on some key fuel parameters (see Section 2.1.3), namely the FMC, surface-to-volume-ratio σ [m^{-1}] of the fuel particles, packing ratio β [-], and mineral fraction. The correction factors for wind and slope are given by:

$$\phi_w = c U^b \quad (3.3a)$$

$$\phi_s = a \tan^2 \gamma_s, \quad (3.3b)$$

where U [m s^{-1}] is the midflame wind speed, γ_s [-] is the slope angle in radians, and $a(\sigma, \beta)$, $b(\sigma, \beta)$, and $c(\sigma, \beta)$ are functions of the surface-to-volume-ratio and packing ratio. The use of the latter functions can lead to a ROS larger than the wind speed, so the maximal wind speed correction factor is artificially limited by a critical wind speed. Note that the basic model by Rothermel (1972) only calculates the maximum fire spread and assumes the wind to be blowing directly uphill. However, this has been extended to scenarios where wind and aspect do not align and for any other direction than that of the head fire (Albini, 1976; Andrews, 1986; Finney, 2004). Using the ROS from Eq. (3.2), the fire line intensity I [kW m^{-1}] can be calculated as:

$$I = \frac{12.61R}{60\sigma}, \quad (3.4)$$

which is a reformulation of Eq. (3.1) by Wilson (1980).

3.5 Simulation and analogue models

3.5.1 Landscape level simulations

Over the last two decades, the further development of remote sensing and GIS applications, along with the rise of (parallel) computers, have created new opportunities for wildfire modelling. During this period, the focus has shifted from building fire behaviour models (as discussed in Sections 3.3 and 3.4) to the simulation of fire spread across a landscape, typically represented by one or more GIS layers (Sullivan, 2009c). This can either be achieved by using existing fire behaviour models as submodels of a simulation model or by using a mathematical construct with an analogous dynamical behaviour (see Section 3.2.2).

As was mentioned in Section 3.2, most operational simulators use (quasi-)empirical fire behaviour models that predict a steady ROS in the head fire direction (Section 3.4). Hence, in order to run simulations across landscapes, the simulation model needs to extend this formulation to all directions, while correcting for varying environmental conditions. Often this is done by assuming local homogeneity in time and space (Trunfio et al., 2011).

Moreover, extra submodels can be included for modelling of, for example, the acceleration from ignition and different fire phenomena (see Section 2.1.6). This requires special care, as the different submodels can rely on different spread mechanisms and assumptions, thus complicating their coupling. Yet, a chain is only as strong as its weakest link. Indeed, even simulations that extend and couple their fire behaviour submodels “perfectly”, critically rely on the quality and assumptions of these submodels and used input data (Sullivan, 2009c). The latter will probably remain the biggest limitation on the accuracy of fire models, due to the costs related to collecting high-quality, high-resolution data (Sullivan, 2009c).

3.5.2 Wind-slope correction

It should be clear that wind and slope play a crucial role in wildfire behaviour and modelling. Their effect is mostly modelled by means of correction factors, which can be based on (quasi-)empirical knowledge or more physically based assumptions. Sharples (2008) reviews some of these correction factors and summarizes their similarities (Table 3.2). He subdivides them into two classes, namely scalar and vector methods. The former are included in one-dimensional fire behaviour models and correct the ROS in a specified (head fire) direction. They can be introduced in a multiplicative or additive way. In the former, the wind-induced ROS (R_w)—which already takes into account the effect of the wind vector (\mathbf{w})—is adjusted by multiplying it with a slope correction factor (σ_s), which depends on the slope angle (γ_s), wind direction (θ_w) and the topographic aspect (γ_a). The additive methods, on the other hand, add a term correcting for both wind and slope to a base ROS (R_0); Rothermel’s model is an example hereof.

Simulation models extend the scalar correction methods to vectors by taking into account the directional effects of wind and slope. The multiplicative approach is vectorised by multiplying the uphill component of the wind-induced ROS vector (\mathbf{R}_w) with the slope correction factor (σ_s), using a slope correction matrix (Σ_s). This approach has the drawback that it ignores the slope effect when the wind vector is aligned perpendicularly to the slope. The additive method is vectorised by means of an equivalent wind vector (\mathbf{U}_{ws}), which is the sum of the wind vector and a vector accounting for the slope effect. This equivalent wind vector is added to a unit vector ($\hat{\mathbf{v}}$) in the direction of the equivalent wind or normal to the fire front.

Table 3.2: General framework for wind-slope correction Sharples (2008).

	Scalar	Vector
Multiplicative	$R_w \sigma_s(\gamma_s, \theta_w, \gamma_a)$	$\mathbf{R}_w \Sigma_s(\gamma_a, \gamma_s)$
Additive	$R_0 (1 + \phi_{ws}(\ \mathbf{w}\ , \theta_w, \gamma_s, \gamma_a))$	$R_0 (\hat{\mathbf{v}} + \mathbf{U}_{ws})$

3.5.3 Simulation models

The generation of a two-dimensional fire spread simulation from a one-dimensional fire behaviour model involves two steps (Sullivan, 2009c):

1. the representation of the fire perimeter;
2. the propagation of this fire perimeter with some kind of propagation algorithm.

It is obvious that these steps are linked. Generally, the fire front is idealised as the interface between the burnt and unburnt areas. There are three main ways to represent a fire perimeter (Mallet et al., 2009; Sullivan, 2009c), being so-called level set functions, vector, and raster representations. These can be placed on a spectrum ranging from continuous to discrete representations (Figure 3.3). *Level set functions* are continuous functions in time and space. Cutting them by a plane parallel to the surface at a given time t , defines the fire perimeter implicitly as the zero-isoline of the transect, in such a way that points with negative function values comprise the burnt region and vice versa (Mallet et al., 2009; Osher and Fedkiw, 2003). *Vector* representations discretise the fire perimeter into a limited number of vertices, which move freely in space according to the propagation algorithm. *Rasters* are the most discrete representations, in which the landscape is discretised in a regular or irregular grid. Its cells comprise a certain area with homogeneous conditions and the fire perimeter constitutes of a group of contiguous cells. It should be noted that there are also vector-raster hybrids (e.g. Clark et al. (2004); Peterson et al. (2009); Trunfio et al. (2011)), along with some other, less frequently used representations (e.g. networks (Hajian et al., 2016)).

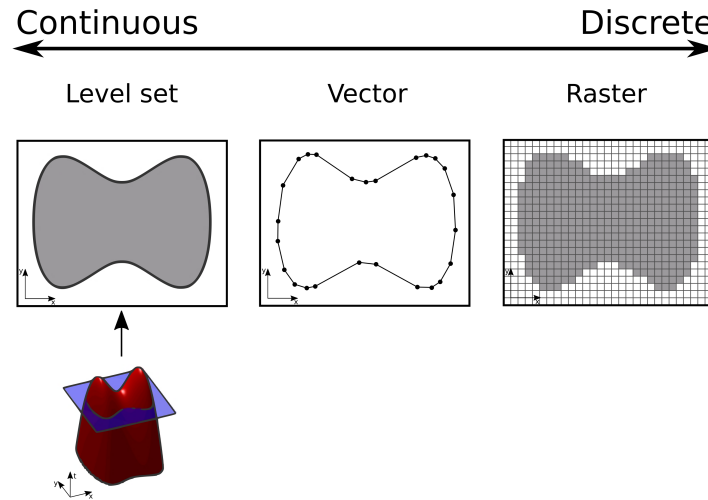


Figure 3.3: Schematic overview of the three main fire perimeter representations, adapted from Alexandrov (2004).

Vector-based simulation

Two main propagation methods are used with the vector representation. The first one is based on *Huygen's wavelet principle* (Anderson et al., 1982). This method considers each point of a fire perimeter (mostly represented as vector) as a source of ignition (Figure 3.4(a)). From each of these points, a hypothetical fire spreads during a time step Δt , after which the new fire perimeter is defined as the hull of the individual perimeters. The hypothetical fires are assumed to ignite independently and under local homogeneous conditions. Their perimeter shape and direction are derived from a predetermined shape template—with an eccentricity that depends on the prevailing wind speed and slope (Alexander, 1985)—and the ROS of the head fire, calculated using a fire behaviour submodel. The backing ROS (i.e. the ROS in the opposite direction of the head fire) can be derived implicitly from the fire shape or can be calculated independently (Finney, 2004).

Although the choice of the shape template is not physically underpinned (Fendell and Wolff, 2001), it is often assumed to be an ellipse, due to its relatively straightforward mathematics (Van Wagner, 1969) and the observation that the resulting shapes reasonably fit real fire shapes (Green, 1983). Richards (1990, 1995) and Knight and Coleman (1993) developed analytical equations for this approach. Figure 3.4(b) shows the elliptic template used by Richards (1990), where a is the flanking ROS, and $c + b = R$, with R the ROS of the head fire.

The wave propagation method does not distinguish burnt from unburnt areas, as the fire perimeter vertices move freely and independently across the landscape. Hence, computationally expensive algorithms are required to account for topological changes, in order to avoid meaningless spread across already burnt areas (Finney, 2004). Moreover, the assumption of

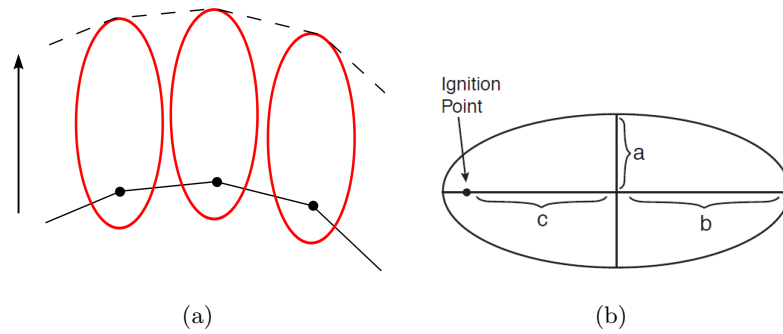


Figure 3.4: Schematic representation of Huygen’s fire perimeter propagation (a) with the elliptic shape template (b), adapted from Sullivan (2009c) and Richards (1990). The fire perimeter at time step t (solid line) is expanded to a new perimeter (dashed) at time $t + \Delta t$. The arrow indicates the forward ROS direction.

independent hypothetical fires ignores the effects of the fire line shape on its spreading behaviour. Still, despite these drawbacks, Huygen’s wavelet propagation method has proven its usefulness, as it has been incorporated into a number of operational fire simulators, including FARSITE (Finney, 2004), Prometheus (Tymstra et al., 2010), and PHOENIX Rapidfire (Tolhurst et al., 2008), developed for the USA, Canada, and Australia, respectively. These simulators are built upon the extension of a national quasi-empirical fire behaviour calculation system—BEHAVE (Andrews, 1986), the FBP (Forestry Canada Fire Danger Group, 1992), and the Australian Fire Spread Meters (Cheney and Sullivan, 2008; McArthur, 1965; Noble et al., 1980), respectively—to landscape-level fire spread simulators. An output example is given in Figure 3.5.

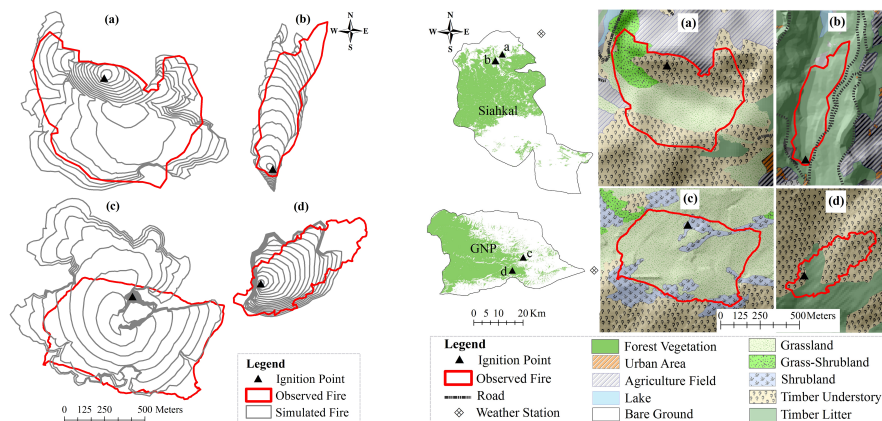


Figure 3.5: An example of fire perimeters obtained with FARSITE, compared to the observed ones of four small (< 60 ha) fires in Iran (Jahdi et al., 2015).

A second vector-based propagation method worth mentioning is Forefire (Filippi et al., 2009b, 2014a), which is a *discrete event front tracking* algorithm. This method considers the vertices of the fire perimeter as agents with three state variables, namely their positions, the environmental conditions at their positions, and a propagation vector. The latter is pointed outward the perimeter and directed along the bisector of the angle with the two neighbouring agents. Forefire does not rely on a predefined shape template, since it uses a simple physically based fire behaviour submodel (Balbi et al., 2007), which is able to calculate the ROS in all directions (and not only in the head fire direction). As opposed to Huygen’s wave propagation method, the states of the agents are changed during discrete events which are scheduled at specific times and ranked in a global time table. This approach treats time as a continuous variable and results in an asynchronous movement of the vertices. The driving events are:

1. travelling a maximum (quantum) distance, which defines the maximum resolution of the simulation;
2. collisions, i.e. movement into a different area or within a minimum distance of another agent.

Asynchronous vertex displacement avoids the re-calculation of steady, slowly moving perimeter parts, due to the constraint on the time step by the fast moving head fire. Moreover, the crossing algorithms only have to be applied for the agents that are triggered by collision. Hence, this approach is especially computationally advantageous in very heterogeneous conditions with a varying ROS along the fire perimeter. An example is presented in Figure 3.6.

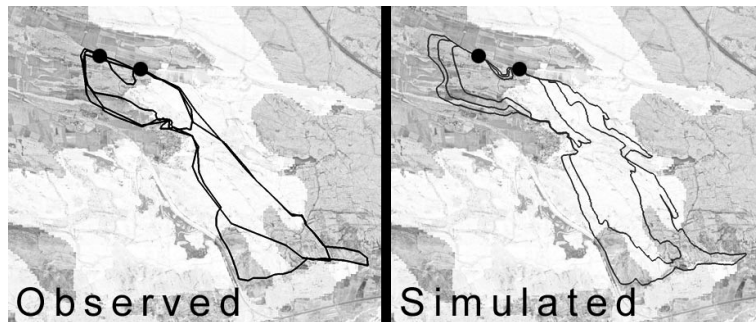


Figure 3.6: An example of fire perimeters obtained with Forefire, compared to observed ones of a fire burning around 800ha in France (Filippi et al., 2009b). The black dots represent the ignition points at 9h40; the perimeters are recorded at 12h, 14h30 and 16h.

Raster-based simulation

Raster simulations are generally based on *near-neighbour proximity* of cellular automata (CA) (von Neumann, 1966). The fire is defined by a finite number of cell states, which can be as simple as “unburnt”, “burning” or “burnt” (Sullivan, 2009c). A cell’s state is updated at discrete time steps, based on the states of the cells in its neighbourhood at the previous time step, using a simple set of rules, which are derived from the used fire behaviour model(s). There are several approaches for implementing and extending CAs (Sullivan, 2009c). Green (1983) identifies two main methods, i.e. cell contact and (heat) accumulation (Figure 3.7).

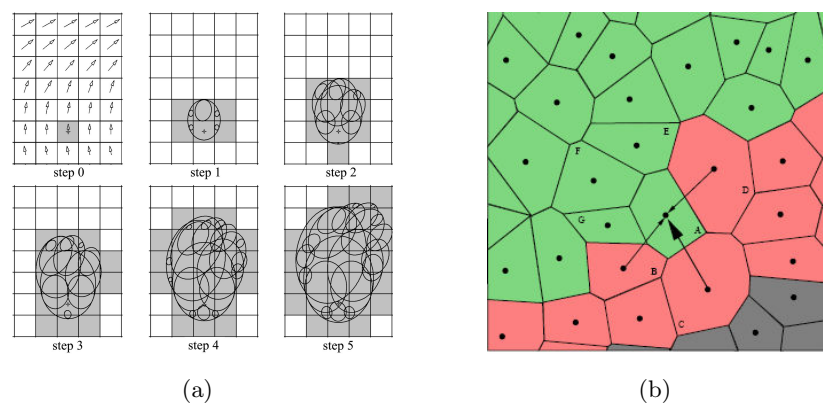


Figure 3.7: Examples of the two main approaches of perimeter propagation based on near-neighbour proximity. In (a), the cell contact method, the shading indicates the burning cells, the ellipses show the calculated fire shapes, and the arrows represent the wind field (Trunfio et al., 2011). In (b), the accumulation method, the green, red and black cells represent unburnt, burning and burnt cells, respectively, while the arrows indicate the heat received by cell A from its neighbours (Johnston et al., 2006).

Kourtz and O’Regan (1971) laid the basis of the cell contact method, in which a fire behaviour model and a shape template are used to calculate the time of arrival of the flame front moving from a burning cell to its unburnt neighbours. An unburnt cell ignites when it is reached by the fire front. This approach is actually very similar to the vector wave propagation, but has two main differences. Firstly, the positions of the new ignition sources are fixed within the adjacent cells. Secondly, the cell states explicitly indicate which cells are burning or burnt. Two notable examples of this approach are IGNITE (Green et al., 1990) and FireStation (Lopes et al., 2002). An example by Trunfio et al. (2011), in which the ignition source is not restricted to the cell centre (as opposed to the previously mentioned examples), is shown schematically in Figure 3.7(a). A weakness of the cell contact approach is that fire spread is only determined by the neighbour with the fastest ROS (Green, 1983).

The accumulation method, on the contrary, also accounts for the cumulative effect of multiple neighbours, because it considers a cell to be ignited when a critical threshold of an accumulated variable (e.g. a virtual heat) is reached (Green, 1983). This method is illustrated schematically in Figure 3.7(b). Hfire (Peterson et al., 2009) is a notable simulator using this approach. The advantage of the raster-based methods over their vector-based counterparts is that they do not allow fire spread across burnt areas. So here is no need for crossover algorithms, as such increasing the computational efficiency. A major drawback, however, is the possible distortion of the fire shape, due to the limited number of spread directions, imposed by the geometry of the grid (Ball and Guertin, 1992; French, 1992; Finney, 2004; Peterson et al., 2009). Several ways to tackle this problem have been proposed over the years, e.g. the use of larger neighbourhoods (Finney, 2002), irregular grids (Johnston et al., 2006), freely definable ignition points in the cells (Trunfio et al., 2011) and optimisation algorithms (Ghisu et al., 2015). However, since most of these models rely on Rothermel’s model for their fire behaviour calculations, they share the same basis as FARSITE and often result in similar predictions (Figure 3.8).

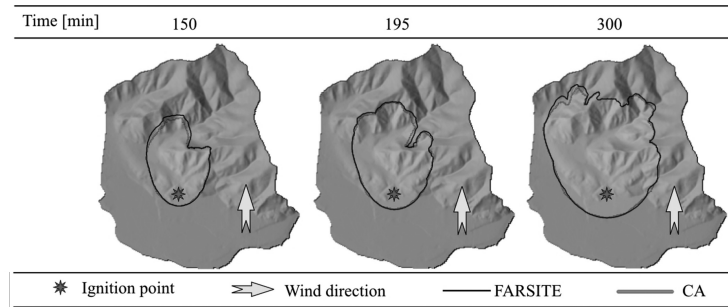


Figure 3.8: An example of fire perimeters obtained by the cell contact model proposed by Trunfio et al. (2011), compared to the ones obtained with FARSITE.

Level set methods

Quite recently, level set methods (Osher and Fedkiw, 2003) have been used to simulate fire front propagation (Mallet et al., 2009; Mandel et al., 2009). These methods use an Eulerian approach, as opposed to the Lagrangian vector-based methods. The fire perimeter is represented as a closed curve Γ . The basic idea is to let Γ evolve using a so-called level set function φ , such that

$$\Gamma(t) = \{x \in \mathbb{R}^2 \mid \varphi(x, t) = 0\}. \quad (3.5)$$

In practice, the signed distance from the fire front Γ is used as level set function, i.e. points x for which $\varphi(x, t)$ lie outside the fire perimeter (Figure 3.9). The level set function is governed by

$$\frac{\partial \varphi}{\partial t} + S \|\nabla \varphi\| = 0, \quad (3.6)$$

where S is the ROS normal to the fire front (Figure 3.9). The initial condition of Eq. (3.6) is derived from the observed fire perimeter at $t = 0$, by calculating the distance of every point to the fire front. The resulting initial-value problem can be solved using a suitable numerical scheme. A more detailed description of this approach can be found in Mallet et al. (2009) and Osher and Fedkiw (2003). Its main advantage is its ease to deal with topological changes (e.g. front mergers), while still resulting in physically meaningful fire shapes (Mallet et al., 2009). This comes at the cost of using the level set function, which has one extra dimension than the fire front. Moreover, retrieving the initial value of φ is a computationally expensive task (Hilton et al., 2015). These issues can, however, be dealt with by efficient algorithms (e.g. Adalsteinsson and Sethian (1995); Sethian (1996)). The main drawbacks of this method are caused by the numerical schemes that can induce numerical dispersion and are not proven to converge for every problem (Mallet et al., 2009; Mandel et al., 2009). The level set method is implemented in SFIRE (Mandel et al., 2009), which will be discussed in Section 3.5.4.

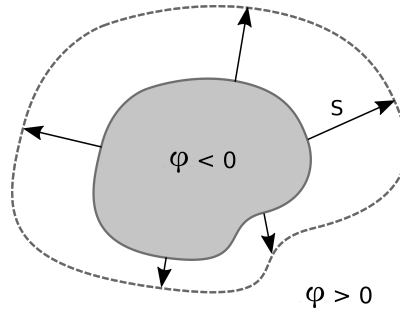


Figure 3.9: A schematic representation of the level set method. The grey area represents the area enclosed by the current fire perimeter.

3.5.4 Coupled fire-atmosphere models

The majority of the simulators discussed in preceding sections only includes one-way interaction between wildfire and environment, i.e. the fire spread is described using a predefined set of environmental conditions. This is often accomplished using a predefined (elliptical) fire shape, which is an approximation of the small-scale fire-atmosphere interactions (Clark et al., 2004; Sullivan, 2009c). Wildfires can, however, have a strong influence on the local weather (see Section 2.1). Hence, excluding these fire-atmosphere feedback processes is known to result in a lower model accuracy (in e.g. FARSITE), especially for extreme fire behaviours, such as high-intensity, plume-dominated fires (Finney, 2004; Pastor et al., 2003). To overcome this shortcoming, several authors propose to couple wildfire models and CFD-based weather prediction models. In addition to the standard ROS prediction, this requires the specification of heat and mass fluxes that influence the atmospheric behaviour and the burning time of the fuel. Compared to the detailed physical wildfire behaviour models, this approach is

computationally more efficient. This follows from the separation of large-scale local atmospheric conditions and the smaller-scale fire front processes—which are modelled using the simple physically based or (quasi-)empirical models (Gollner et al., 2015). However, it has to be noted that the coupling with (quasi-)empirical fire behaviour models is not evident given their assumptions, which results in having to rely on highly subjective parameters (Gollner et al., 2015). Some notable examples of coupled fire-atmosphere models are WRF-Fire (Coen et al., 2013) and WRF-SFIRE (Mandel et al., 2011, 2014), which are both based on Rothermel’s fire behaviour model, and MESO-NH/ForeFire (Filippi et al., 2009a), which is based on the quasi-physical model by Balbi et al. (2009) (Figure 3.10).



Figure 3.10: An example of observed (red) and simulated perimeters of a fire of 25 ha in Corsica (Filippi et al., 2011). The blue and green perimeters are simulations of MESO-NH/ForeFire at $t = 50$ min and 240 min, respectively; the yellow perimeter results from the uncoupled model (ForeFire) at $t = 240$ min.

3.5.5 Analogue models

A different approach in wildfire simulation is the use of so-called analogue models. The common thread of these models is that they evolve dynamics that share similarities with wildfire spread (Frigg and Hartmann, 2012; Sullivan, 2009c), but are not based on fire behaviour submodels. Many examples are presented in Sullivan (2009c), including several CA-based models, artificial neural networks, Markov chains and reaction-diffusion models. These models can provide a different (theoretical) perspective on the subject (e.g. insights in critical behaviour, self-organisation and the fractal character of the fire line), but hardly find their way into practical tools. Moreover, analogues intended for operational use are hard to calibrate, since they are intrinsically empirical and thus rely on experimental or historical data (Sullivan, 2009c).

Two examples of stochastic simulators—with an intended practical use—are the CA model of Alexandridis et al. (2008, 2011) (Figure 3.11) and the percolation model EMBYR (Hargrove et al., 2000). Table 3.3 provides a brief summary of the main (dis)advantages of the discussed modelling approaches.

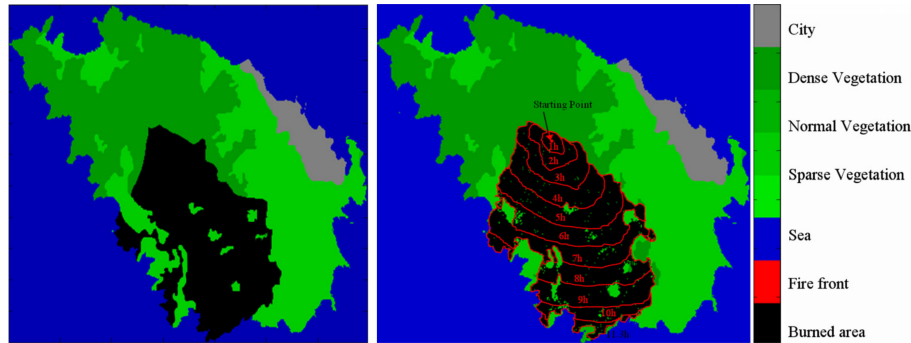


Figure 3.11: An example of burnt areas of a fire in Spetse, Greece, obtained from observation (left) and simulation (right), using a CA (Alexandridis et al., 2008)

Table 3.3: Main advantages and disadvantages of wildfire of different simulation methods.

Model type	Advantages	Disadvantages
Vector-based	<ul style="list-style-type: none"> realistic fire shapes 	<ul style="list-style-type: none"> difficulties with topological changes
Raster-based	<ul style="list-style-type: none"> computationally efficient 	<ul style="list-style-type: none"> fire shape distortions
Level set method	<ul style="list-style-type: none"> easily deals with topological changes realistic fire shapes computationally efficient 	<ul style="list-style-type: none"> stability and convergence of numerical schemes
Coupled fire-atmosphere	<ul style="list-style-type: none"> includes atmospheric feedbacks 	<ul style="list-style-type: none"> subjective coupling parameters computationally demanding
Analogues	<ul style="list-style-type: none"> often stochastic 	<ul style="list-style-type: none"> difficult calibration

3.6 Uncertainty in wildfire modelling and simulation

From the general description presented in Chapter 2, it is clear that a wildfire is an extremely variable, nonlinear and turbulent phenomenon. Moreover, the environmental data can be of a very coarse (spatio-temporal) resolution as compared to their variability. Therefore, the study and management of wildfires entails a lot of uncertainties (Thompson and Calkin, 2011). Yet, the vast majority of fire behaviour models and simulators are deterministic in nature and therefore do not account for uncertainty. In recent years, there is an increasing interest in addressing this issue (Cruz and Alexander, 2013; Thompson and Calkin, 2011), mainly using ensemble methods and data assimilation.

Ensemble methods—which are also applied for meteorological forecasts (Sivillo et al., 1997)—incorporate stochasticity in the deterministic simulators by considering some of the input variables as random variables with a known distribution. The resulting model is used for a Monte Carlo simulation. Examples hereof are presented in, amongst others, Cruz (2010), Finney et al. (2011), and Hajian et al. (2016). Since no stochasticity is implemented in the deterministic model structure, the output of every single Monte Carlo simulation is still considered to provide the best prediction under the given set of conditions. Hence, this approach does not improve the model accuracy, but it does provide the possibility to perform a quantitative risk assessment (Cruz, 2010; Finney et al., 2011).

Data assimilation methods, on the other hand, go one step further. The aim of these methods is to increase the simulation accuracy, by repeatedly incorporating new observation data into a running model and adjusting its simulation results (Cruz and Alexander, 2013). Of course, while doing this, the uncertainty of the assimilated data has to be taken into account, for instance using Ensemble Kalman Filters (Srivastava et al., 2016).

3.7 Wildfire modelling in Belgium

Due to its high population density and long history of cultivating and building upon available space, Belgium lacks vast wildlands. Consequently, wildfires are bounded to relatively small areas and can quickly reach the WUI, thus imposing a threat to neighbouring communities. Despite this risk, little research has been undertaken on (the modelling of) wildfires in Belgium. Hence, fuel classification and model parametrisation for the local vegetation is still lacking. Moreover, few data are available on historical wildfires in Belgium; only fairly big (> 100 ha), recent (after 2011) wildfires have been documented in sufficient detail to allow for testing of real-time wildfire simulators.

The dissertation by Depicker et al. (2016) focuses on the development of a wildfire risk map for Belgium based on recorded historical ignitions (Figure 2.7(a)). Several risk maps are proposed, one of which is based on a logistic regression using the population density, land cover class and sandy soil texture as predictors (Figure 3.12). Depicker et al. (2016) subsequently use this risk map as a basis a CA-based model, which is tested on one historical wildfire. In the next chapters, we will continue along this path.

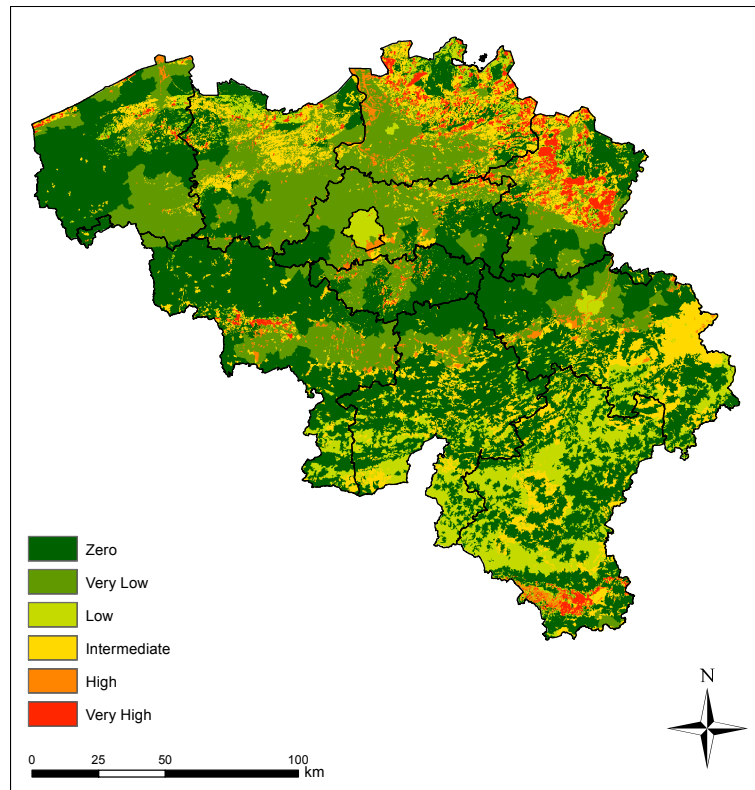


Figure 3.12: A wildfire risk map for Belgium, based on logistic regression (Depicker et al., 2016).

CHAPTER 4

Study areas and model description

After the general overview of wildfire models (Chapter 3), it is time to put these models into practice. The aim of the present and the next chapters is to evaluate a number of available wildfire simulators in an operational context for Belgium. This evaluation is done for seven recent fires, which are discussed in Section 4.1. Section 4.2 will detail on the selected models and their settings.

4.1 Case description

4.1.1 Overview

The basis of this dissertation is a dataset of registered fires, which was provided by the European Forest Fire Information System (EFFIS). The latter is maintained by the Joint Research Centre (JRC) of the European Commission (EC). This dataset consists of seven fires that occurred between 2011 and 2015 in Belgium and the Netherlands (Table 4.1 and Figure 4.1). Based on MODIS satellite imagery and the CORINE map, the following data were available:

1. the start date of the fire;
2. the recorded perimeter in vector format;
3. fuel classes and canopy cover in raster format;
4. elevation, slope and aspect in raster format.

The spatial resolution of all the raster data is 100 m. In the remainder of this section a summary of the selected wildfires is given; a complete overview of their features is presented in Figures 4.9 through 4.22 at the end of this chapter.

Table 4.1: Overview of the wildfire dataset.

Case	Location	Year	Area (ha)	
			EFFIS	Reports
1	High Fens	2011	1399	1365 ^a
2	Kalmthout Heath	2011	555	448 ^a
3	The Hoge Veluwe National Park	2014	396	350 ^a
4	Meeuwen-Gruitrode	2011	226	350 ^b
5	Büllingen	2015	80	-
6	Butgenbach	2015	29	-
7	Oldebroek Heath	2015	22	-

^a fire report, ^b news report

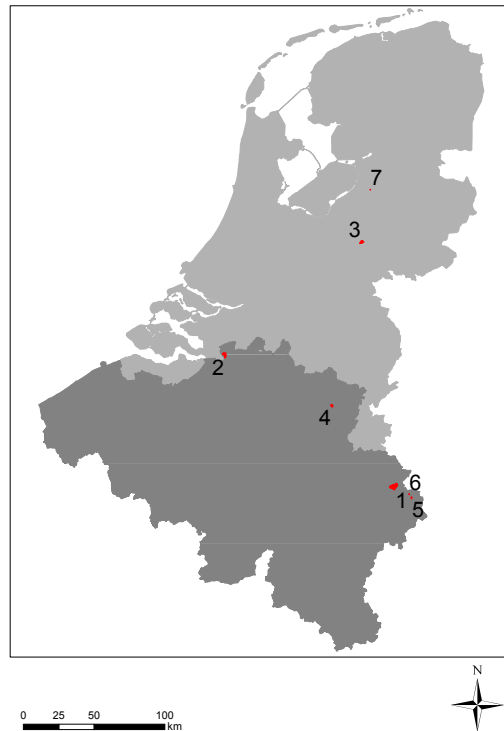


Figure 4.1: Locations of the wildfires in Belgium (1,2,4,5,6; dark) and the Netherlands (3,7; light).

4.1.2 Wildfire perimeter

The final wildfire perimeters were determined on the basis of MODIS imagery with a spatial resolution of 250 m (Joint Research Centre, 2015). These images are updated two times a day and analysed by a combination of automatic and manual processes in EFFIS (Joint Research

Centre, 2015). The perimeters are accompanied by a start and end date, which are the times of the first and last update, respectively. However, these do not necessarily correspond to the actual ignition and extinction times (Joint Research Centre, 2015). An example hereof is illustrated in Figure 4.2; the perimeters of Case 1 were updated until 1 May 2011, although the wildfire was reportedly under control 27 April 2011. For large wildfires (Cases 1–4) a fire or news report could be found that documents the actual time of first sight and/or the time at which the wildfire was under control. Furthermore, these reports also provide (approximate) observations of the total burnt area (Table 4.1).

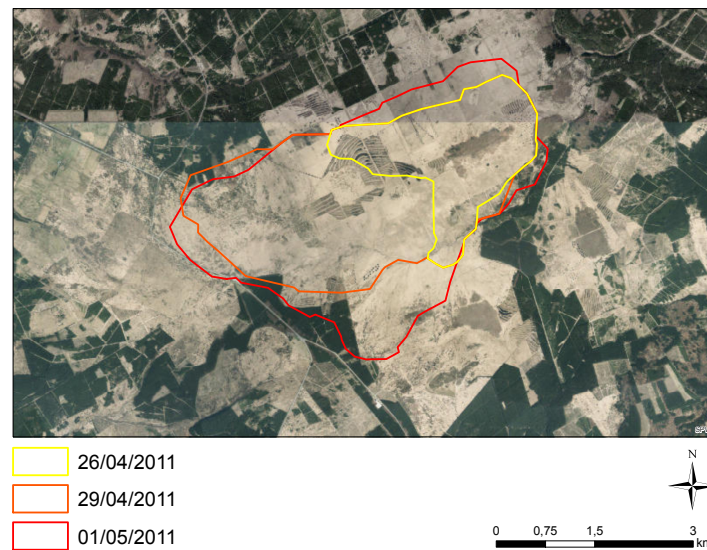


Figure 4.2: Three recorded perimeters of Case 1.

For Cases 1 and 2, the two biggest wildfires in the dataset, a more detailed perimeter was available, based on high-resolution satellite imagery. This enabled an accuracy check of the EFFIS perimeters (Table 4.2 and Figure 4.3). In both cases, the EFFIS perimeter overestimates the actual burnt area. Moreover, small unburnt enclaves inside the fire perimeter are not mapped, which is a known limit of the EFFIS data (Joint Research Centre, 2015). Some burnt areas are, however, still left unaccounted for (approximately 10% of the reported burnt area). The maximal distance between the unregistered perimeter part and the EFFIS perimeter is 536 m and 454 m for Case 1 and 2, respectively. In conclusion, the coarse resolution of the MODIS imagery (approximately 40 ha) leads to significant errors on the recorded perimeter. The impact of this discrepancy is expected to be relatively larger for the other fires as these are smaller. Especially the quality of the two smallest fire perimeters is highly questionable, since their burnt area is lower than the resolution (Joint Research Centre, 2015). Note that most Belgian wildfires are smaller than the resolvable area given by this resolution, hence the reliability of this method for wildfire perimeter registration is limited in the Belgian context.

Table 4.2: Comparison of the wildfire perimeters registered by EFFIS and those in the fire reports of Cases 1 and 2. The values are expressed as area percentages of the envelope of both perimeters.

	Case 1	Case 2
True +	80.6	66.1
False +	10.8	25.8
False –	8.6	8.1

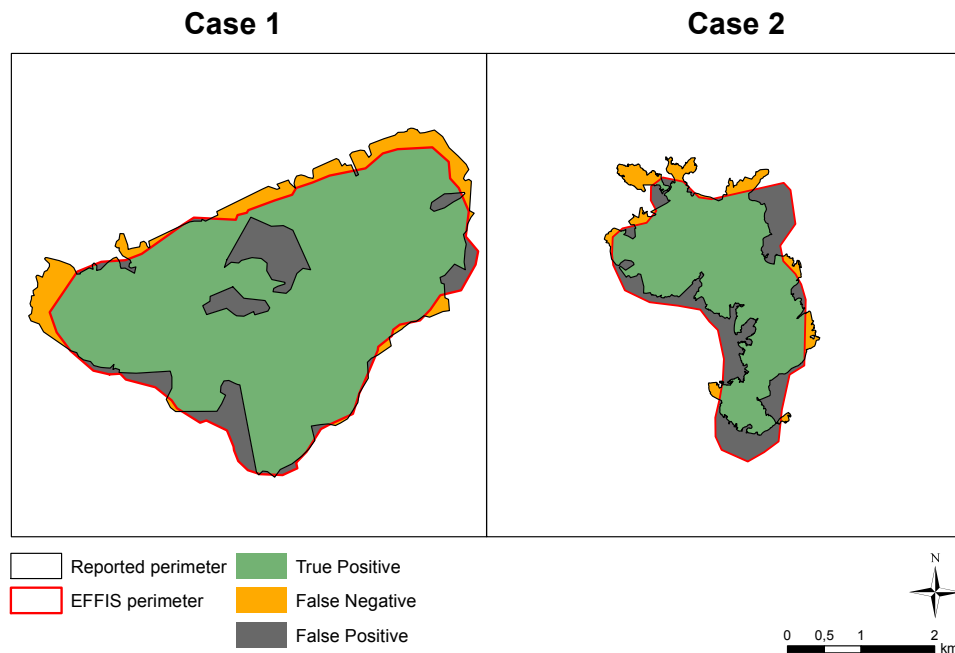


Figure 4.3: Comparison of the wildfire perimeters registered by EFFIS and those in the fire reports of Cases 1 and 2.

4.1.3 Fuel complex

The fuel maps in Figures 4.9 to 4.15 originate from the JRC FUELMAP project (Joint Research Centre, 2011). This project aimed at the development of a unified pan-European fuel mapping and classification system, by combining different (remote sensing) datasets, which resulted in 42 fuel classes—from here referred to as JRC classes—at a spatial resolution of 250 m (Toukiloglou et al., 2013). The JRC also provided a table to convert these classes into the USDA National Forest Fire Laboratory (NFFL) fuel classes (Anderson, 1982), which are used by most wildfire simulators. The reader is referred to Appendix A for a full description of these classifications.

Figure 4.4 presents the distribution of fuel classes according to the JRC FUELMAP (horizontal axis) and NFFL (color scheme) classification, within the wildfire perimeters. Note that all cases are dominated by the same two JRC classes, namely classes 1 and 8, which represent peat bogs and temperate moors and heathlands, respectively. This prevalence does not come as a surprise, since these fuels can dry out very fast, which is necessary to sustain a big wildfire in the moist climate of Belgium. Moreover, temperate heathlands in Belgium are being colonised by the invasive grass species *Molinia caerulea* (Marrs et al., 2004). These grasses do not only cause extensive fuel built-up, but they also thrive after a wildfire, as was the case in the Kalmthout Heath (Case 2) after the fires in 1996 and 1997 (Jacquemyn et al., 2005).

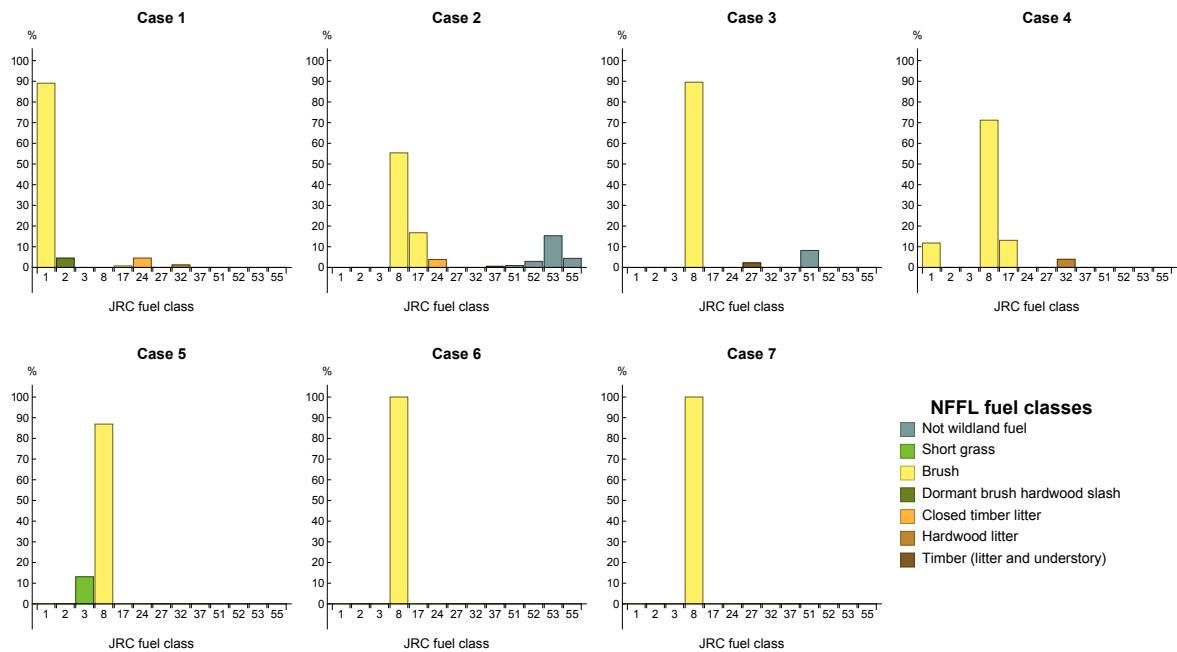


Figure 4.4: Overview of fuel classes according to the JRC FUELMAP (horizontal axis) and NFFL (bar colors) classification, as percentages of the burnt area. See Appendix A for a full description of these classifications.

Notice in Case 2 the relatively high percentages of urban and barren areas (JRC class 53) inside the fire perimeter. These correspond to areas in the Kalmthout Heath that are actually dunes (JRC class 40, Figure 4.5(b)). This error is expected to have a considerable impact on the fire spread simulation as dune fuels should be reclassified to the NFFL class “Short Grass”, while the urban and barren classes do not support fire propagation in the simulations.



Figure 4.5: Landscape of the Kalmthout Heath (Case 2), with areas of heathland (a) and dunes (b).

4.1.4 Topography and street maps

The maps of slope and aspect in Figures 4.9 to 4.15 show that the wildfires in Flanders and the Netherlands (Cases 2, 3, 4 and 7) all occurred on practically flat terrain. Note, however, that the coarse spatial resolution of 100 m has a smoothing effect and local variations in elevation and slope remain unresolved. Figure 4.1.3 illustrates this for Case 2. Thus, only the data of wildfires in The Ardennes (Cases 1, 5 and 6) show significant average slopes ($> 1\%$). Case 1 is located on top of a hill and is thus subjected to the prevailing weather to a greater extent, while Cases 5 and 6 are located in valleys.

Only Cases 1 and 3 reached large, asphalted, roads. In both cases, the EFFIS perimeters indicate that the fires crossed these roads at some point. Yet, this seems very unlikely, since such wide roads act as fire corridors that can only be crossed by extreme (spotting) fires. Moreover, these roads are used by the fire department as strategic blockades from which they can launch their attacks. The reports of these cases mention indeed that the wildfires were stopped at the big roads, which again points out a drawback of the coarse resolution of the EFFIS perimeters. Moreover, in all cases the (burnt) area is transected by numerous dirt roads, walking paths, cycle trails and even a small river (Case 1) which can all act as barriers or retardants for the spreading surface fire, but are not included in the data.

4.1.5 Weather

For the use of a dynamical wildfire simulator in an operational context, one would have to rely on weather forecasts using a (mesoscale) weather model. However, weather forecast data by the European Centre for Medium-Range Weather Forecasts (ECMWF) are available only for fire cases after August 2011. Hence, historical data of the wind vector, cloud cover, relative humidity (RH), and temperature from nearby weather stations are used instead in this work (Figures 4.16 to 4.22). Precipitation data are not included, as no weather stations recorded any precipitation for either of the cases during the period of interest. These dry conditions are also reflected by the low RH values, when comparing these to the long-term monthly average of around 73% for a normal month of April or May in Belgium (KMI, 2017). This is of course expected, as the risk of (large) wildfires increases in dry weather conditions.

The weather data are extracted from Wolfram Mathematica's database (Wolfram Research Inc., 2016). For most cases, these data come from the weather station closest to the centroid of the fire perimeter, as determined using ArcMap (ESRI, 2011). Only for Case 1 and 4, the data were interpolated between the two and three closest stations, respectively, via inverse distance weighing (De Smith et al., 2007). For every case, the start of the time series is set three days prior to the ignition, in order to account for the weather conditions leading up to the wildfire. As the original temporal resolution varied between stations and observations (with time steps ranging from 1 minute up to 1 hour and more), all time series were resampled to a single temporal resolution of 30 minutes by linear interpolation.

As is common for all these weather variables, their observed values vary significantly, with clear day-night variations. Thus, larger fires (Cases 1–4) show, unsurprisingly, more variation during their (longer) burning periods than the smaller fires (Figure 4.6). It might be reasonable to expect relatively high wind speeds during large wildfires and vice versa, but this is not clearly observed.

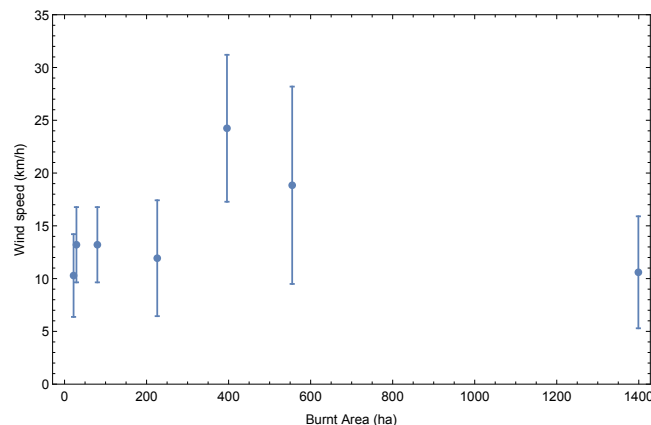


Figure 4.6: Plot of average wind speed and standard deviations during the wildfires versus the burnt area.

4.1.6 Wildfire ignition and progress

As the observed MODIS perimeters only provide a very rough idea of ignition times and locations, these data are preferably retrieved from other sources. For Cases 1–4 news or fire reports are available. These document the time of first sight, which is here assumed to be the time of ignition. Ignition locations can be derived from a reported map (Cases 1–3), or estimated based on the location description (Case 4). Since a news report on the latter case states that the fire started when a burning car was towed through the heath towards a nearby road (Houben, 2011), the ignition source may be envisaged as a line instead of a point. For the small fires (Cases 5–7), however, no news or fire report is available, so the ignition time has to be based on the MODIS observations. For these cases, the ignition location is estimated as the centroid of the section of the burnt area facing the average wind direction. Table 4.1 and Figure 4.7 provide an overview of the results hereof.

There is a large variability in available information concerning the progress and duration of the wildfires between the different cases—even more than for what concerns the ignition data. For example, only for Case 1 there are multiple fire perimeters available, but as was mentioned before, these could not reliably be used as time-stamped snapshots of different stages of the wildfire. Moreover, a news report of Case 4 mentions the recurrence of several fire hotspots after the fire was reportedly under control, but there are no details on the locations thereof (Houben, 2011). Last but not least, the interventions by fire fighters are only documented (at a reasonable level of detail) in the fire reports of Cases 2 and 3. Hence, for the sake of comparability, all wildfires are assumed to spread continuously during their burning period, while ignoring the actions of fire fighters.

For Cases 1–4, it is assumed that the fire spreads from the first time it is spotted, until the time it was reportedly under control by the fire fighters. The rationale behind this is to perform a simulation of the worst case scenario, which would typically be done by the fire department at the start of a wildfire. It is expected that the simulations will (strongly) over-estimate the size of the wildfire, especially in regions where the fire fighters were active. For Cases 5–7, the simulations are run until the observed burnt area is reached, as there are no reliable data on the duration of these wildfires. These simulations are therefore regarded as worst case scenarios, but rather serve as an extra way to compare the simulations in terms of ROS and shape of the final perimeter.

Table 4.3: Overview of the fire dataset, provided by the JRC.

Case	Area (ha)	Ignition		Duration (h)	Ignition location	
		Date	Time		Lon (°E)	Lat (°N)
1	1399	2011/04/25	16:26 ^a	38 ^a	6.124846	50.539370
2	555	2011/05/25	11:56 ^a	55 ^a	4.434590	51.383916
3	396	2014/04/20	08:41 ^a	12 ^a	5.874427	52.095529
4	226	2011/05/07	14:00 ^b	8 ^b	5.511101*	51.050103*
					5.509102*	51.050312*
5	80	2015/04/23	12:30 ^c	-	6.265952	50.455384
6	29	2015/04/21	12:30 ^c	-	6.242140	50.477850
7	22	2015/04/14	12:27 ^c	-	5.976461	52.418578

based on ^afire report, ^bnews report, or ^cperimeter meta-data

*estimated line ignition between two points

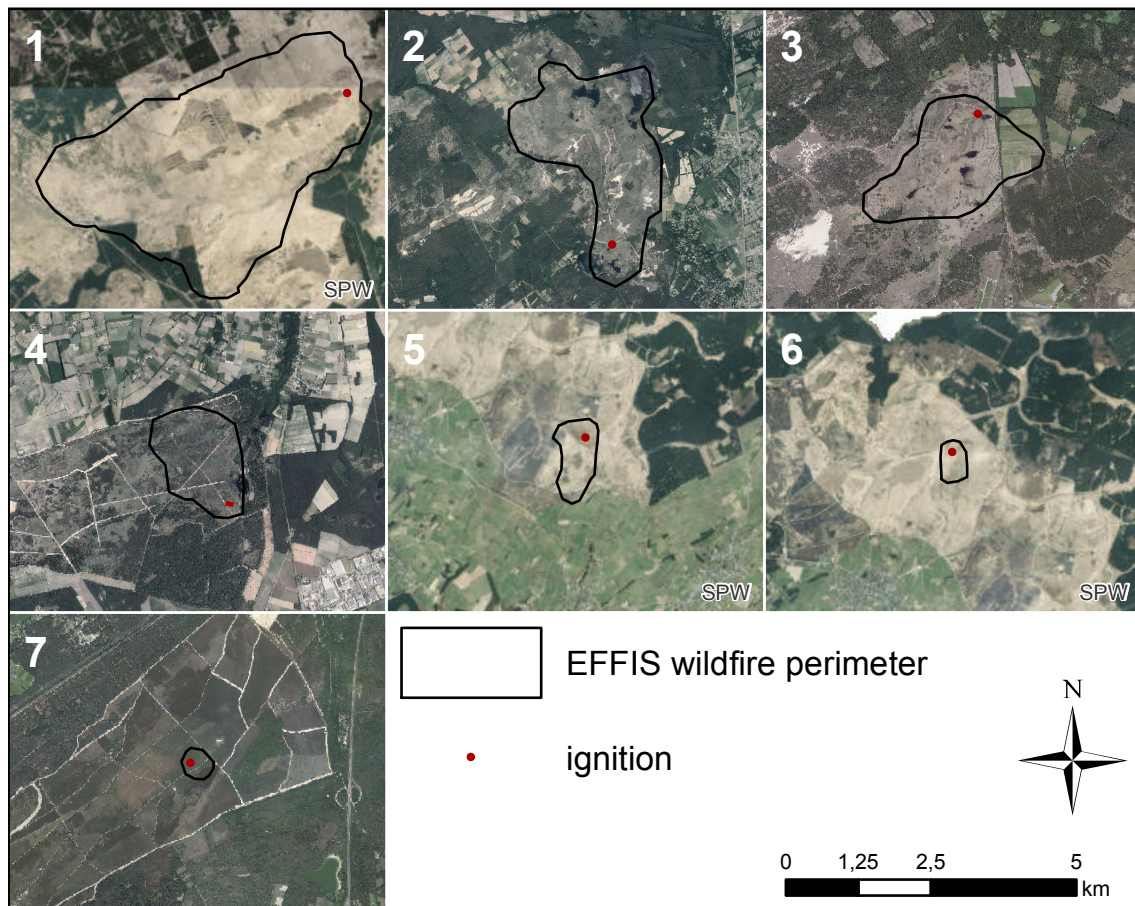


Figure 4.7: Fire perimeters and approximate ignition locations for the selected wildfires (Table 4.3).

4.2 Model description and settings

In this chapter, three wildfire simulators are evaluated using the dataset described in Section 4.1, namely FARSITE (Finney, 2004), ForeFire (Filippi et al., 2009b, 2014a), and the CA-based model (Depicker et al., 2016). A general overview of these models is presented in Table 4.4. The rest of this section will detail on their underlying mechanics, settings and usage.

Table 4.4: Overview of the evaluated wildfire simulators.

Name	Model type	Level of development	Reference
FARSITE	simulation model	operational	Finney (2004)
ForeFire	simulation model	research phase	Filippi et al. (2009b, 2014a)
CA analogue	analogue model	early research phase	Depicker et al. (2016)

4.2.1 FARSITE

In Chapter 3, FARSITE is named as the current standard of wildfire simulation models. It is implemented in free, open source software with a graphical user interface (GUI). It is based on the fire behaviour model BEHAVE (Andrews, 1986), which includes the quasi-physical model of Rothermel (1972) and fuel moisture models (e.g. Rothermel et al. (1986)), and Huygen’s wavelet principle, as implemented by Finney (2004). This basis module is extended with additional submodels describing crown fire, spotting, point-source fire acceleration (Finney, 2004). Yet the more complicated the model, the more data and/or parameters are needed. Hence, in addition to the surface spread (and fuel moisture) model, only the acceleration model is used here. Several options regarding settings and types of input data are available, but only those that were used in this work are discussed.

Fire acceleration and fuel moisture submodel

The fire acceleration model is adapted from the FBP (Alexander et al., 1992). It corrects for the time lag between ignition and reaching the equilibrium ROS, given by the fire behaviour model. This model assumes a negative exponential function that reaches by default 90% of the equilibrium ROS at 20.02 and 7.68 min for point and line ignitions, respectively. Finney (2004) notes that the ROS in FARSITE is often overestimated due to the continuously accelerating and decelerating wildfire (as a result of the highly variable wind). Hence, besides the acceleration model, also a subjective adjustment factor can be specified per fuel class.

The dead FMC is critical in determining the fire behaviour (see Sections 2.1 and 3.4), but hard to measure due to its highly dynamic nature. FARSITE thus makes use of dead fuel moisture models to estimate this parameter for different fuel types (e.g. the one by Rothermel et al. (1986) for fine fuels). These models make use of the time lag concept (Section 2.1.3) and the equilibrium moisture content. The latter strongly depends on the local weather conditions (air temperature, RH, solar radiation, and precipitation), which are in turn affected by local topography and site conditions (e.g. the canopy cover). Hence, in order to account for spatial variability of the FMC at the time of ignition, the FARSITE user can run the dead fuel moisture model for a specified amount of time prior to the ignition (the so-called conditioning period). FMC of live fuels is assumed to remain constant at its initial value throughout the simulation.

Model inputs and settings

FARSITE requires several input data and parameters to be specified in a project file, which forms the basis of a simulation. The input data include landscape, wind, and weather files, which consist of the data discussed in Section 4.1 (see Table 4.5). A file containing the initial FMC of the present fuel classes also has to be provided. Since no data are available of the latter, default values are used, which are tuned by considering the previously discussed conditioning period. This period is set to three days, as it is assumed that this is sufficient to estimate the FMC of fine fuels (time lag classes 1 h and 10 h), which are the most important for the ROS (Section 2.1.3). Besides these input data, the parameters of the present fuel classes, including the previously discussed ROS adjustment factor, are also specified in the project file. These are all kept at their default values.

Apart from the parameters in the project file, some additional model parameters are specified prior to starting the FARSITE simulation. These include the wildfire duration, time step, spatial resolution and the selection of the submodels used. The time step, i.e. the maximal period in which the environmental variables are considered to be constant (Finney, 2004), is set at 30 min, which is the temporal resolution of the wind data. The spatial resolution is determined by the perimeter and distance resolution, which define the maximal distance between the perimeter vertices and the maximal horizontal spread before new landscape information is used, respectively. Both are set to 50 m, since no additional meaningful precision is gained at values lower than half of the spatial resolution of the landscape data (Finney, 2004).

Table 4.5: Overview of the input data, needed in a FARSITE project.

	Landscape	Wind	Weather
Data type	static (GIS rasters)	dynamic (spatially uniform)	dynamic (spatially uniform)
Variables	Elevation [m] Slope [degrees] Aspect [degrees] Canopy cover [%] Fuel classes	Hour [hhmm] Wind speed [km/h] Wind direction [degrees] Cloud cover [percentage]	Precipitation [mm/d] Precipitation start and end [hhmm] Daily T_{\min} and T_{\max} [°C] Daily RH_{\min} and RH_{\max} [%] Times of daily T_{\min} and T_{\max} [hhmm] Elevation [m]

4.2.2 ForeFire

In Section 3.5 the discrete event front tracking algorithm of ForeFire was presented as an alternative for Huygen’s wavelet principle, though it has not yet reached the level of development of FARSITE. Besides a web application with limited functionality, and which is moreover restricted to wildfires in France (Demo ForeFire API V1, 2017), there is no software available with a GUI like FARSITE. The open-source code is available for researchers and developers via a git repository (ForeFire API). This code can be compiled to, among others, a C++ simulation core with a Python/NumPy interface. Since the web application is the closest thing to an operational ForeFire tool, we opted to use its settings in the Python/NumPy interface. ForeFire is implemented in a modular software architecture, with the possibility to extend and couple it with different submodels (Filippi et al., 2014a). Moreover, the user can choose from a set of different fire behaviour models or can implement new ones.

Fire behaviour model

The physically-based Balbi model (Balbi et al., 2009), which was modified by Filippi et al. (2014b), is used in combination with ForeFire, as this is also the model used in the ForeFire web tool. Just as Rothermel’s model, it is built around an energy balance, yet the components of this balance are derived from physical/geometrical considerations, rather than experimental data. These derivations rely on the following assumptions (Balbi et al., 2009):

1. the fire front is a radiative panel with a triangular cross-section;
2. the radiative heat transfer is dominant (at long range);
3. (radiative) preheating of the vegetation takes place only under the flame;

4. the fraction of energy emitted as radiation by the flame (χ) is a decreasing function of the flame surface-to-volume ratio (σ);
5. the velocity vector into the flames is a combination of the wind vector and natural convection of the flame;
6. the gasses are ideal, the thermodynamic transformations isobaric;
7. there exists an average flame temperature and ignition temperature;
8. the gas inflow into the flame is stoichiometric (at a constant ratio of 8.3 kg air/kg pyrolysis gas);
9. the fuel distribution is locally homogeneous;
10. the mass exchange rate due to pyrolysis is constant.

Note that some of these are strong assumptions (e.g. Assumptions 2, 3, 7; see Section 2.1.7). The resulting model is a single algebraic equation that links the stationary ROS to the tilt angle (γ) of the fire front towards the unburnt fuel. The latter depends on the wind, slope, and the front normal. This model has been modified by Filippi et al. (2014b) to account for the effect of the local front depth (λ) and curvature (κ) on the ROS (R):

$$R = R_{fuel} + R_{flame}, \quad (4.1)$$

where R_{fuel} and R_{flame} are the contribution of the fuel undergoing pyrolysis (i.e. short range heat transfer) and of the flames (i.e. long range heat transfer), respectively. These components are given by:

$$R_{fuel} = \frac{\left(1 - e^{-\frac{\lambda \beta_d(\beta)}{4}}\right) \epsilon_f B T_i^4 d_{fb}}{2 W [c_{p,f} (T_i - T_a) + M h_w]}, \quad (4.2a)$$

$$R_{flame} = \chi h \dot{\sigma} f(\gamma, \kappa, \lambda), \quad (4.2b)$$

where $\beta_d(\beta)$ [-] is a radiation dumping ratio that depends on the packing ratio, ϵ_f [-] the fuel emissivity, B [$\text{W m}^2 \text{K}^4$] the Stefan-Boltzmann constant, $c_{p,f}$ [$\text{J kg}^{-1} \text{K}^{-1}$] the heat capacity of the fuel, T_i and T_a [K] the ignition and air temperature, M [%] the FMC, h_w [J kg^{-1}] the latent heat, $\dot{\sigma}$ [$\text{kg m}^{-2} \text{s}^{-1}$] the mass exchange rate due to pyrolysis, and $f(\gamma, \kappa, \lambda)$, a function depending on the local front characteristics.

Model inputs and settings

Similarly to a FARSITE project file, most input data for ForeFire are packed into a netcdf file, containing GIS rasters of the elevation, fuel classes, and wind vector field(s). Note the more limited data requirements compared to FARSITE. This is because the current ForeFire distribution does not include submodels (such as the dead fuel moisture model), apart from the fire behaviour model. Hence, all fuel parameters are static and defined in a fuel table file for every fuel class. The fuel classification/parametrisation used here is the one from the ForeFire web-application, based on the CORINE land cover (LC) classes (Tables 4.6 and 4.7). Note that this parametrisation is still premature as only the fuelbed depth (d_{fb}) varies between the burnable fuel classes. Hence, (spatial) variability of important parameters such as the FMC is left unaccounted for.

ForeFire is run from a Python script in which the simulation parameters and ignition information (coordinates, date and time) are specified. Since it only accepts closed perimeters as ignitions sources, the simulations start from a triangular perimeter, of which the centroid coincides with the ignition point, or a polygon surrounding the ignition line (Table 4.3). Important parameters again include the perimeter and distance resolution, yet the effect of these parameters is different than in FARSITE. The perimeter resolution now also determines the minimal size of the triangular ignition perimeter, so it is set to a smaller value (20 m). As was explained in Section 3.5, ForeFire is event driven, yet the size and number of time steps have to be specified to produce perimeters at regular time intervals (here, 30 min). Consequently, the distance resolution now also determines the maximal error between the simulated and the produced perimeter at a given time. To make this error practically negligible, the distance resolution is kept at 1 m.

Table 4.6: CORINE LC classes with the corresponding JRC fuel classes and ForeFire parameters.

fuel class ID		CORINE class description	FMC		W [kg fuel m ⁻²]		d_{fb} [m]
CORINE	JRC		dead	live	dead	live	
111	53	Continuous urban fabric	0.15	0.5	0	0	0
231	3	Pastures	0.13	0.5	0.6	1.28	2
241	51	Annual crops associated with permanent crops	0.13	0.5	0.6	1.28	1.6
243	52	Agriculture with natural vegetation	0.13	0.5	0.6	1.28	1.6
311	32	Broad-leaved forest	0.13	0.5	0.6	1.28	1.6
312	24, 27	Coniferous forest	0.13	0.5	0.6	1.28	1.6
313	37	Mixed forest	0.13	0.5	0.6	1.28	1.6
322	1, 2, 8, 17	Moors and heathland	0.13	0.5	0.6	1.28	2.6
512	55	Water bodies	0.13	0.5	0.6	1.28	0

Table 4.7: ForeFire parameters that are constant for all present fuel classes.

Parameter	Value	Units
ρ_b	500	[kg m ⁻³]
σ dead	2400	[m ⁻¹]
live	5700	[m ⁻¹]
ρ_a	1	[kg m ⁻³]
T_a	300	[K]
T_i	600	[K]
$c_{p,f}$	1800	[J kg ⁻¹ K ⁻¹]
h_w	2300000	[J kg ⁻¹]
h	15000000	[J kg ⁻¹]
χ	0.3	[-]

4.2.3 CA-based model

The final model selected for reviewing has been proposed by Depicker et al. (2016). It is a CA-based model using a square two-dimensional grid. The state of a cell c_i at time t , denoted as $S(c_i, t)$, reflects the number of time steps after the ignition of cell c_i . So, at time t , c_i is unburnt if $S(c_i, t) = 0$, burning if $S(c_i, t) > 0$ and $S(c_i, t) < n_{burn}$, and burnt if $S(c_i, t) \geq n_{burn}$, where n_{burn} is the number of time steps to completely burn the fuel enclosed in a cell. The state of every cell is governed by a stochastic transition function, which is evaluated at discrete time steps, and is given by

$$S(c_i, t + 1) = \begin{cases} S(c_i, t) + 1, & \text{if } S(c_i, t) > 0, \\ 1, & \text{if } S(c_i, t) = 0 \wedge \varepsilon < p_i, \\ 0, & \text{otherwise,} \end{cases} \quad (4.3)$$

with ε a random number between 0 and 1 and p_i the probability that cell c_i will ignite in the next time step. The latter depends on the cell's neighbourhood N_i and is calculated as

$$p_i = p_{veg} \left(1 - \prod_{c_j \in N_i} (1 - p_j) \right), \quad (4.4)$$

where p_{veg} and p_j are the intrinsic ignition probability and the probability that the wildfire spreads from a neighbouring cell c_j to cell c_i , respectively. The factor between parentheses thus denotes the total probability that a fire will spread from at least one of the cells in N_i to c_i . Here, N_i is the Moore neighbourhood, i.e. the eight cells surrounding c_i , while p_{veg} and p_j are given by

$$p_{veg} = (1 + e^{2.283 - 2.413 x_1 - 1.884 x_2 - 2.020 x_3 - 2.545 x_4 - 2.143 x_5})^{-1}, \quad (4.5a)$$

$$p_j = \begin{cases} \frac{1}{(1 + \psi_1 e^{-\psi_2 \mathbf{w} \cdot \hat{\mathbf{v}}}) (1 + \psi_3 e^{-\psi_4 \gamma_s})}, & \text{if } S(c_j, t) > 0 \text{ and } S(c_j, t) < n_{burn} \\ 0, & \text{if } S(c_j, t) = 0 \text{ or } S(c_j, t) \geq n_{burn} \end{cases} \quad (4.5b)$$

Equation (4.5a) was derived on the basis of a logistic regression (Depicker et al., 2016), taking into account five categorical predictors, namely the LC classes shrubland (x_1), broadleaved forest (x_2), mixed and coniferous forest (x_3), wetland (x_4), and the sandy soil texture class (x_5). Since categorical predictors can only take a value of 0 or 1, Eq. (4.5a) can yield ten different values greater than zero (Table 4.8). As this equation is constructed from a dataset of ignition locations of historical fires, the (strong) assumption is made that the ignition probability during a wildfire is the same as the wildfire risk before ignition. Hence, we slightly modified Eq. (4.4), by replacing p_{veg} by p'_{veg} , where

$$p'_{veg} = \min(\alpha p_{veg}, 1), \quad (4.6)$$

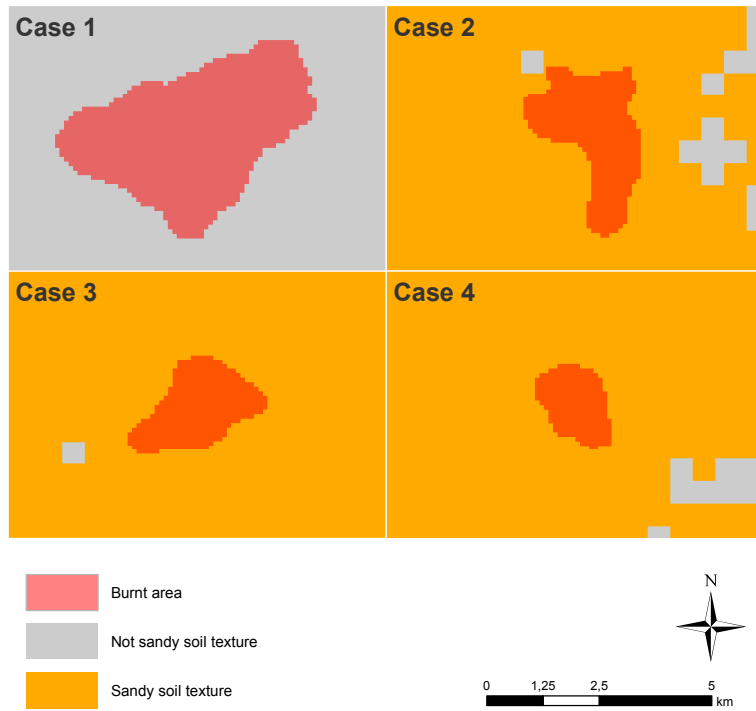
with α a scaling factor greater than 0. This way it is assumed that the intrinsic ignition probability during a wildfire is proportional to the wildfire risk, up to a value of 1. This modified model will be referred to as CA2, and the original one as CA1. p_j is calculated as a function of the component of the wind vector (\mathbf{w}) in the direction of wildfire spread (denoted by the unit vector $\hat{\mathbf{v}}$) and the slope angle (γ_s). Moreover, Eq. (4.5b) contains four parameters ($\psi_{1,2,3,4}$), whose value should be obtained through model calibration.

Table 4.8: Possible values for p_{veg} , according to Eq. (4.5a).

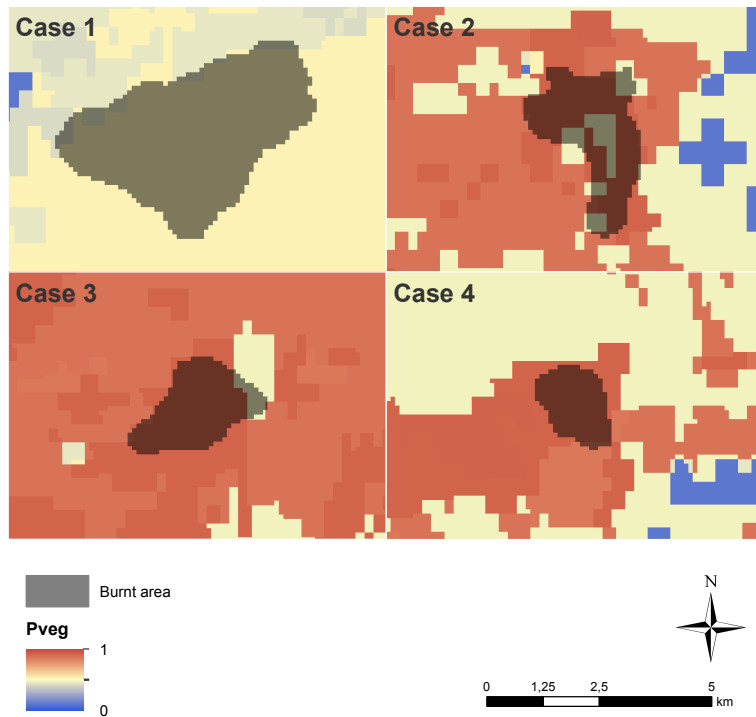
Texture	Land cover class				
	Others	Shrubland	Broadleaved forest	Coniferous\ mixed forest	Wetland
Not sandy	0.093	0.532	0.402	0.435	0.565
Sandy	0.465	0.907	0.851	0.868	0.917

Model inputs and settings

The main inputs of CA1 and CA2 are geographic (raster) data of elevation, LC classes, and soil texture, wind vector data during the whole wildfire duration and the ignition perimeter. In order to preserve comparability, the LC classes are again derived from the fuel maps of the JRC (Section 4.1). The soil texture maps are also provided by the JRC and originate from Ballabio et al. (2016). Since the calibration and evaluation of the CA-based model will be confined to Cases 1–4 (see Chapter 6), only the soil texture (Figure 4.8(a)) and p_{veg} maps (Figure 4.8(b)) of these cases are shown here. Contrary to FARSITE and ForeFire, which rely on pre-determined parameters for the fuel classes, the few model parameters α , $\psi_{1,2,3,4}$, and n_{burn} are yet to be calibrated (see Chapter 6). Note that n_{burn} should preferably depend on the state of the fuels within a cell. Yet, as the studied cases involve more or less the same fuel types (see Section 4.1), it is assumed that this parameter is approximately the same for all cells. Besides, there are two important parameters that have to be specified, namely the temporal resolution of the simulation (Δt), and the grid size, defined by the spatial resolution (Δx) and the number of grid cells (n_{cells}). These parameters not only have a large influence on the computation time, but also determine the maximal ROS, which is limited to $\frac{\Delta x}{\Delta t}$. Moreover, Δt affects the interpretation of p_i , since the latter is the probability that a cell ignites during one time step. Δx is fixed by the spatial resolution of the input data (100 m), while Δt is fixed at 7.5 min, limiting the maximal ROS to 800 m/h. Finally, n_{cells} was set to 120x120, 100x100, 80x80 and 40x40 cells for Cases 1–4, respectively. These choices are mainly based on practical considerations regarding the computational demands of the current model implementation.



(a)



(b)

Figure 4.8: Soil texture (a) and p_{veg} (b) maps of Cases 1–4, together with the rasterized burnt areas.

Case 1: High Fens

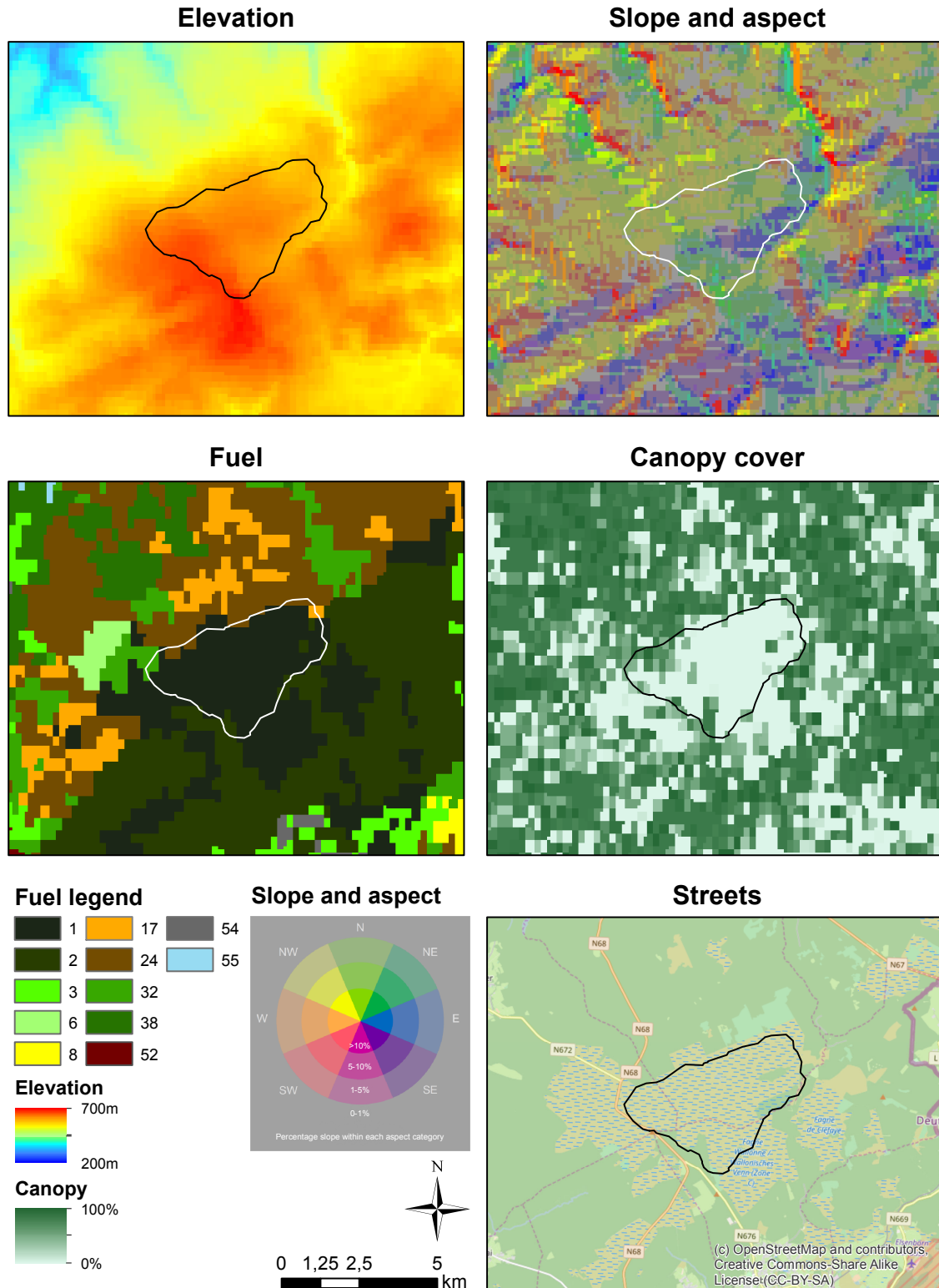


Figure 4.9: Geographical data of wildfire Case 1.

Case 2: Kalmthout Heath

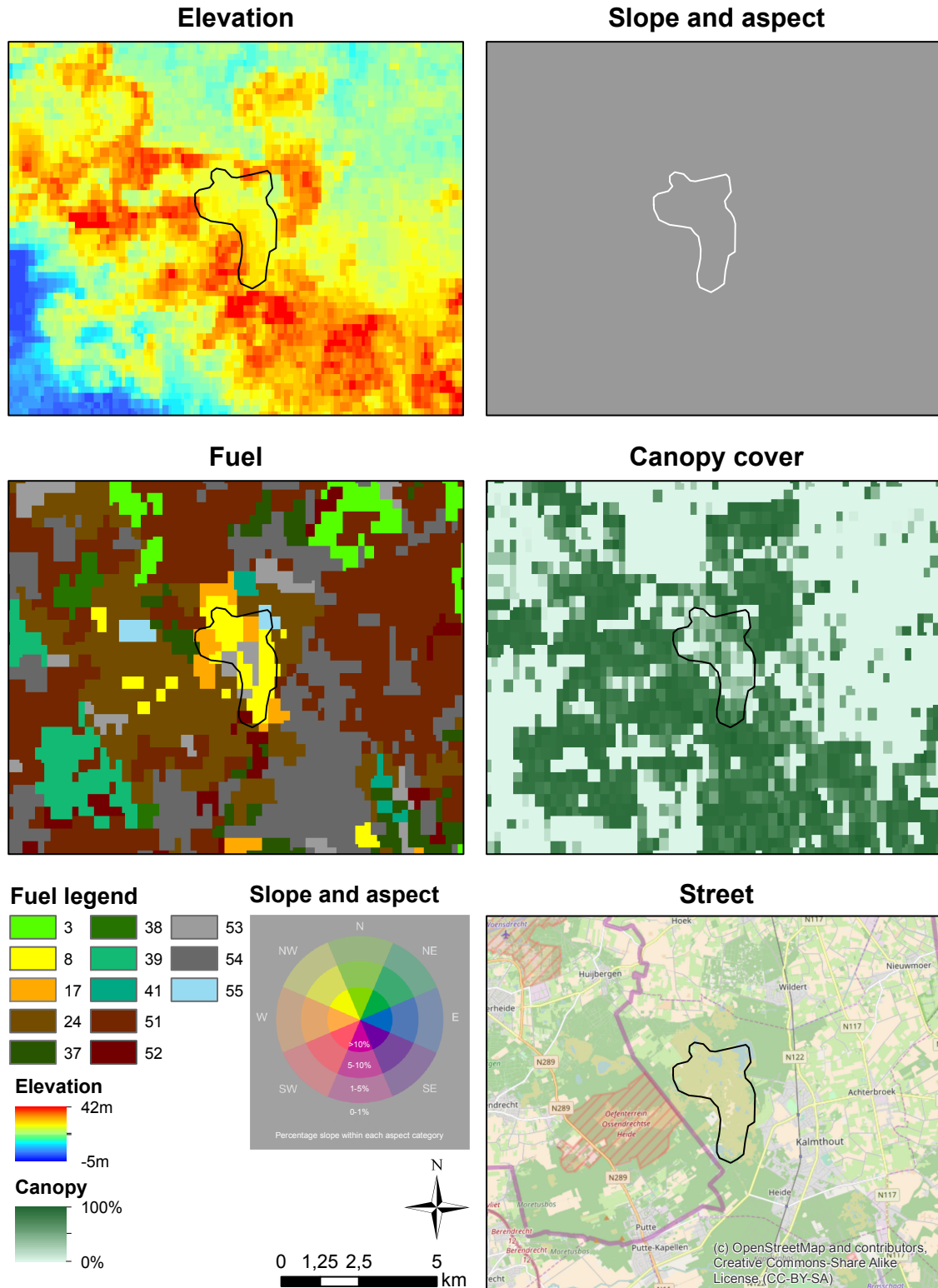


Figure 4.10: Geographical data of wildfire Case 2.

Case 3: The Hoge Veluwe National Park

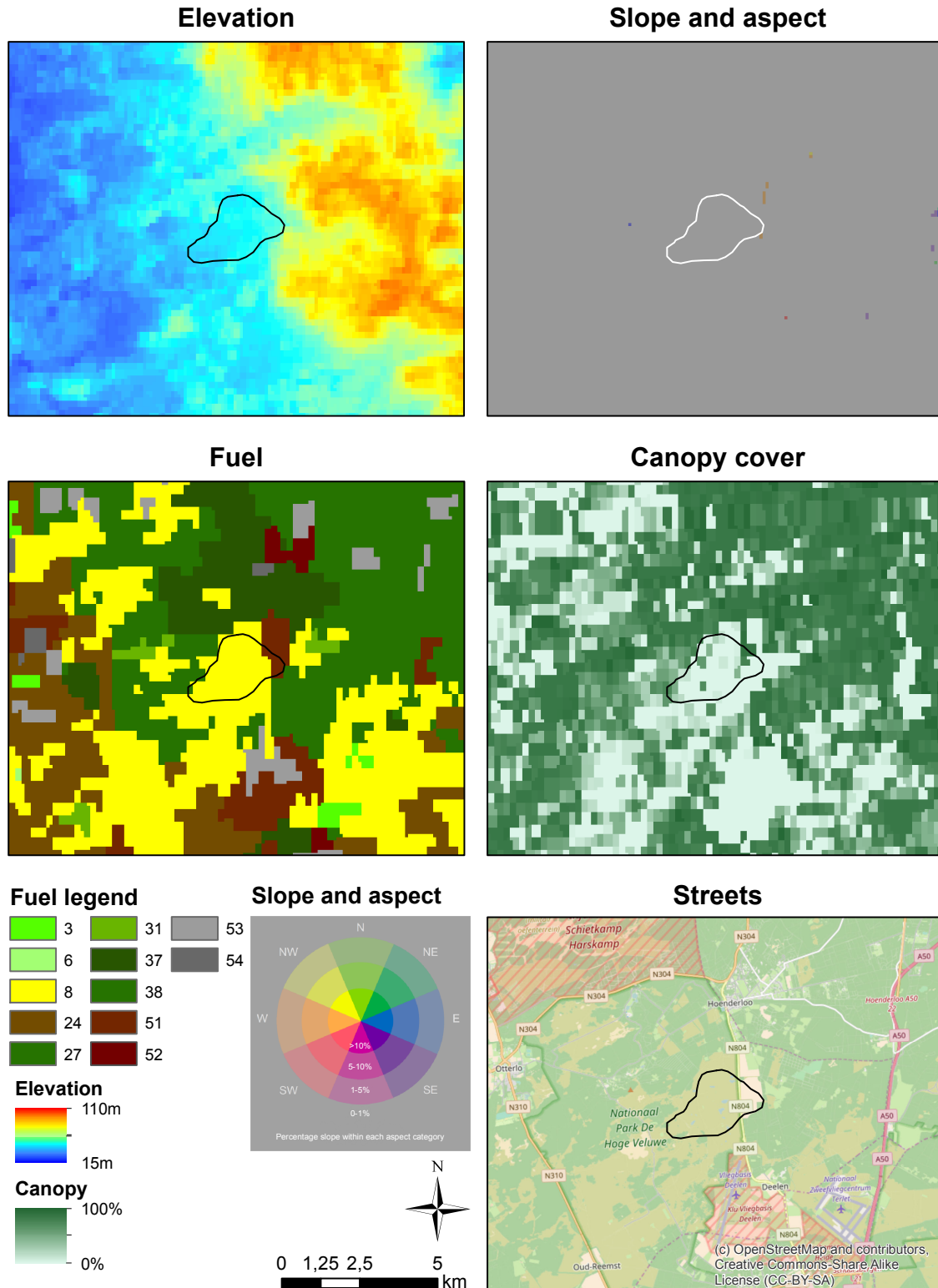


Figure 4.11: Geographical data of wildfire Case 3.

Case 4: Meeuwen-Gruitrode

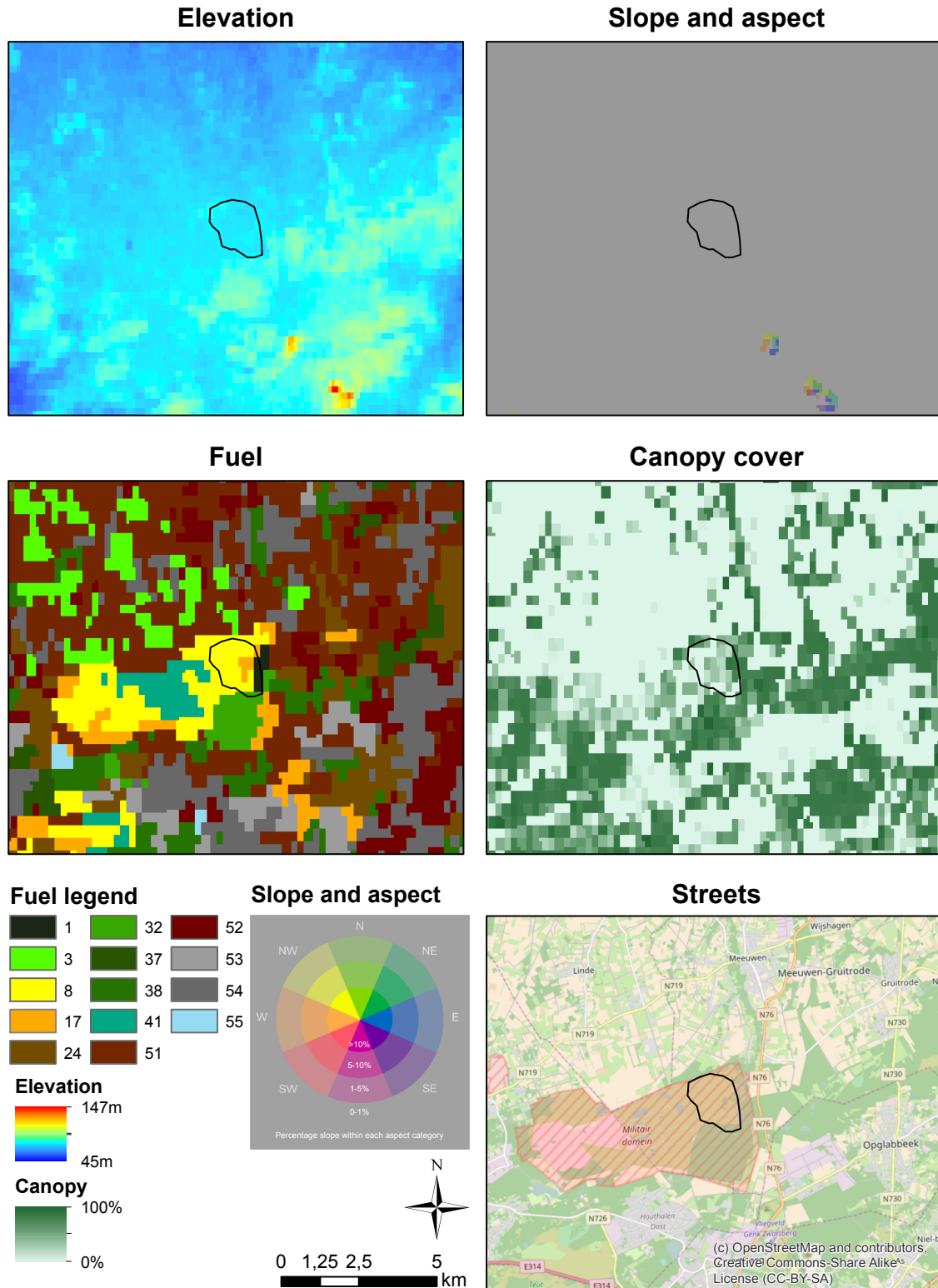


Figure 4.12: Geographical data of wildfire Case 4.

Case 5: Büllingen

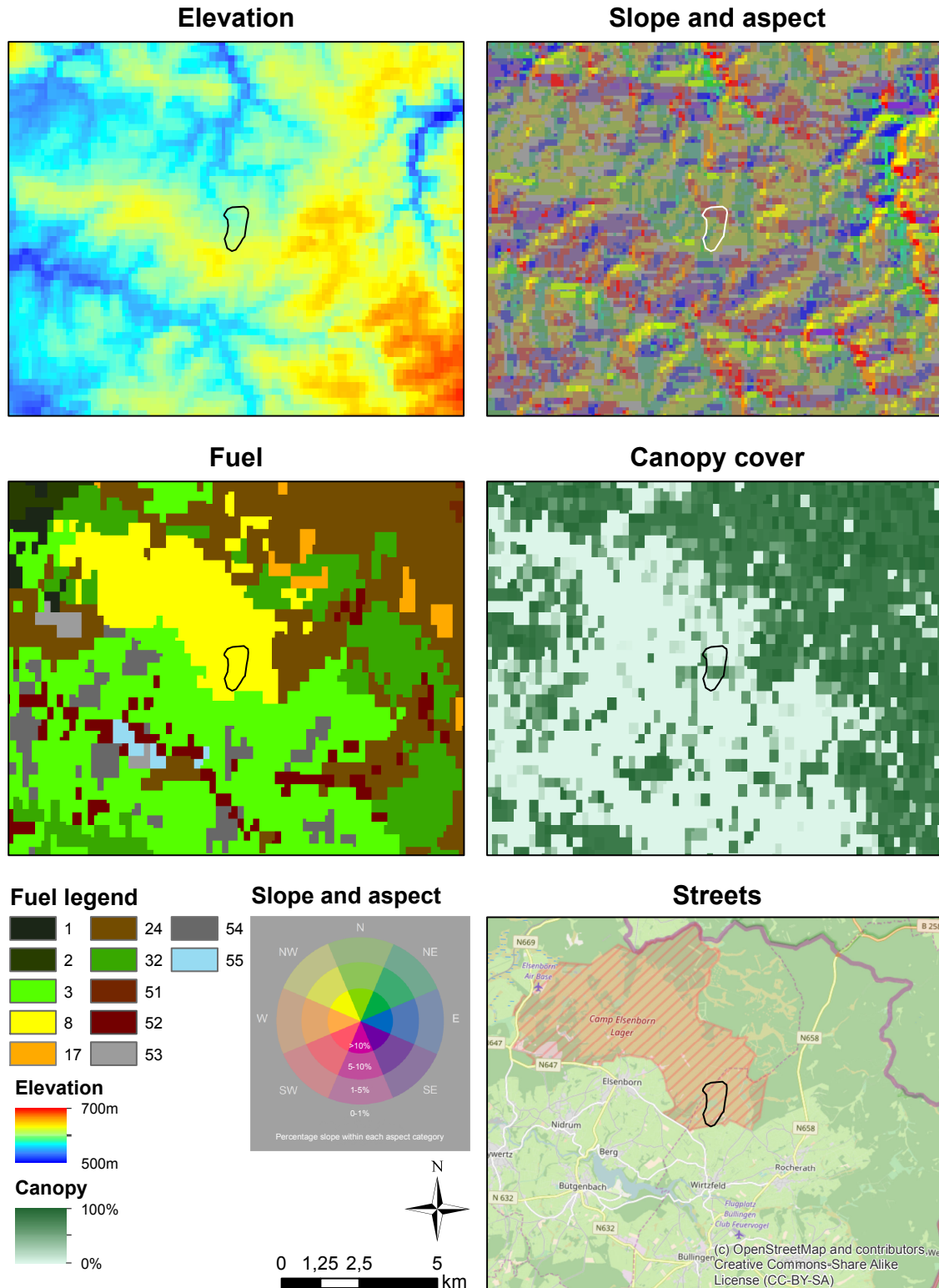


Figure 4.13: Geographical data of wildfire Case 5.

Case 6: Bütgenbach

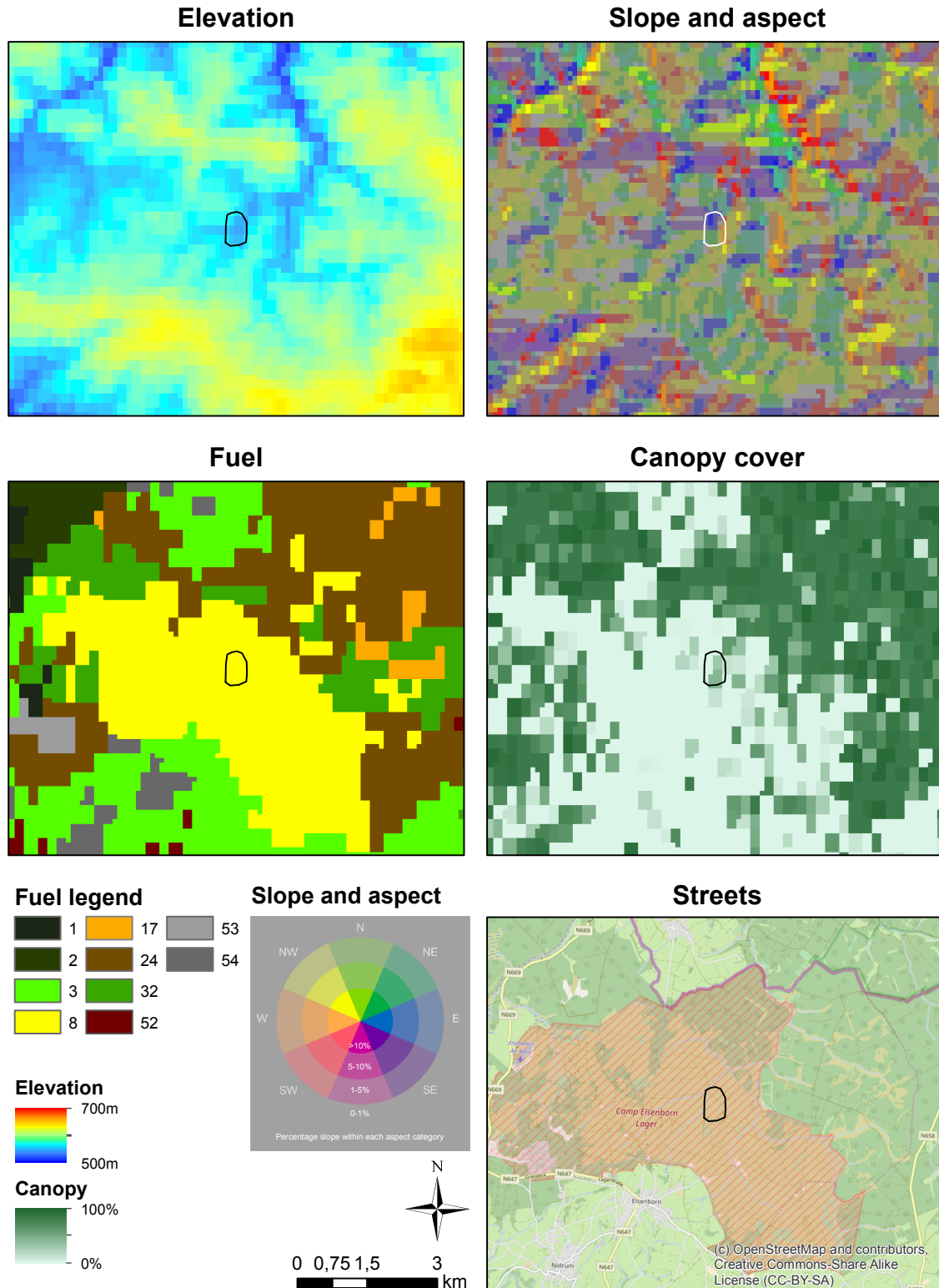


Figure 4.14: Geographical data of wildfire Case 6.

Case 7: Oldebroek Heath

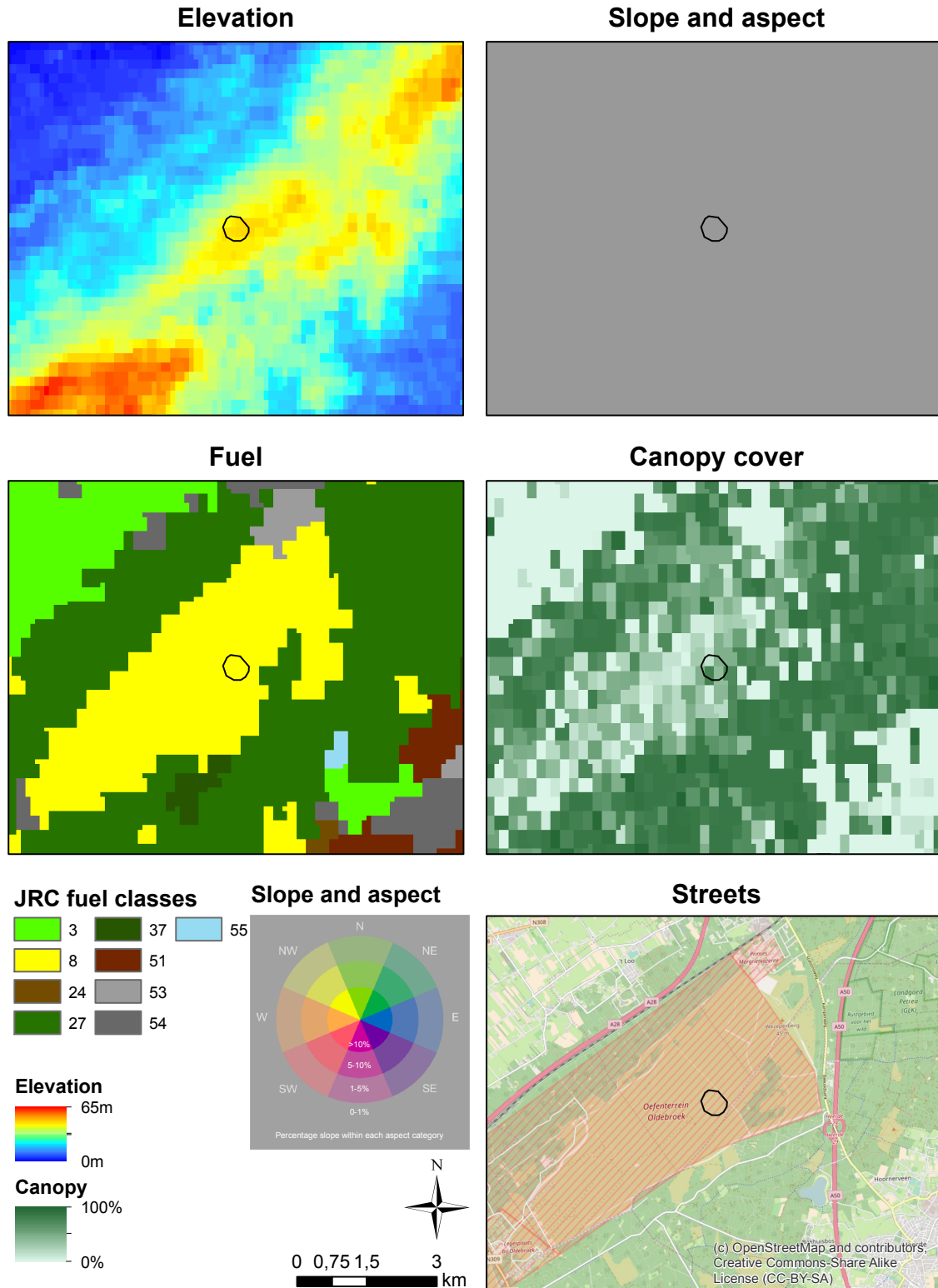
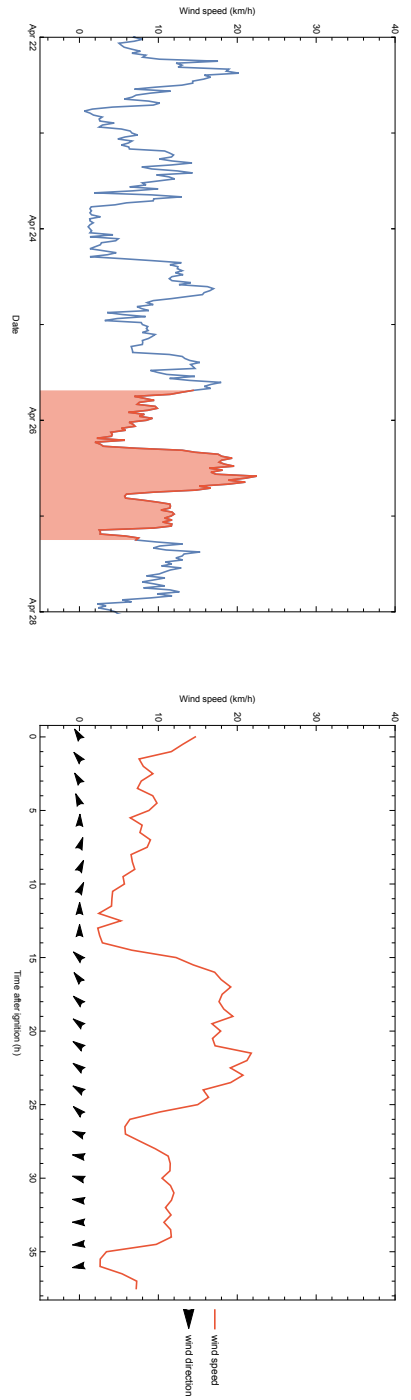
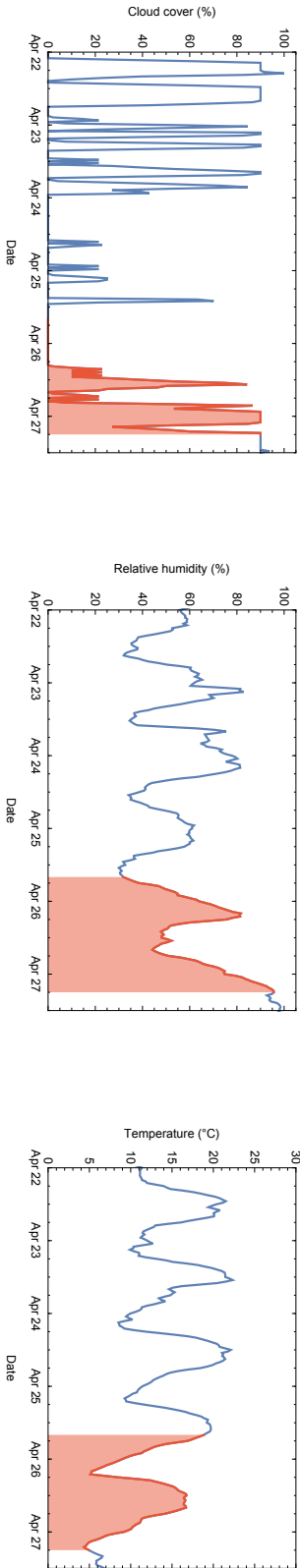


Figure 4.15: Geographical data of wildfire Case 7.



(a)



(b)

Figure 4.16: Overview of the wind data (a) and cloud cover, relative humidity and temperature (b) for wildfire Case 1. The fire duration is marked in red; the wind arrows in (a) point in the direction in which the wind is blowing.

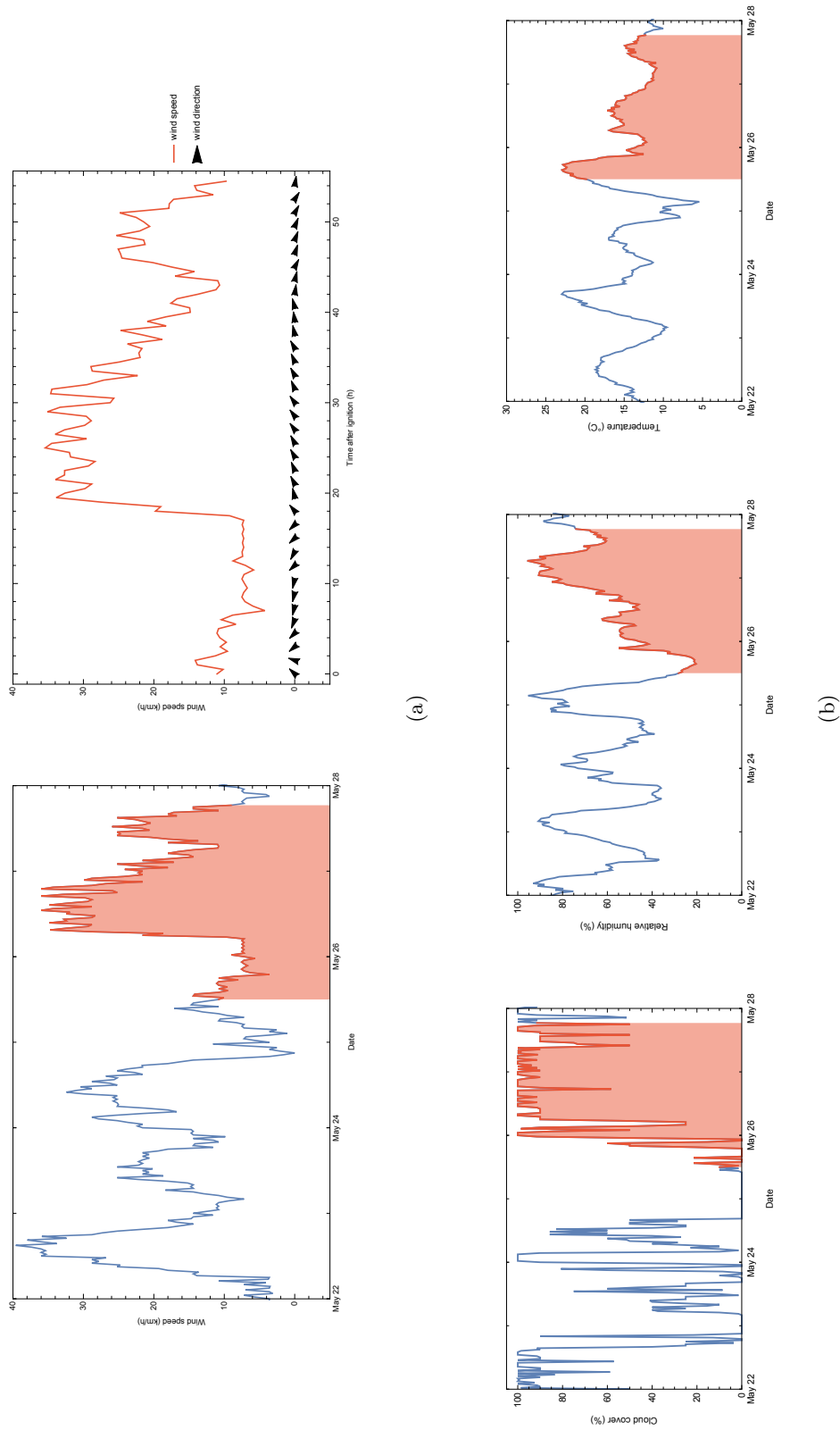


Figure 4.17: Overview of the wind data (a) and cloud cover, relative humidity and temperature (b) for wildfire Case 2. The fire duration is marked in red; the wind arrows in (a) point in the direction in which the wind is blowing.

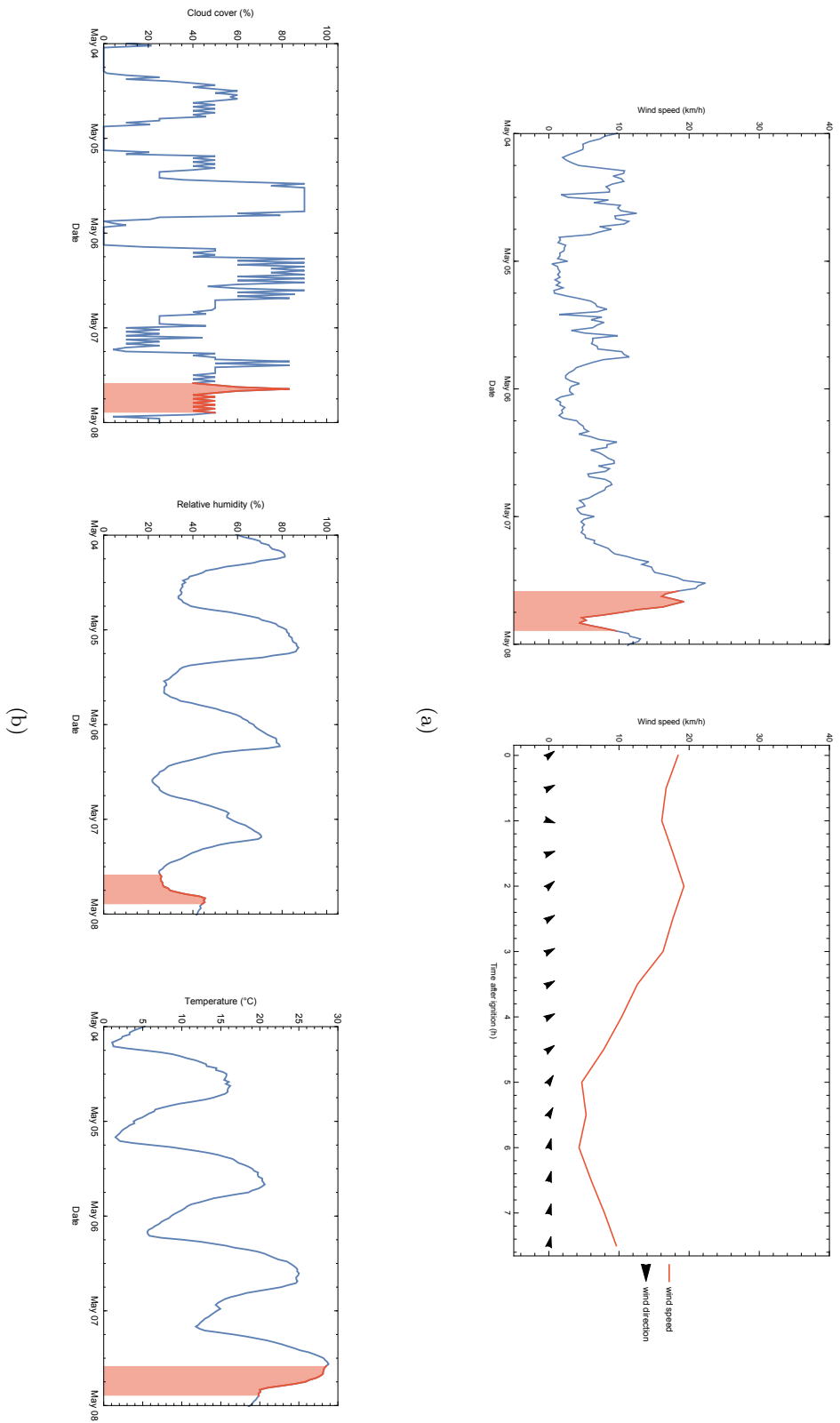


Figure 4.18: Overview of the wind data (a) and cloud cover, relative humidity and temperature (b) for wildfire Case 3. The fire duration is marked in red; the wind arrows in (a) point in the direction in which the wind is blowing.

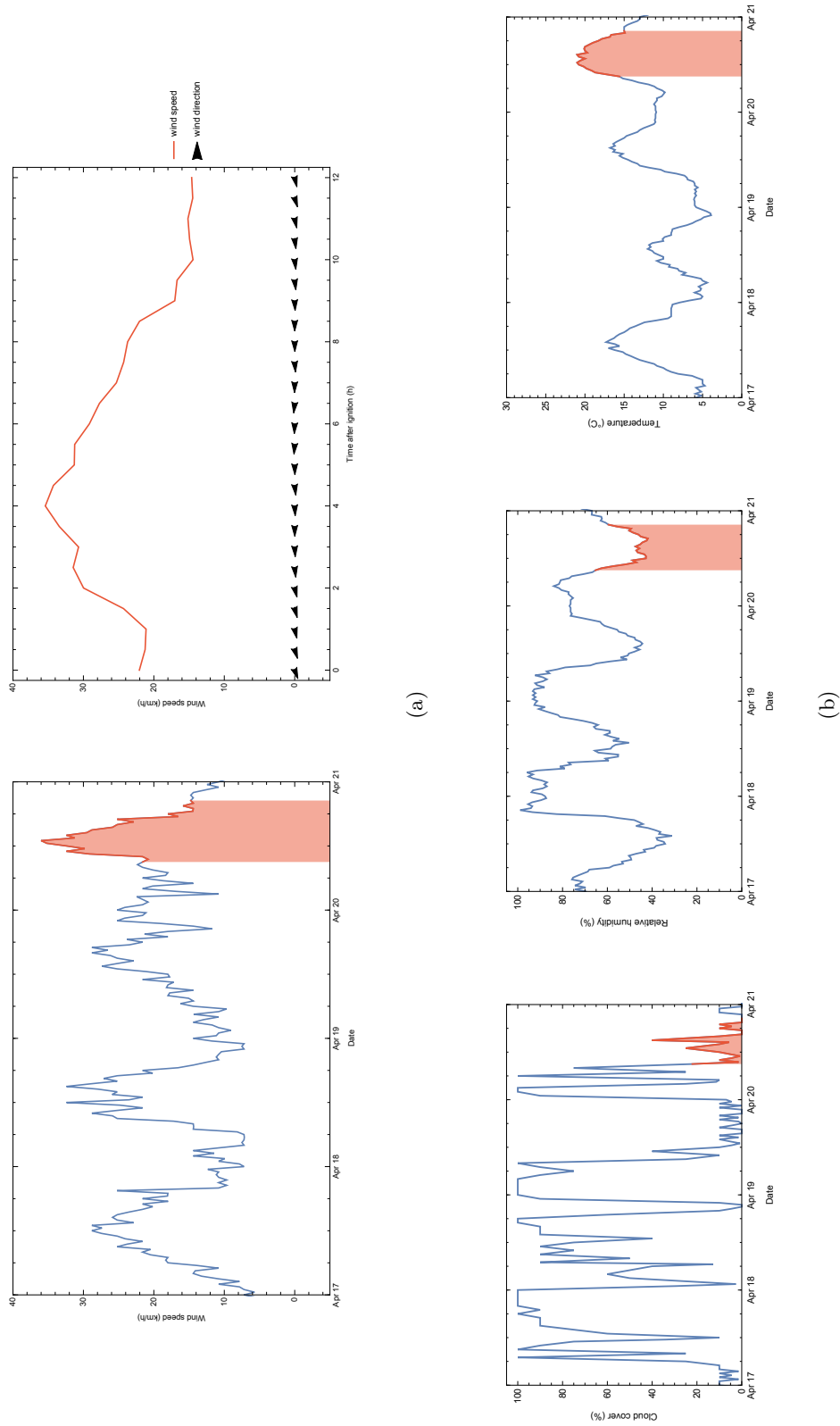


Figure 4.19: Overview of the wind data (a) and cloud cover, relative humidity and temperature (b) for wildfire Case 4. The fire duration is marked in red; the wind arrows in (a) point in the direction in which the wind is blowing.

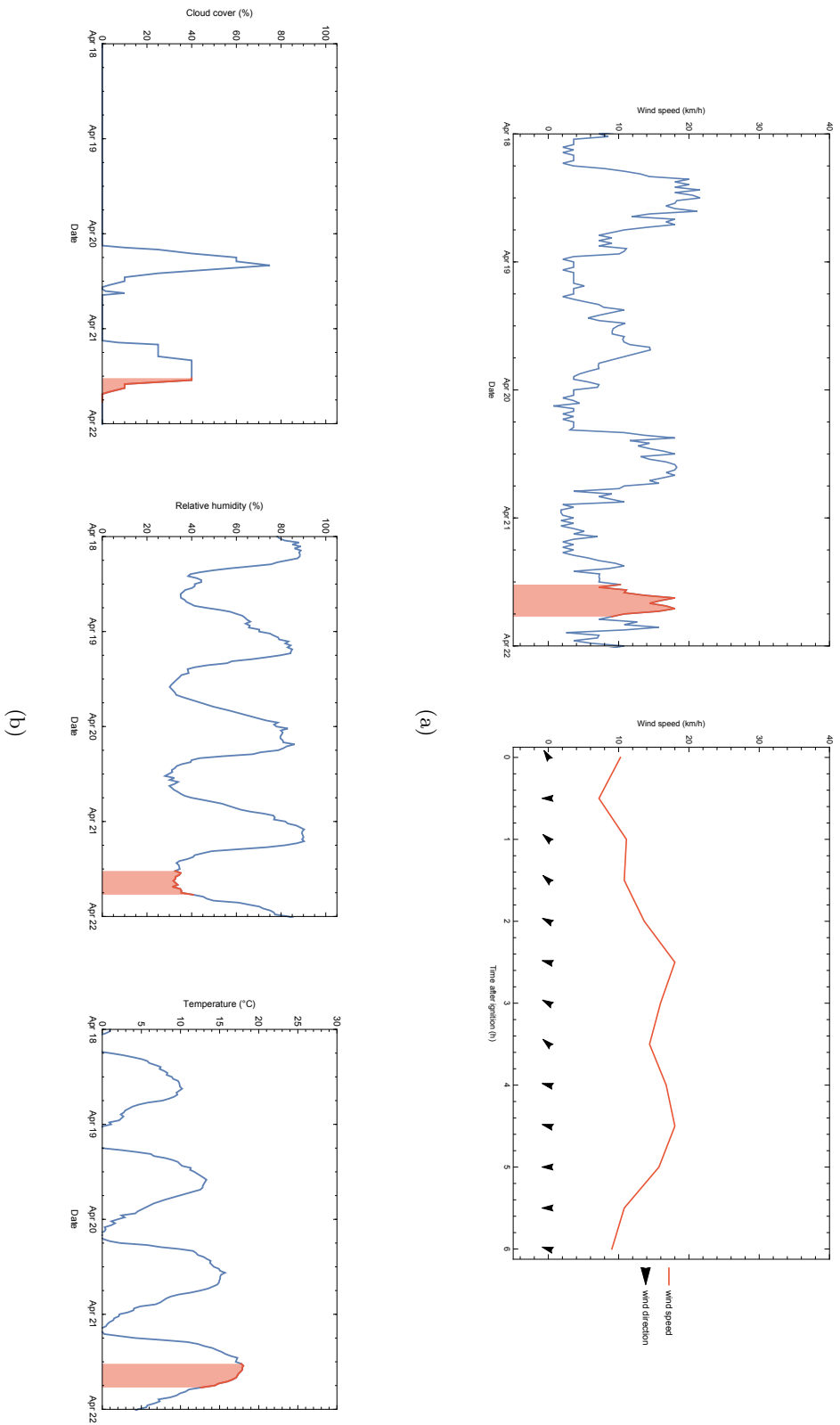


Figure 4.20: Overview of the wind data (a) and cloud cover, relative humidity and temperature (b) for wildfire Case 5. The wind arrows in (a) point in the direction in which the wind is blowing. In absence of a known fire duration, the first 6 hours after ignition are marked in red.

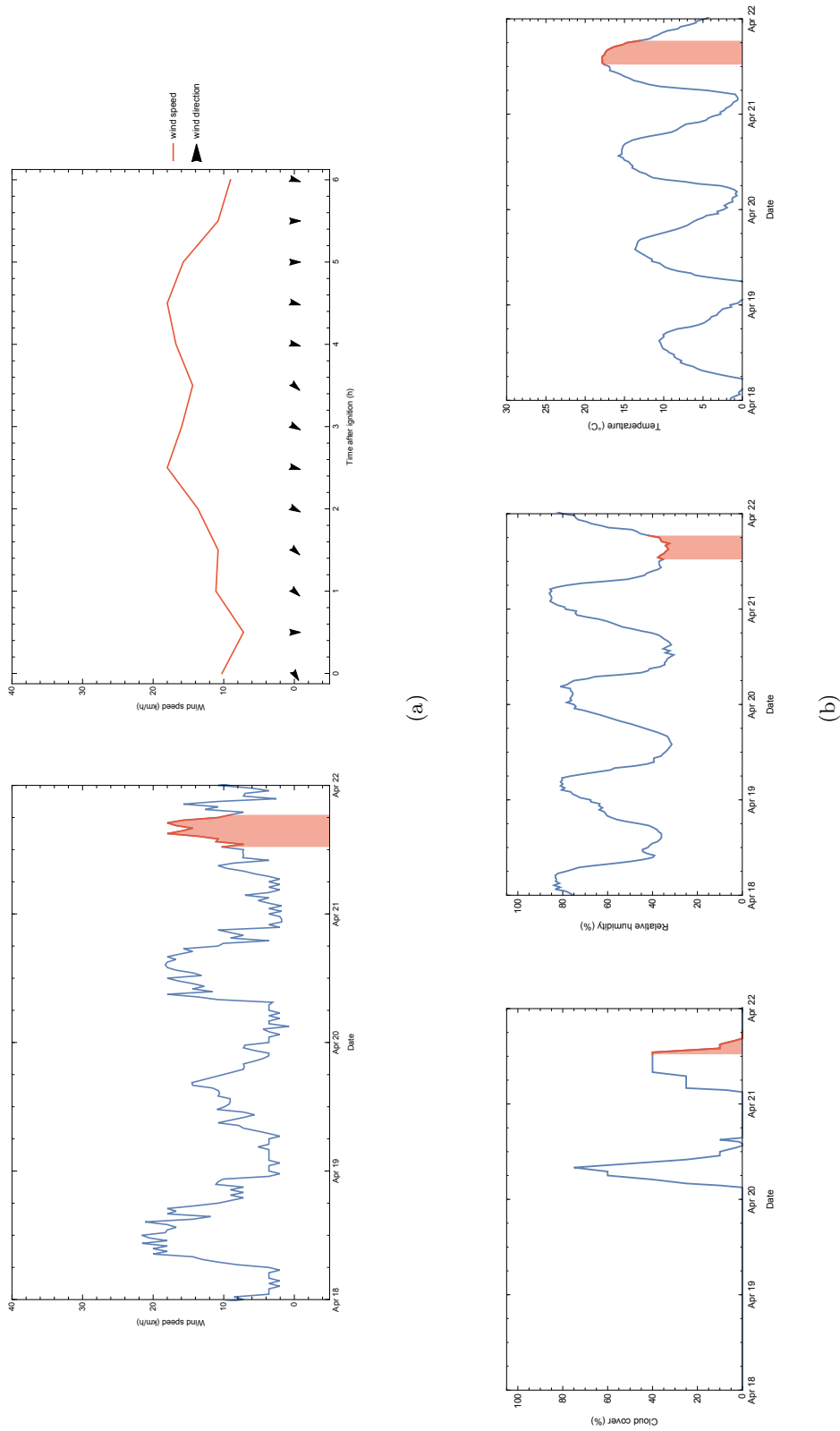


Figure 4.21: Overview of the wind data (a) and cloud cover, relative humidity and temperature (b) for wildfire Case 6. The wind arrows in (a) point in the direction in which the wind is blowing. In absence of a known fire duration, the first 6 hours after ignition are marked in red.

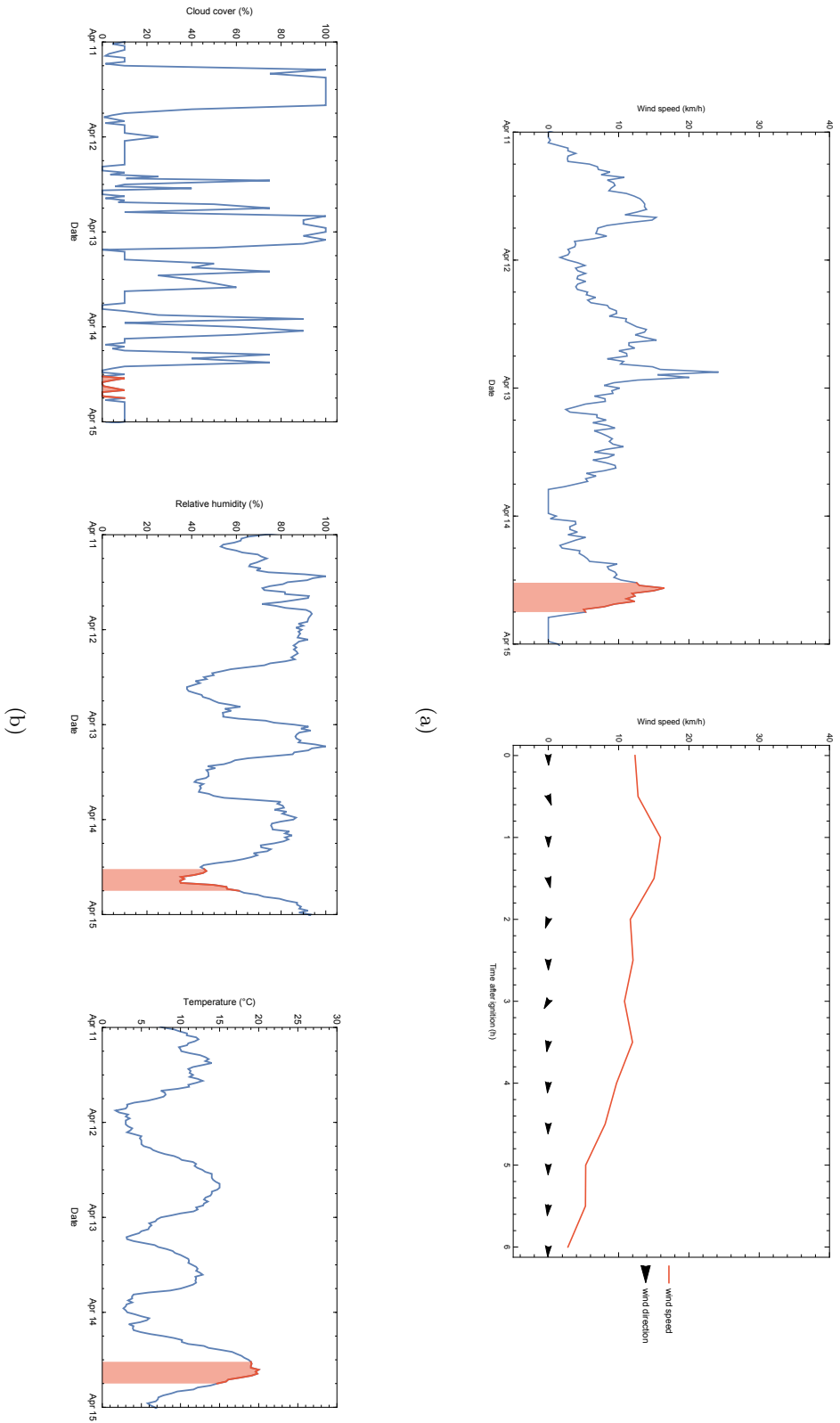


Figure 4.22: Overview of the wind data (a) and cloud cover, relative humidity and temperature (b) for wildfire Case 7. The wind arrows in (a) point in the direction in which the wind is blowing. In absence of a known fire duration, the first 6 hours after ignition are marked in red.

CHAPTER 5

A evaluation of FARSITE and ForeFire

In this chapter FARSITE and ForeFire (Chapter 3 and Section 4.2) are reviewed in terms of how they perform in a Belgian context. In Section 5.2 benchmark simulations are carried out, using the (readily) available data. Section 5.3 then focuses on two specific cases, incorporating relevant terrain information and assessing the impact thereof.

5.1 Model evaluation

The model evaluation will be based on the simulated area at the end of the documented wildfire duration, throughout the remainder referred to as “End”, and the time at which the simulated area has reached the same size as the observed burnt area. The latter usually cannot be observed directly, since the perimeters are simulated at fixed time steps. It is thus inferred from a linear interpolation between the time instances leading to the last (“Inner”) simulated areas smaller than, and the first (“Outer”) larger than the observed burnt area. The area that is burnt between those time points is from here on referred to as the “Inter” area. These two characteristics are compared qualitatively and quantitatively with the observed perimeters, using maps and accuracy measures, respectively. The latter reflect the areas that are correctly simulated (True +), falsely simulated (False +), and falsely left unaffected (False –). These measures are expressed as area percentages of the hulls that enclose the observed and simulated (End or Outer) burnt areas.

5.2 Benchmark simulations

The rationale of a benchmark simulation, using the data and settings as described in Chapter 4, is to evaluate the models (in their currently available state) in what would be an operational setting. The results are first discussed per model, and a general discussion is presented in Section 5.4. Finally, since the wildfire duration is available only for the larger wildfires (Cases 1–4), these will be discussed separately from the smaller ones (Cases 5–7).

5.2.1 FARSITE

Cases 1–4

The results of the benchmark simulations for Cases 1–4 are presented in Figure 5.1 and Tables 5.1 and 5.2. It is apparent that FARSITE generally underestimates the burnt area during the documented wildfire duration (End); only for Case 1 the observed burnt area is reached in silico within the recorded time frame. In order to reach a simulated area that agreed with the observed one, the simulated time for Cases 2–4 had to be the double of the wildfire duration. Yet, the results beyond the documented end are highly speculative since these also passed the end of the recorded weather data. These results are rather surprising, as FARSITE is known to generally overestimate the ROS and burnt area (Finney, 2004).

Table 5.1: Burnt areas simulated with FARSITE and corresponding wildfire durations for Cases 1–4, as shown in Figure 5.1.

Case	End	Inner	Inter	Outer	Observed
1 Area (ha)	1544	1382	1399	1415	1399
Duration (min)	2280	2040	2055	2070	2280
2 Area (ha)	257	554	555	557	555
Duration (min)	3300	7920	7929	7950	3300
3 Area (ha)	279	393	396	400	396
Duration (min)	720	1620	1633	1650	720
4 Area (ha)	116	219	226	226	226
Duration (min)	450	1020	1049	1050	450

Table 5.2: Accuracy measures of FARSITE simulations for Cases 1–4, expressed as area percentages of the hull enclosing the simulated perimeters.

	Case 1		Case 2		Case 3		Case 4	
	End	Outer	End	Outer	End	Outer	End	Outer
True +	26.7	27.5	29.5	27.4	29.2	29.5	43.1	66.5
False +	39.8	36.6	11.5	36.4	24.2	35.6	5.3	16.7
False –	33.6	35.9	58.9	36.1	46.6	34.9	51.6	16.8

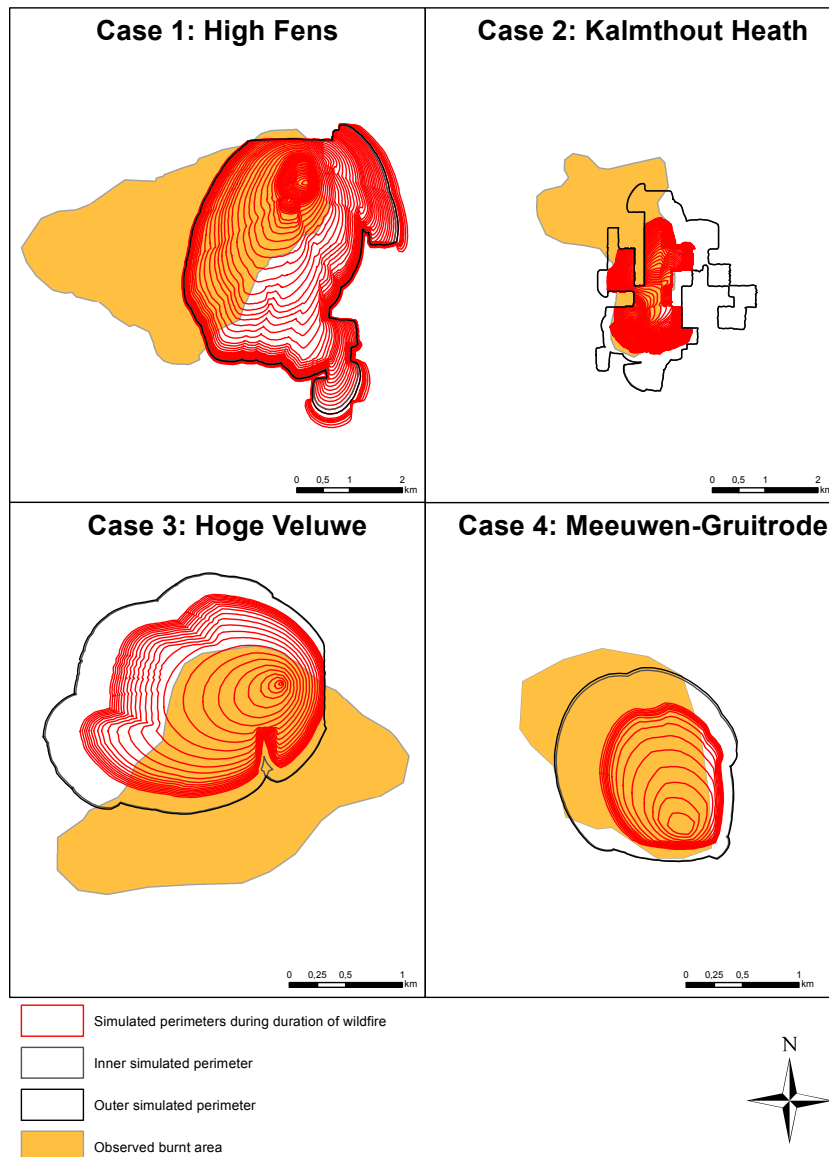


Figure 5.1: Results of FARSITE simulations for Cases 1–4.

From Figure 5.1 and Table 5.2 it is also clear that the simulated perimeters are of a poor quality. Within the recorded duration of the wildfire the true positives vary between 26.7 % and 43.1 %, while the false negatives go from 33.6 % up to 58.9 %. Simulations stretching beyond the observed wildfire duration only improve the quality for Case 4, raising the correctly simulated portion of the (outer) hull area to 66.5 %. For the other cases, increasing the simulation time does not significantly increase the percentage of true positives. On the contrary, it is even lowered by 2.1 % for Case 2. When we compare the in situ and in silico perimeters to the wind data (Figures 4.16–4.19), it is clear that the former closely align with the prevailing wind direction at the start of the wildfire (roughly the first half of the burning period), while the latter align with the wind direction at the end of the wildfire (roughly the second half of the burning period).

This can be explained as follows. Wildfires can initially spread relatively fast as they are not yet fought by fire fighters. When these commence their suppressive actions, the wildfire spread gets retarded, until it is eventually stopped. This is of course not a gradual process, as larger fires are more difficult or even impossible to stop and changing weather conditions can cause re-ignitions and sudden outbursts in different directions. Still, for our cases it can be stated that the larger part of the burnt area was reached in the first half of the burning period. However, as was mentioned before, no data regarding the actions of the fire fighters could be included in the simulations. This makes that the simulated spread is only governed by the weather data. Especially in Cases 1 and 2, the wind direction and speed change considerably in the second half of the burning period, which clearly affects the shape of the simulated fire perimeter. Moreover, due to the use of the acceleration submodel, the wildfire also spreads—under the same environmental conditions—at a higher ROS later on in the simulation.

Finally, the effects of the coarse fuel map resolution can clearly be observed for Case 2. This is due to the fact that the land cover in and around the Kalmthout Heath is relatively heterogeneous, as it is located very close to the WUI (Figure 4.10). Moreover, in Section 4.1 it was already explained that some dune areas inside the observed perimeter are (wrongly) classified as “urban and barren”. Since urban land is considered unburnable, the simulations are abruptly stopped when the fire front reaches such areas, as can be observed in Figure 5.1.

Cases 5–7

The results of these simulations are presented in Figure 5.2 and Tables 5.3 and 5.4. They are remarkably better in terms of the shape of the simulated perimeter. For the outer perimeters (Outer), the proportion of true positives varies between 57.7 % and 63.3 %, while the false negatives vary between 3.0 % and 16.7 %. Keep in mind, however, that these simulations are not restricted by a recorded burning period, like Cases 1–4, as no wildfire duration was recorded. Hence, it is expected that the simulated burning periods overestimate the true ones.

Table 5.3: Burnt areas simulated with FARSITE and corresponding wildfire durations for Cases 5–7, as shown in Figure 5.2.

Case	Inner	Inter	Outer	Observed
5 Area (ha)	80	80	120	80
5 Duration (min)	240	240	270	
6 Area (ha)	27	29	42	29
6 Duration (min)	150	153	180	
7 Area (ha)	11	22	23	22
7 Duration (min)	90	118	120	

Table 5.4: Accuracy measures of FARSITE simulations for Cases 5–7, expressed as area percentages of the hull enclosing the simulated perimeters.

	Case 5		Case 6		Case 7	
	Inner	Outer	Inner	Outer	Inner	Outer
True +	69.1	57.7	75.2	63.3	50.2	62.8
False +	15.4	37.0	10.1	33.7	0.0	20.4
False –	15.5	5.3	14.6	3.0	49.8	16.7

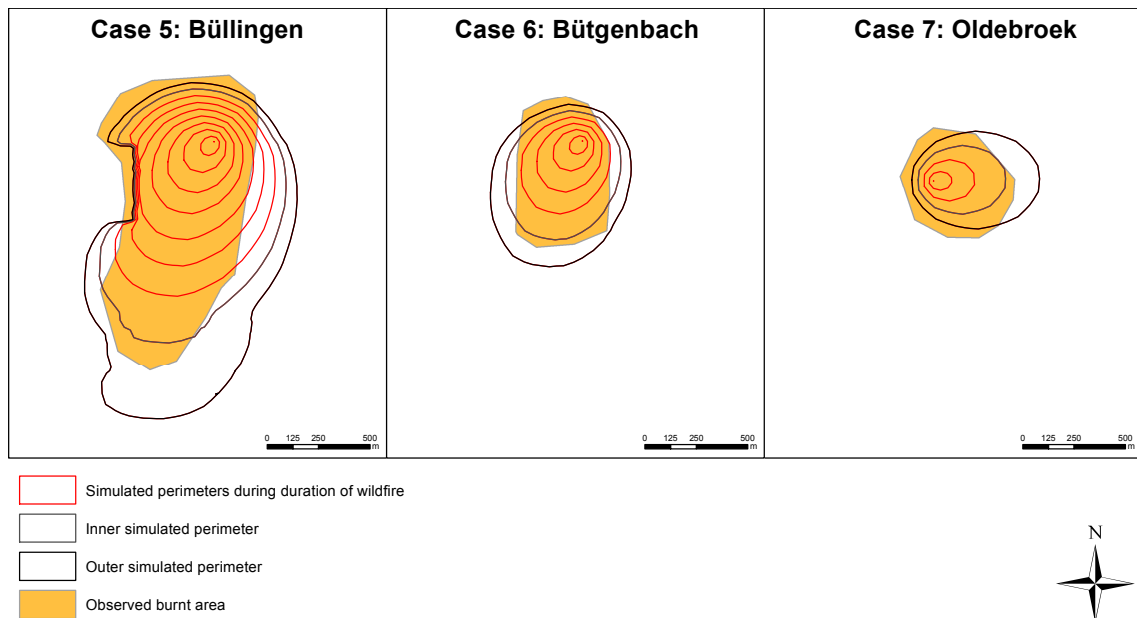


Figure 5.2: Results of FARSITE simulations for Cases 5–7.

5.2.2 ForeFire

Cases 1–4

The results of the benchmark simulations for Cases 1–4 with ForeFire are presented in Figure 5.3 and Tables 5.6 and 5.5. In contrast to the FARSITE simulations, these results do not underestimate the perimeter at the end of the documented wildfire periods (End). The observed burnt area is always reached within this time frame. Especially for Cases 1–2 these simulated times (13 and 10h, respectively) seem fairly realistic. For Cases 1–3 this leads to a proportion of true positives for Outer that is respectively 17.7 %, 7.2 % and 8.1 % higher than those obtained for the FARSITE simulations, whereas it is 4.5 % lower for Case 4. The proportion of false negatives is between 2.8 % and 8.9 % lower as compared to FARSITE. Hence, the ForeFire simulations of these cases are more accurate than those by FARSITE.

Table 5.5: Burnt areas simulated with ForeFire and corresponding wildfire durations for Cases 1–4, as shown in Figure 5.3.

Case	End	Inner	Inter	Outer	Observed
1 Area (ha)	11657	1333	1399	1420	1399
Duration (min)	2280	750	773	780	2280
2 Area (ha)	16287	511	555	568	555
Duration (min)	3300	570	593	600	3300
3 Area (ha)	1994	388	396	461	396
Duration (min)	720	330	333	360	720
4 Area (ha)	542	212	226	256	226
Duration (min)	450	240	250	270	450

Cases 5–7

The results of the ForeFire benchmark simulations for Cases 5–7 are presented in Figure 5.4 and Tables 5.8 and 5.7. These results are, in terms of true positives and false negatives, less accurate than those obtained with FARSITE. Moreover, it can be noticed that the shape of the western perimeter boundary for Case 5 is more accurately captured by FARSITE (Figure 5.2). Since the area beyond this boundary has a higher canopy cover percentage (Figure 4.13), the better performance of FARSITE in this respect can be attributed to its fuel moisture model. On average, the observed burnt area is reached approximately 30% faster with ForeFire, as compared to FARSITE.

Table 5.6: Accuracy measures of ForeFire simulations for Cases 1–4, expressed as area percentages of the hull enclosing the simulated perimeters.

	Case 1		Case 2		Case 3		Case 4	
	End	Outer	End	Outer	End	Outer	End	Outer
True +	12.0	45.2	3.4	34.6	16.8	37.6	41.8	62.0
False +	88.0	27.9	96.6	33.5	80.6	36.4	58.2	24.0
False –	0.0	26.9	0.0	31.9	2.5	26.0	0.0	14.0

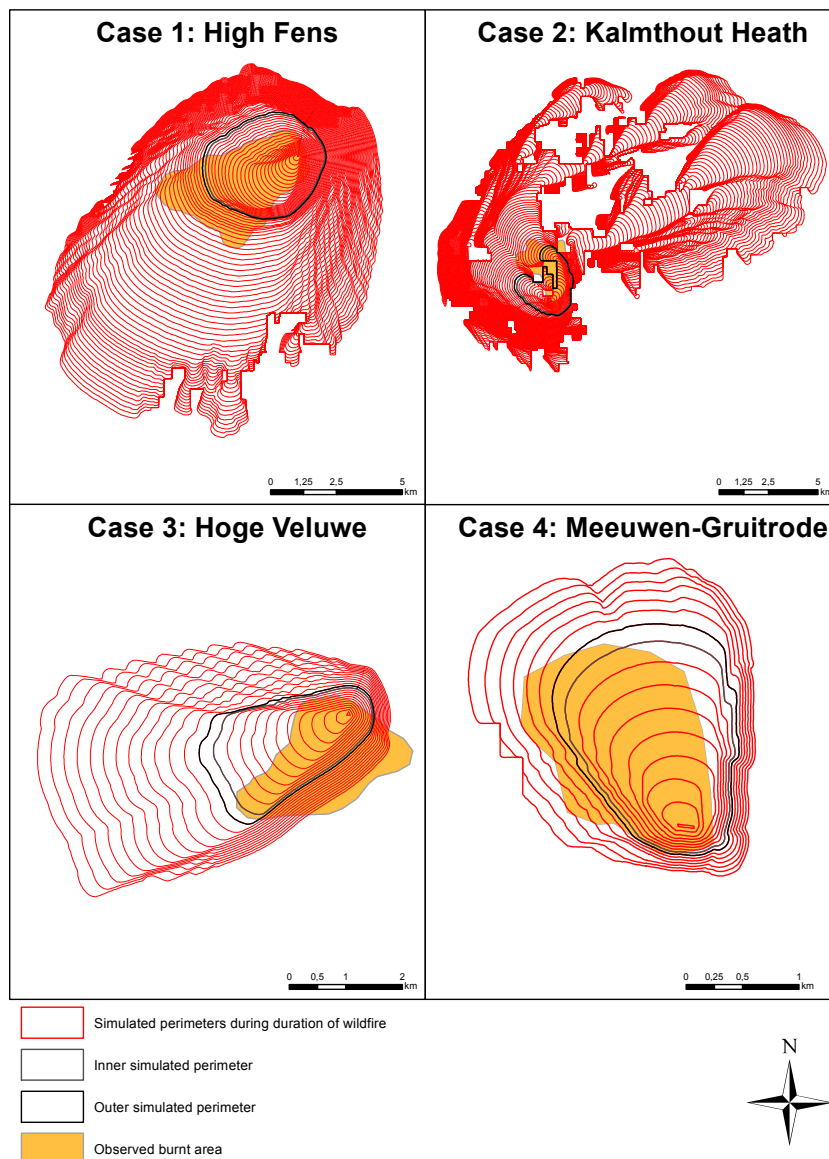


Figure 5.3: Results of ForeFire simulations for Cases 1–4.

Table 5.7: Burnt areas simulated with ForeFire and corresponding wildfire durations for Cases 5–7, as shown in Figure 5.4.

Case	Inner	Inter	Outer	Observed
5 Area (ha)	63	80	90	80
5 Duration (min)	150	169	180	
6 Area (ha)	22	29	39	29
6 Duration (min)	90	102	120	
7 Area (ha)	11	22	25	22
7 Duration (min)	60	84	90	

Table 5.8: Accuracy measures of ForeFire simulations for Cases 5–7, expressed as area percentages of the hull enclosing the simulated perimeters.

	Case 5		Case 6		Case 7	
	Inner	Outer	Inner	Outer	Inner	Outer
True +	59.7	61.1	69.9	62.8	47.6	49.4
False +	10.5	24.3	3.9	30.7	1.8	30.2
False –	29.8	14.5	26.2	6.5	50.6	20.3

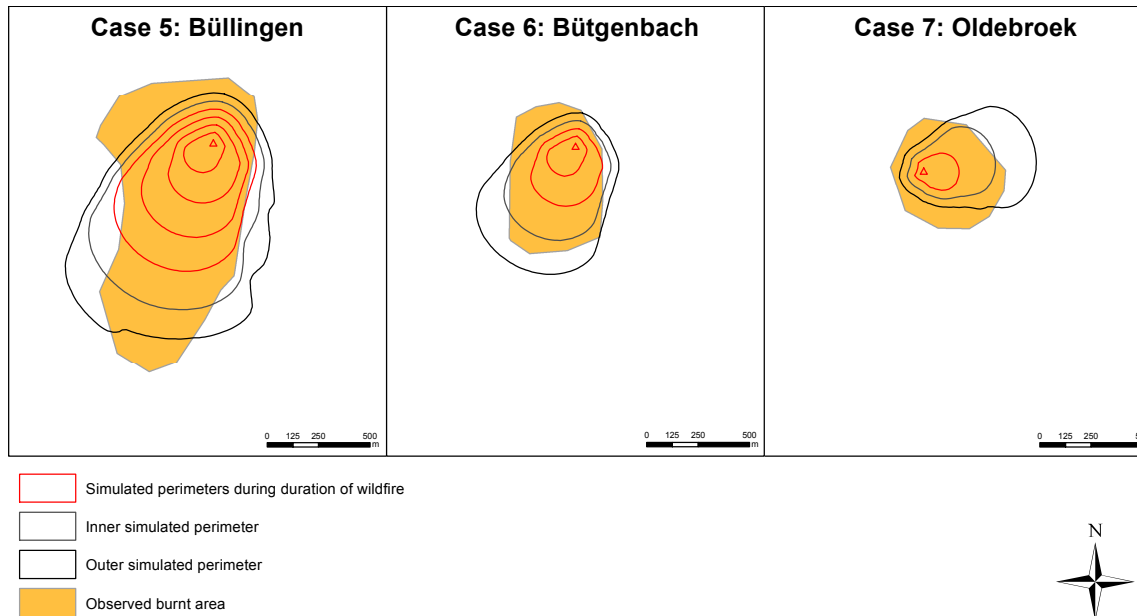


Figure 5.4: Results of ForeFire simulations for Cases 5–7.

5.3 Incorporation of detailed terrain information

In Section 4.1 it was revealed that the available geographic data are of a coarse spatial resolution and thus do not capture important details, such as roads. Hence, the relatively low accuracy of the simulation results in Section 5.2 should not come as a surprise. In order to improve the accuracy of the simulations for the two largest wildfires (Cases 1 and 2), their fuel maps are both adjusted to better reflect the terrain conditions.

5.3.1 Case 1

In this case, we added the main road at the west side of the observed perimeter, which acts as a barrier. The river Helle at the East side is also partly included. For the latter, we assumed that it acted as a barrier up to the point where it was crossed by the observed perimeter. These barriers were specified as separate GIS vector files in FARSITE. For ForeFire, they had to be included in the fuel map, of which the spatial resolution was increased to 10 m. These adjustments are presented along with the resulting simulation results in Figure 5.5. Tables 5.9 and 5.10 again provide the simulated areas and fire durations, and accuracy measures, respectively. The most obvious effect of including these barriers is the retardation of the simulations. Contrary to the benchmark simulations, the FARSITE simulations do now not reach the observed burnt area within the wildfire duration (Table 5.9). When comparing the outer simulated areas (Outer), a slight improvement in accuracy for both models is observed. Indeed, the proportion of true positives is approximately 4 % higher, while the proportions of false positives and negatives are both approximately 2 % lower.

Based on these results, adding barriers looks promising, since this wildfire was indeed stopped at the road and river (with or without the help of fire fighter actions). Furthermore, we could have included more (smaller) roads that coincide with the wildfire perimeter, as such increasing the accuracy of the (outer) perimeters. However, in reality, these roads will not always stop wildfires, as they could be crossed by spotting or, when overgrown by weeds for example, even by surface fires. Hence, including them in fuel maps that are to be used for operational purposes, should not be done without expert knowledge.

Table 5.9: Burnt areas simulated with FARSITE and ForeFire and corresponding wildfire durations for Case 1 with adjusted fuels, as shown in Figure 5.5.

Model		End	Inner	Inter	Outer
FARSITE	Area (ha)	1070	1392	1399	1425
	Duration (min)	2280	2640	2646	2670
ForeFire	Area (ha)	4813	1330	1399	1409
	Duration (min)	2280	810	836	840

Table 5.10: Accuracy measures of FARSITE and ForeFire simulations for Case 1 with adjusted fuels, expressed as area percentages of the hull enclosing the simulated perimeters.

	FARSITE		ForeFire	
	End	Outer	End	Outer
True +	33.0	31.1	29.0	49.4
False +	24.6	35.0	70.9	25.6
False -	42.4	33.9	0.1	25.1

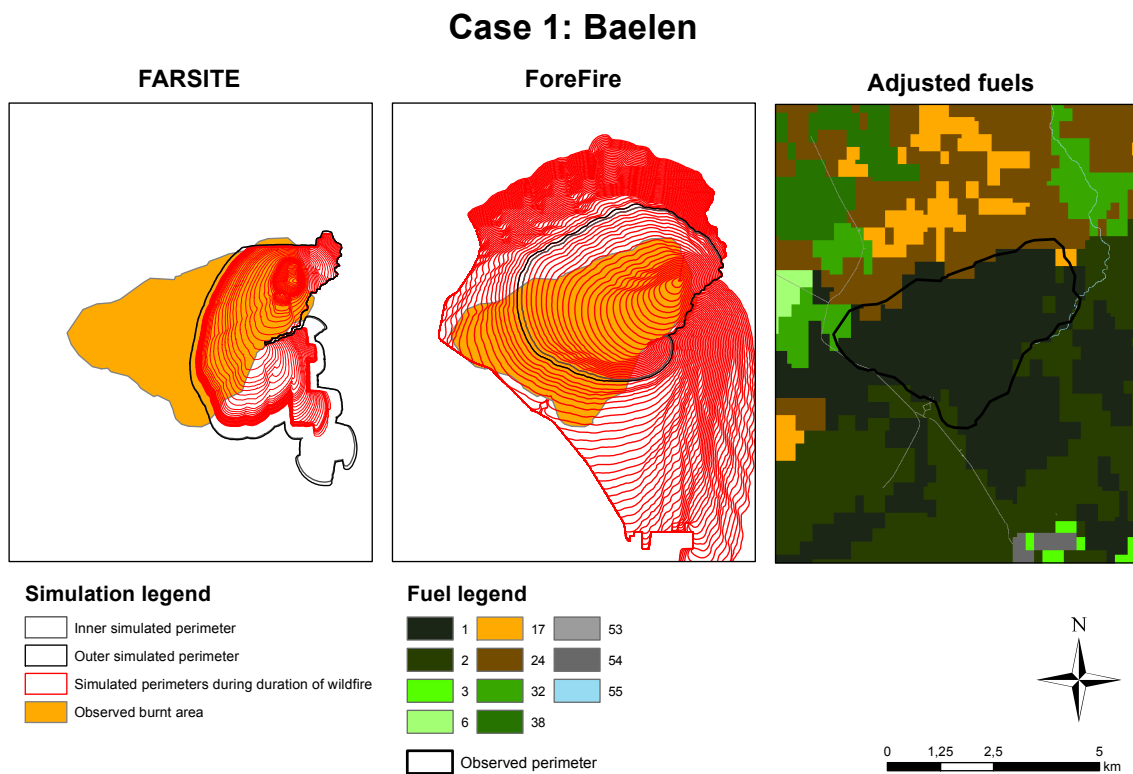


Figure 5.5: Results of FARSITE and ForeFire simulations for Case 1 with adjusted fuels.

5.3.2 Case 2

For this case, the original fuel data was adjusted by reclassifying the dune areas in the Kalmthout Heath from urban and barren to dune fuels (Figure 5.6). This increases the quality of the simulations for both models (Figure 5.6, Tables 5.11 and 5.12). The proportion of true positives of the outer simulated perimeters is approximately 15 % higher, as compared to those obtained with the original data (Table 5.2). This is due to the fact that the simulated fire is slowed down, rather than completely stopped when reaching dune areas. Hence, the simulations are also markedly sped up, as the observed burnt area is reached 23 % and 17 % faster with FARSITE and ForeFire, respectively (Table 5.11). From these results we may conclude that, given the coarse resolution of the available fuel maps, care should be taken when including unburnable wildland fuel classes, since these can act as impenetrable blockades. Mainly in areas close to the WUI, urban fuel types, such as large gardens, should be classified as burnable fuels.

Table 5.11: Burnt areas simulated with FARSITE and ForeFire and corresponding wildfire durations for Case 2 with adjusted fuels, as shown in Figure 5.6.

Model		End	Inner	Inter	Outer
FARSITE	Area (ha)	294	546	555	553
	Duration (min)	3300	6030	6069	6060
ForeFire	Area (ha)	18649	525	555	585
	Duration (min)	3300	480	495	510

Table 5.12: Accuracy measures of FARSITE and ForeFire simulations for Case 2 with adjusted fuels, expressed as area percentages of the hull enclosing the simulated perimeters.

	FARSITE		ForeFire	
	End	Outer	End	Outer
True +	32.0	43.0	3.0	48.8
False +	13.7	28.4	97.0	27.6
False -	54.3	28.6	0.0	23.6

Case 2: Kalmthout Heath

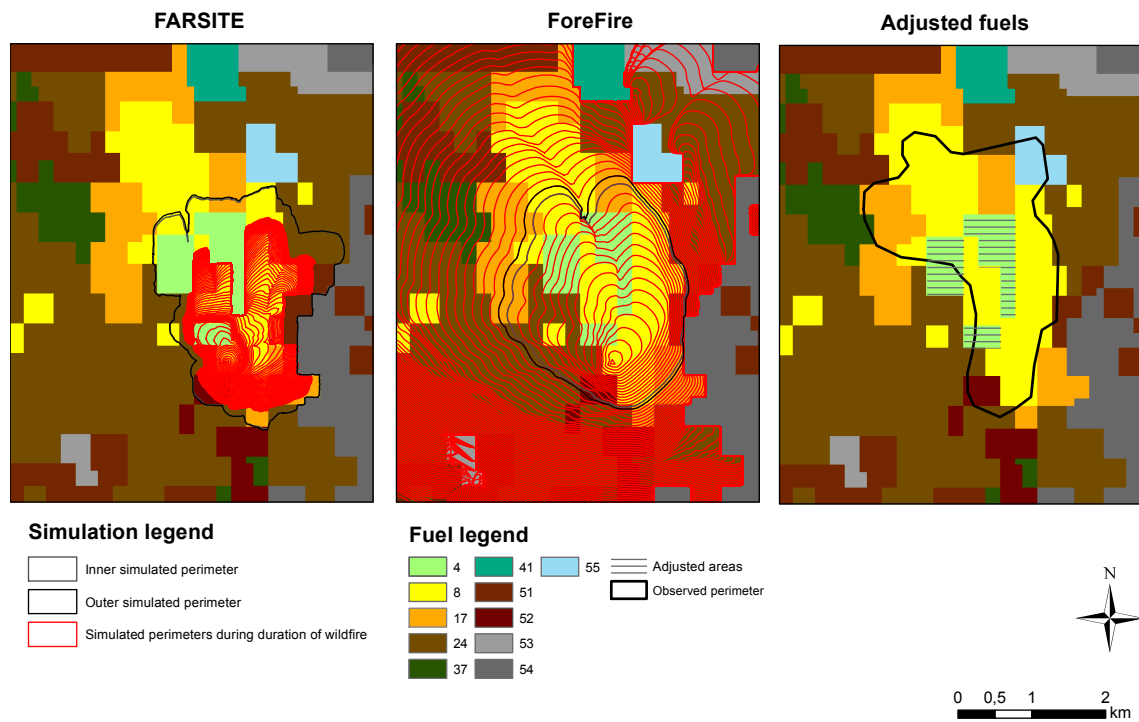


Figure 5.6: Results of FARSITE and ForeFire simulations for Case 2 with adjusted fuels.

5.4 General discussion and conclusion

Here we will present a more general discussion regarding the performance of FARSITE and ForeFire in an (operational) context for Belgium. The models will be evaluated on the basis of their simulations and their usability.

5.4.1 Simulation results

The simulations results obtained with FARSITE and ForeFire (Sections 5.2 and 5.3) are generally characterized by low accuracies, especially those for the two largest wildfires (Cases 1 and 2). This becomes even more striking when comparing our results with examples found in literature (see Figures 3.5 and 3.6). The reasons behind these low accuracies are hard to pin down, but the poor quality of the available data (see Section 4.1) clearly plays a major role. This relates to the coarse resolution of the GIS raster layers, uncertainty of the weather data (especially the wind vectors), and the limited and uncertain information on the progression of the wildfires (e.g. the ignition location, wildfire duration, recorded perimeters, and lack of data on fire fighter actions). Mainly the latter is troublesome for this study, as few conclusions can be drawn regarding the simulated wildfire dynamics.

Due to the coarse resolution of the available data, important terrain data such as roads are not included in the simulations, which also contributes to the low accuracies. Indeed, the (ad hoc) adjustments for Cases 1 and 2 (Section 5.3), resulted in (significantly) improved accuracies. Furthermore, the fuel models used by both simulators are not adequately calibrated for the Belgian fuels. These are based on classifications which were developed on continental scales and strongly simplify the actual fuel complex (Keane et al., 2001; Duka and Ioannilli, 2016). The development of detailed fuel maps will thus be a necessary step in making more effective wildfire simulators for Belgium. Indeed, Arca et al. (2007) and Salis (2008) also conclude from their evaluations of FARSITE in a Mediterranean context that reasonably accurate simulations are only to be expected when adapted fuel models are used. For the four Italian wildfires that were simulated with such models, the reported simulation results are significantly more accurate than the simulated (End and Outer) perimeters that were presented here, with on average 62 % true positives and 2 % false negatives. Since most (large) wildfires in Belgium and the Netherlands are located in moors and heathlands, a focus on mapping and classifying these vegetation types might be a good starting point.

In contrast to the geographical data, the uncertainty of weather data is only expected to increase in an operational context. In the presented simulations, this uncertainty stems mainly from measuring and interpolation errors of the historical data. In an operational context, the meteorological data will come from extrapolated on-site measures or mesoscale weather models, which are characterized by even higher uncertainties.

There is a large difference between the FARSITE and ForeFire simulations, mostly with respect to their dynamics. The simulations with ForeFire overestimate the burnt area within the documented fire duration—as was expected in these worst-case simulations—while those with FARSITE generally underestimate the spread. As was mentioned, the latter comes as a surprise, when comparing with the literature. Indeed, Salis (2008) performed simulations with the standard fuel models for four Italian wildfires between 19 ha and 145 ha, and reports simulated areas that are 1.5 up to 15 times the observed ones. Moreover, the simulations by Jahdi et al. (2015) also resulted on average in (slight) overestimations of the burnt areas (Figure 3.5). For the optimal combination of standard fuel models, they report simulated burnt areas that are on average 14 % larger than the observed ones. A possible reason for the underestimation observed here might again be the poor quality of the (fuel) data used, since FARSITE relies on complex and data-driven submodels. Moreover, it can not be ruled out that for some of the latter, suboptimal default settings for the were used. ForeFire, on the other hand, is in its current version much simpler than FARSITE and relies on fewer data inputs. Hence, it is mostly affected by wind speed and direction. This brings us to another main conclusion. The presented simulations do not provide more relevant information than the fact that the wildfires will spread mainly along the prevailing wind direction, so their added value in an operational context would be very limited.

5.4.2 Usability

An important aspect concerning the practical usability of operational real-time wildfire simulators is their computational cost. In this aspect, FARSITE and ForeFire scored comparably well, as the corresponding simulations are completed much faster than real-time on a desktop machine. Perimeters smaller than 1500 ha are, at the current settings and resolutions, simulated within a minute. However, if more detailed data—with a higher spatio-temporal resolution—would be used, the required computational power and simulation time are expected to increase. Furthermore, we only accounted for the simulation time, while neglecting the time spent on (manual) preparatory work (e.g. generating simulation files) or communication. This brings us to the second and final aspect, namely the ease of use, which was generally bad for both models. Although FARSITE is the most user-friendly, it still requires training and expert knowledge. This is due to the fact that there are numerous options, settings, and data requirements. Moreover, it is not regularly updated and still contains bugs. ForeFire, on the other hand, is still in the early development stage. Hence, it requires (basic) programming knowledge and is thus only usable for researchers and developers.

From all this, we may conclude that both models are not yet ready to be used in an operational setting for Belgium.

CHAPTER 6

Calibration and evaluation of the CA-based model

As described in Section 4.2.3, the CA-based model by Depicker et al. (2016) still requires calibration before it can be applied for simulation purposes. Depicker et al. (2016) have made a first attempt in doing so, using the three perimeters of the Baelen wildfire (Case 1) and a repeated hill climbing algorithm (Russell and Norvig, 2010) that minimises the difference between the observed and simulated burnt areas. Yet, this calibration has two main weaknesses. Firstly, it lacks a validation step, due to the very limited dataset. Secondly, it uses the three observed EFFIS perimeters (Figure 4.2) as time-stamped snapshots, while it was shown in Section 4.1 that these are not reliable. Hence, Sections 6.1–4 aim at recalibrating the CA-based model and evaluating it in the light of its applicability in an operational context. In Section 6.4 we will assess the sensitivity of the calibrated model, with respect to uncertainty in the wind data inputs, by means of a global sensitivity analysis. Finally, Section 6.5 we will give some concluding remarks on the results of this chapter.

6.1 Evaluation of pre-calibrated parameters

Before recalibrating the CA-based model, the parameter set obtained by Depicker et al. (2016) is evaluated for the new data of Case 1 (Table 4.3, Figures 4.9 and 4.16). These parameter values ($\alpha = 1$, $\psi_1 = 9.3$, $\psi_2 = 7.9$, $\psi_3 = 6.6$, $\psi_4 = 5.7$, and $n_{burn} = 15$) were obtained under the assumption that the dates in the meta-data of the three EFFIS perimeters are real time stamps. Hence, the simulated period between the first and last perimeter is 5 days, which is more than three times the reported wildfire duration (Table 4.3). Since Δt and the wildfire duration—and thus the resulting number of simulated steps (n_{steps})—derived from the new data differ from those in Depicker et al. (2016), the parameter interpretations also differ (see Section 4.2.3). This is most notably for n_{burn} , and its value is therefore rescaled, so that the ratio n_{burn} to n_{steps} remains constant, resulting in a new value of 19. A burn frequency

map resulting from 100 repeated simulations using this modified parameter set is shown in Figure 6.1. The value of each cell c_i in this map is the fraction (f_i) of the simulations in which the cell had ignited by the last time step. Average accuracy measures are obtained by taking the sum of f_i over the truly predicted, overestimated and underestimated areas, and subsequently dividing these values by the area (S_h) of the hull enclosing the observed (O) and simulated burnt cells. These measures are thus given by

$$T_+ = \sum_{i|c_i \in O} \frac{f_i}{S_h}, \quad (6.1a)$$

$$F_+ = \sum_{i|c_i \notin O} \frac{f_i}{S_h}, \quad (6.1b)$$

$$F_- = \sum_{i|c_i \in O} \frac{1 - f_i}{S_h} \quad (6.1c)$$

$$S_h = \sum_O 1 + \sum_{i|c_i \notin O} f_i. \quad (6.1d)$$

As such, no subjective thresholds had to be employed for determining which parts of the burn frequency maps are considered to be burned or not. Equations (6.1a–c) resulted in 15% true positives (T_+), 3% false positives (F_+), and 82% false negatives (F_-), which is considerably less accurate than the measures reported by Depicker et al. (2016) (i.e. approximately 61%, 23%, and 17%, respectively). This can be attributed to following reasons. Firstly, the average wind speed during the wildfire is 36% lower in the new data. Secondly, $\psi_{1,2,3,4}$ are not rescaled, though the number of time steps (and hence their practical interpretation) differs. Last but not least, the fact that Depicker et al. (2016) calibrated starting from a well-developed initial perimeter has probably the largest effect on the parameter values, since this calibration did not include the initial acceleration phase of the wildfire.

6.2 Case-dependent calibration

6.2.1 Method

The next step in the calibration of the CA-based model is to perform a similar procedure as Depicker et al. (2016) on the larger and more accurate dataset containing Cases 1–4 (Section 4.1). The goal is to assess for every case if there exists a parameter set that results in accurate simulations of the observed burnt area. This problem of finding an optimal parameter set is tackled by minimizing an objective function (Ω):

$$\Omega = \frac{F_- + F_+}{T_+}. \quad (6.2)$$

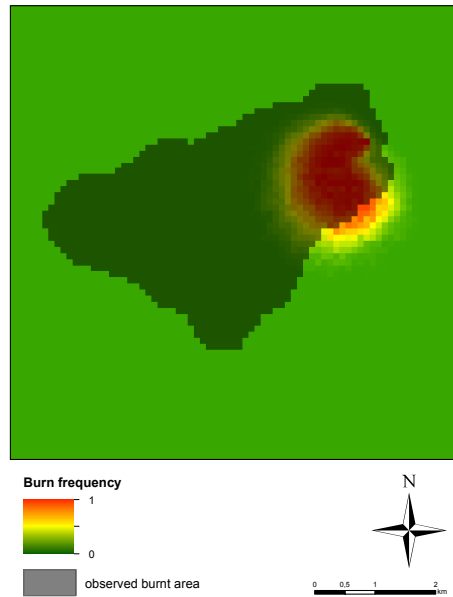


Figure 6.1: Burn frequency map of Case 1 resulting from 100 repeated simulations of the CA-based model with $\alpha = 1$, $\psi_1 = 9.3$, $\psi_2 = 7.9$, $\psi_3 = 6.6$, $\psi_4 = 5.7$, and $n_{burn} = 19$.

A quick assessment of the variability of Ω was done by evaluating this function ten times for different numbers of simulations (Figure 6.2). This was performed for Case 4, using the rescaled parameter set found by Depicker et al. (2016). Note that the variability of the values of Ω seems to become relatively limited from 24 repetitions. Based on this result and practical considerations regarding the available computational power, this number of repetitions is used when evaluating Ω during the calibration stage. The resulting burn frequency maps, obtained with the optimal parameter set, are generated on the basis of 48 runs, for the sake of (smoother) visualisation.

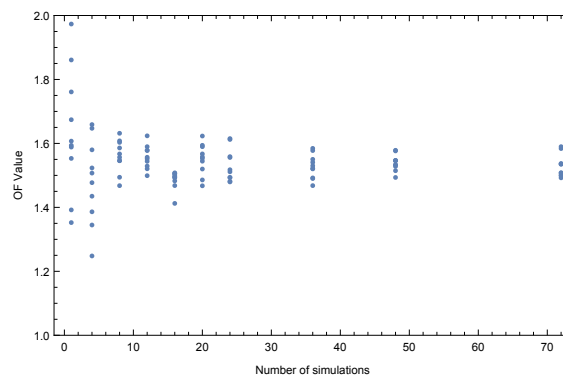


Figure 6.2: Variability of the values of Ω with respect to the number of repeated simulations.

Additionally, some constraints are imposed when solving the optimisation problem, namely that all parameters are positive and that n_{burn} is an integer smaller than n_{steps} . The Nelder-Mead method (Nelder and Mead, 1965), as implemented in Wolfram Mathematica (Wolfram Research Inc., 2016), is used for finding the (global) minimum of this constraint minimisation. The optimal parameters of the calibration by Depicker et al. (2016) are used as a starting point for this method, with the exception of n_{burn} , for which the initial value $n_{steps}/2$ is chosen. Finally, the calibration was performed for both CA1 and CA2 (Section 4.2.3).

6.2.2 CA1

Two things immediately catch the eye, when observing the evolution of the Ω -values versus the number of evaluations of the Nelder-Mead algorithm (Figure 6.3). Firstly, all but Case 2 converge to (relatively) stable Ω -values within 50 evaluations. Secondly, there is a large difference between Cases 1 and 4 on the one hand, and Cases 2 and 3, on the other hand, both in terms of the optimal Ω value and the variability after convergence. Only for Case 4 the optimal Ω value found is lower than 1, meaning that there are more true positives than falsely simulated cells, and for Case 1 this value is just above 1. For Case 2 and 3, the optimal values are considerably higher. This distinction between the cases is also visible in the values of $\psi_{1,2,3,4}$ of the optimal parameter sets (Table 6.1). These values are very similar for Cases 1 and 4, but differ considerably from those of Cases 2 and 3, which are much higher. The latter leads to spread probability values (p_j) that are very close to 1, when wind and slope are aligned with the spread direction, and very close to 0 when this is not the case (Eq. (4.5b)). Conversely to $\psi_{1,2,3,4}$, n_{burn} varies greatly between all cases, leading to cell burning durations between 6 h and 22 h.

The burn frequency maps, obtained with the optimal parameter sets are presented in Figure 6.4 and Table 6.2. For all cases, the most distinctive feature of these maps is the generally round shape of the burnt areas. This indicates that the simulated wildfire spread depends little on the wind data, which is caused by the high $\psi_{1,2,3,4}$ values.

Note that the shapes and accuracy measures of the burn frequency maps for Cases 1, 3, and 4 are still similar to those of the outer simulated perimeters obtained with FARSITE (Figure 5.1, Table 5.2), and—to a lesser extent—to those obtained with ForeFire (Figure 5.3, Table 5.6). The latter is probably due to the fact that the CA-based model was calibrated using the entire reported wildfire durations, whereas the outer perimeters of ForeFire are reached (much) sooner. The burn frequency map for Case 2 differs more from the ones found with both FARSITE and ForeFire, since the CA-based model is less affected by heterogeneous fuel map of this case, than the other models. Yet, the patterns of the underlying p_{veg} data are still visible (Figure 4.8(b)). Finally, the burn frequency maps overestimate the observed burnt areas, except for Case 3, which is slightly underestimated. This overestimation is greatly due to the roundness of the simulated perimeters.

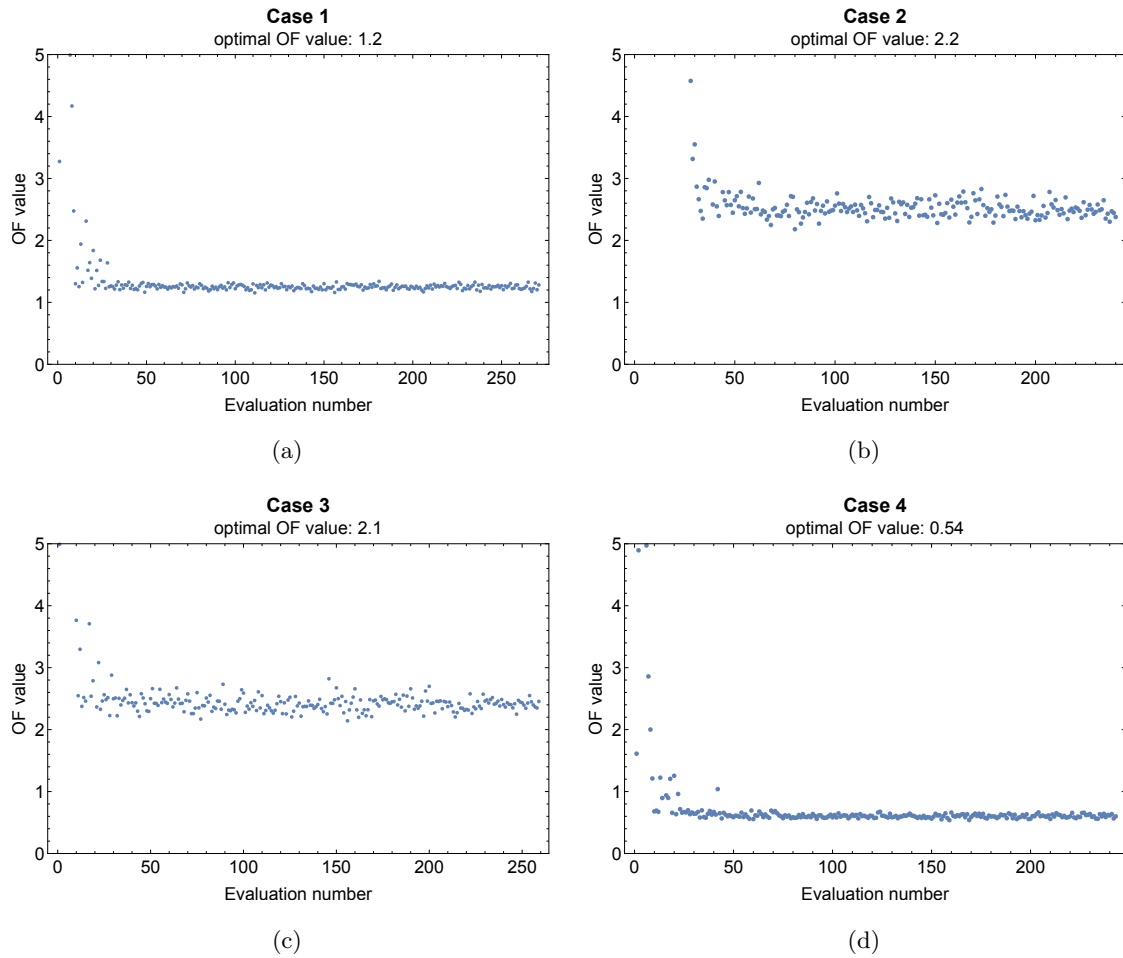


Figure 6.3: Value of the objective function Ω (OF) versus the number of evaluations by the Nelder-Mead algorithm in the case-dependent calibration of CA1 for Cases 1–4.

Table 6.1: Optimal parameter sets for the case-dependent calibration of CA1.

Case	α	ψ_1	ψ_2	ψ_3	ψ_4	n_{burn}
1	1	13.66	11.46	12.58	7.50	177
2	1	52.05	39.12	35.74	31.13	78
3	1	19.77	17.71	15.74	10.71	60
4	1	13.90	11.77	11.72	6.71	49

Table 6.2: Accuracy measures and burnt areas of the simulations obtained with the case-dependent calibrated parameter set of CA1 for Cases 1–4.

	Case 1	Case 2	Case 3	Case 4
True +	44.5	27.4	29.3	62.5
False +	16.5	52.7	35.2	25.8
False –	39.0	19.9	35.6	11.7
Area (ha)				
Simulated	1912	937	395	273
Observed	1398	553	397	229

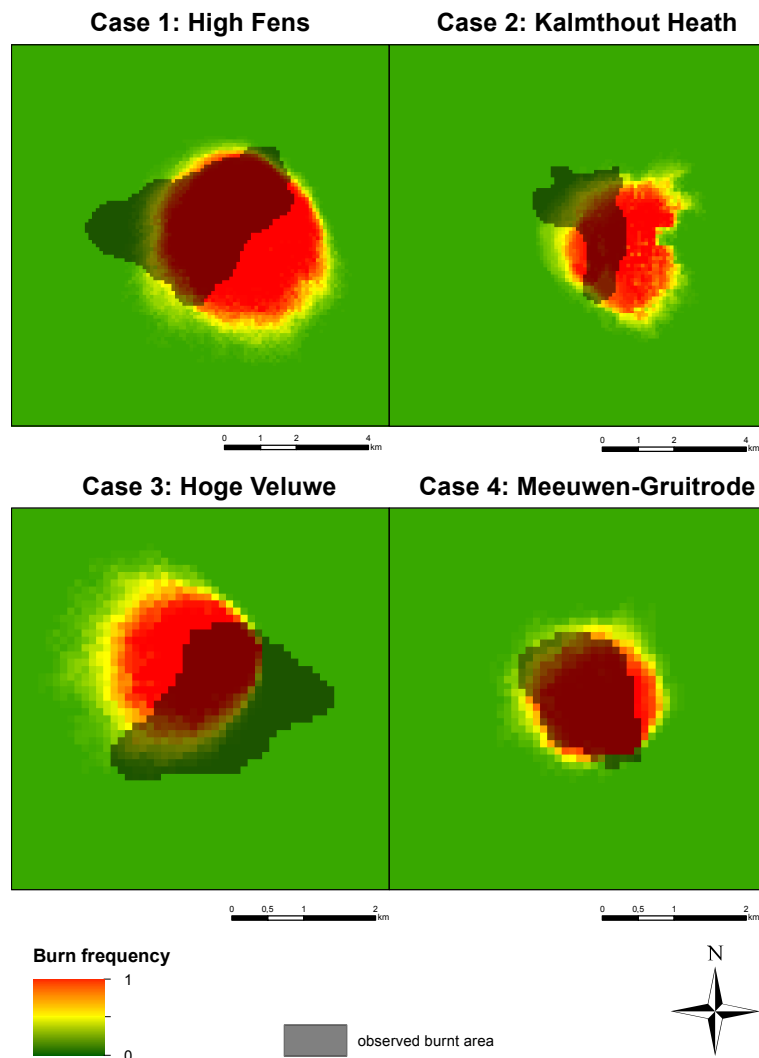


Figure 6.4: Burn frequency maps obtained with the case-dependent calibrated parameter set of CA1 for Cases 1–4.

6.2.3 CA2

The calibrated parameters of CA2 are presented in Table 6.3. The evolution of the Ω values differs little from the one of the calibration of CA1, and is thus not reported explicitly. Yet, the number of evaluations before convergence is about 1.5 times higher for all cases.

Looking at the calibrated α -values, we again perceive a distinction between Cases 1 and 4, and Cases 2 and 3. While the α -values of the former two cases stay relatively close to unity, those of the latter, are more extreme. For Case 3, this cancels the effect of p_{veg} (Figure 4.8(b)). Introducing the extra parameter also has an effect on the other parameters. This is most striking for Case 2, for which ψ_{1-4} are all approximately 80% lower, while n_{burn} is almost three times higher, compared to the values for CA1 (Table 6.1). It is also the only case for which the new parameter set significantly affects the resulting burn frequency map, largely by increasing the simulated burnt area (Figure 6.5, Table 6.4).

Table 6.3: Optimal parameter sets for the case-dependent calibration of CA2.

Case	α	ψ_1	ψ_2	ψ_3	ψ_4	n_{burn}
1	0.94	16.96	13.12	11.90	9.18	236
2	0.29	10.08	7.64	8.03	6.18	306
3	4.21	25.37	20.06	17.20	13.23	76
4	1.36	19.14	15.57	13.52	10.73	51

Table 6.4: Accuracy measures and burnt areas of the simulations obtained with the case-dependent calibrated parameter set of the CA2 for Cases 1–4.

	Case 1	Case 2	Case 3	Case 4
True +	44.6	27.3	28.8	62.1
False +	37.3	65.9	37.2	26.0
False –	18.1	6.8	34.0	11.9
Area (ha)				
Simulated	1826	1512	417	273
Observed	1398	553	397	229

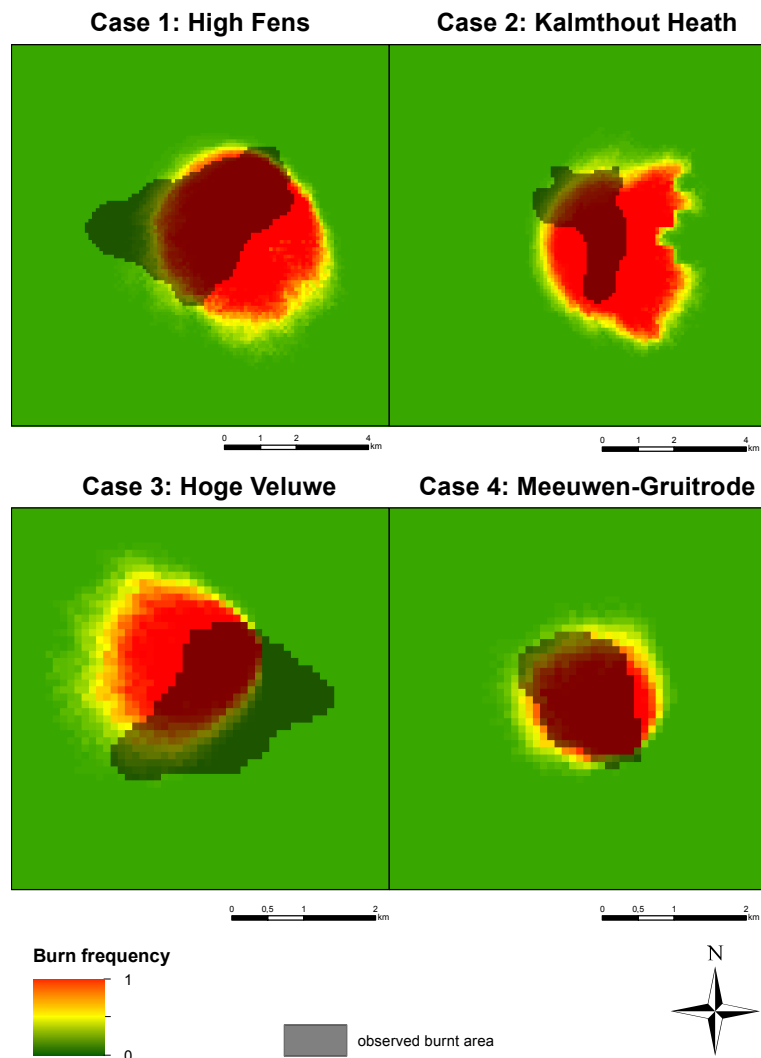


Figure 6.5: Burn frequency maps obtained with the case-dependent calibrated parameter set of CA2 for Cases 1–4.

6.3 Overall calibration

As a last step in the calibration, the predictive power of the CA-based model is assessed. Considering our small dataset, we opt for a leave-one-out-cross-validation method, which uses three cases for calibration and subsequently validates with the remaining case. During this calibration stage, the three cases are evaluated simultaneously in every evaluation, and the Ω is now the average of the objective function that was used for the case-dependent calibration (Eq. 6.2). As the latter is defined as a ratio of areas, all cases are treated regardless of their size or duration.

Figure 6.6 shows that the Nelder-Mead algorithm converges within 50 evaluations for all cases. Note that, if Case 2 is included in the calibration (Figures 6.6(a),(c),(d)), Ω converges to values between 2.6 and 3.1, while a significant improvement in the (optimal) Ω -value is observed when it is left out (Figure 6.6(b)). The resulting parameter set is also markedly different from the others (Table 6.5), as is the resulting burn frequency map (Figure 6.7 and Table 6.6). Including Case 2 in the calibration dataset results in substantial underestimations of the burnt area, and when used for validation, the burnt area is overestimated. This does not really come as a surprise, since similar observations were made with the ForeFire simulations (Figure 5.3).

The overall calibration was also performed for CA2. However, since the results thereof did not provide more relevant information, these are not further discussed here.

Table 6.5: Optimal parameter sets for the overall calibration of CA1.

Case	α	ψ_1	ψ_2	ψ_3	ψ_4	n_{burn}
1	1	28.60	25.08	23.60	13.62	77
2	1	17.61	15.89	13.42	9.31	133
3	1	23.81	18.64	20.70	10.80	266
4	1	26.46	23.22	21.08	13.08	245

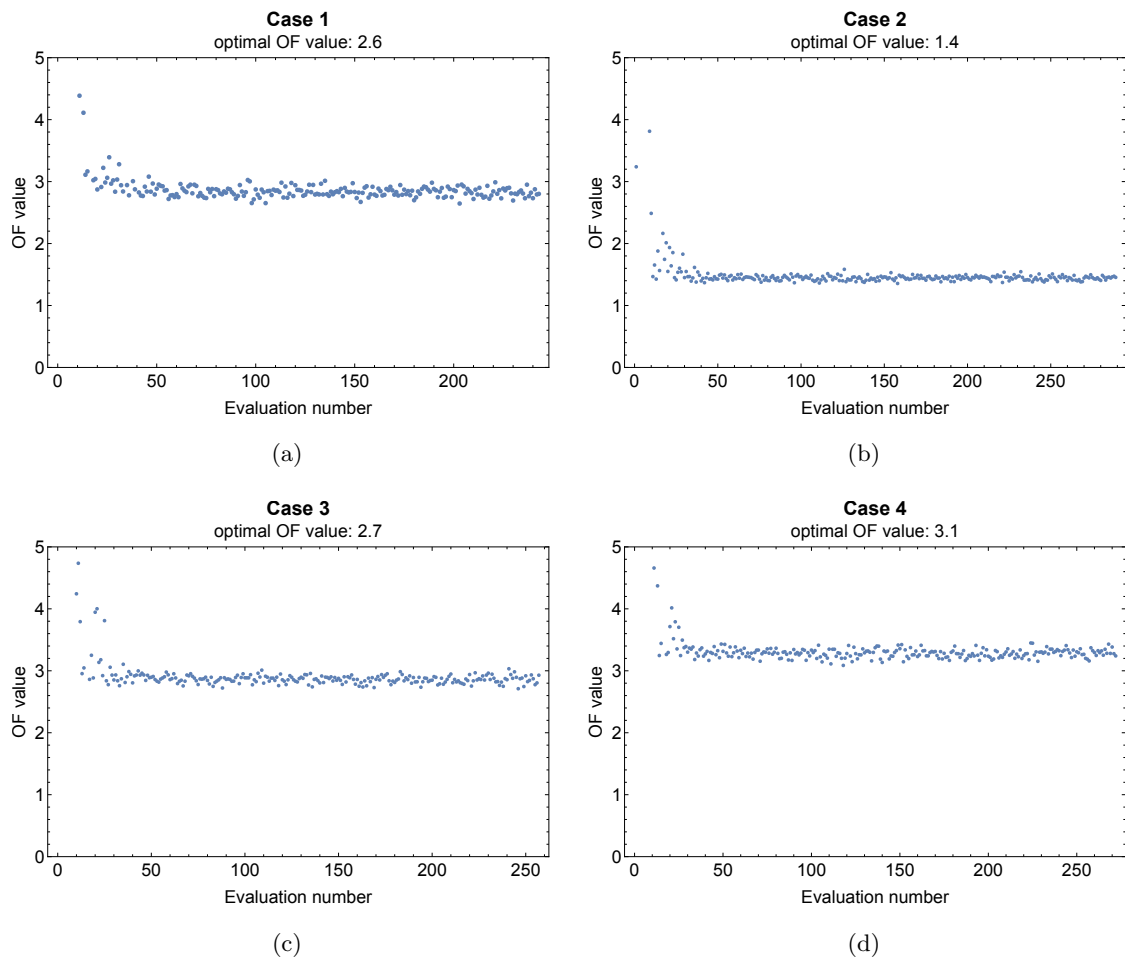


Figure 6.6: Value of the objective function Ω (OF) versus the number of evaluations by the Nelder-Mead algorithm in the case-dependent calibration of CA1 for Cases 1–4, using the remaining three cases as calibration data.

Table 6.6: Accuracy measures and burnt areas of the simulations obtained with the overall calibrated parameter set of CA1 for Cases 1–4.

	Case 1	Case 2	Case 3	Case 4
True +	23.8	10.1	27.1	38.2
False +	8.1	89.9	19.6	5.4
False –	68.1	0.0	53.2	56.4
Area (ha)				
Simulated	485	5476	231	106
Observed	1398	553	397	229

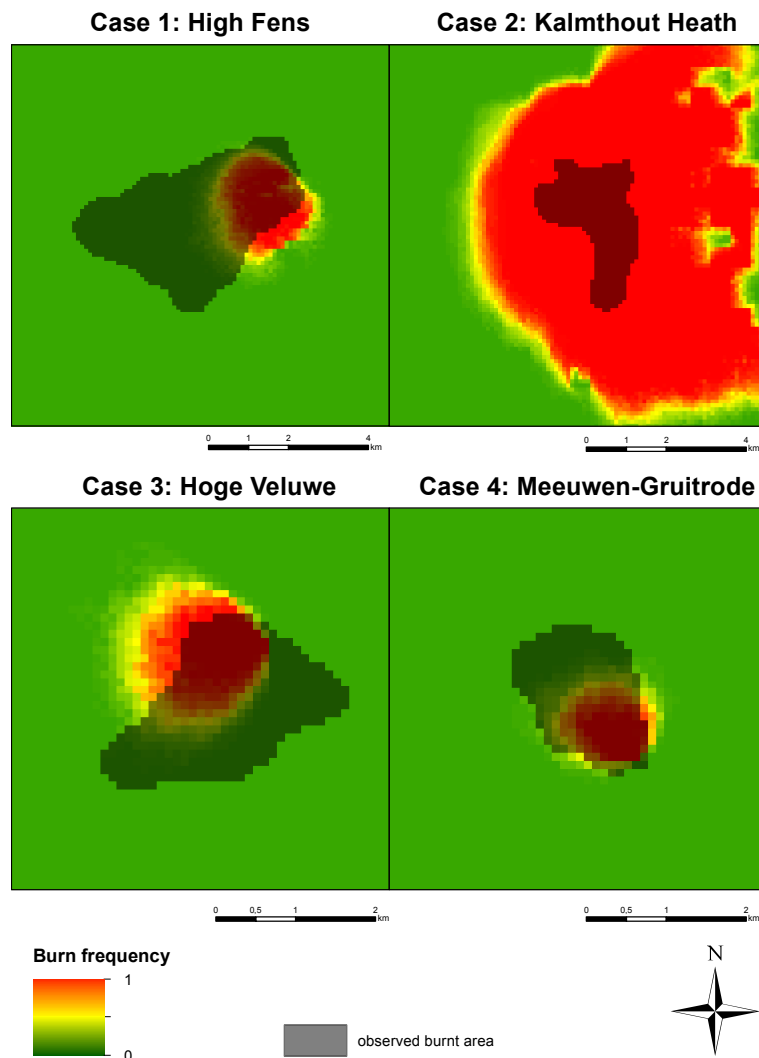


Figure 6.7: Burn frequency maps obtained with the overall calibrated parameter set of CA1 for Cases 1–4.

6.4 Sensitivity analysis

As was mentioned throughout this dissertation, wildfire spread models are characterised by many uncertainties. Hence, it is informative to examine how these uncertainties propagate through the simulations and what their main sources are. The designated method for this purpose is a combined uncertainty and global sensitivity analysis (GSA) (Lilburne and Tarantola, 2009; Ligmann-Zielinska, 2013; Saltelli et al., 2008). Depicker et al. (2016) have performed a GSA of the calibrated model parameters of their CA-based wildfire model (Section 4.2.3). This GSA was not spatially explicit, in that it used aggregated statistics of the simulations, rather than their outputs (Ligmann-Zielinska, 2013). Here, we will perform a spatially explicit GSA of the wind direction and speed for the Case 2 (Figure 4.17(a)). The goal is to construct sensitivity maps that reveal whether or not the (calibrated) model outputs are sensitive to uncertainties in the wind (direction and speed) data inputs, and if so, which areas are most affected by these uncertainties.

6.4.1 Method

Ligmann-Zielinska (2013) proposes a spatially-explicit GSA, which is used in this section. The method is model-independent, meaning that it does not rely on assumptions regarding the model structure. The GSA is based on repeated simulations with varying inputs, which are sampled from probability distributions. The model's sensitivity to the involved inputs is subsequently assessed by assigning proportions of the total variance in the outputs to these inputs. Finally, these variances are used to compute sensitivity index (SI) values, so that a high SI value indicates a high sensitivity of the model to the input. As the GSA is spatially-explicit, SIs are calculated independently for each of the cells. Hence, the result is a sensitivity map for all input parameters under study.

Parameter sampling

In our GSA the sensitivity of CA1 is analysed with respect to two inputs, namely the wind direction and wind speed. Their perturbations are obtained by adjusting the wind data (Section 4.17(a)) as follows

$$\tilde{\mathbf{w}} = \delta_U \begin{bmatrix} \cos \delta_\theta & -\sin \delta_\theta \\ \sin \delta_\theta & \cos \delta_\theta \end{bmatrix} \cdot \mathbf{w}. \quad (6.3)$$

As such, the wind vector \mathbf{w} is rotated counter-clockwise by δ_θ degrees and rescaled by a factor δ_U . The values of δ_U and δ_θ are constant as we want to assess the model's sensitivity for a constant bias on the wind data (e.g. due to interpolation or measurement errors). In order to find appropriate distributions for these parameters, we compared the average wind direction and speed, during the entire wildfire duration of Case 2, of the ten weather stations closest to

the observed perimeter (Figure 6.8). The widths of the ranges of these averages are 38° and 2.94 ms^{-1} , respectively. In order to prevent preferential sampling, we chose to sample the adjusted wind direction and speed within ranges around the original values, that are of the same width as the those of the values in Figure 6.8. Hence, δ_θ and δ_U are randomly sampled from the uniform distributions $U(-19, 19)$ and $U(0.6, 1.4)$, respectively.

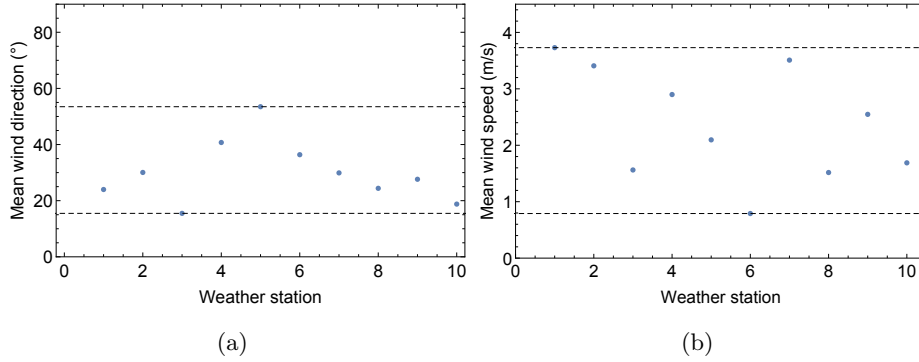


Figure 6.8: Mean wind direction (a) and speed (b) data during the entire wildfire duration of Case 2, from ten weather stations (station 1 is closest to the observed perimeter, 10 is the furthest). Minimal and maximal values are marked with dashed lines.

Calculation of sensitivity maps

For calculating the sensitivity indices, the method of Sobol' was used (Sobol', 1993), which consists of four steps. Firstly, two matrices A and B , of dimensions $(N, 2)$, are constructed by sampling N sets $(\delta_\theta, \delta_U)$. Here, we have chosen N to be 1000. Secondly, two extra matrices C_1 and C_2 are created using the first and second column from A , respectively, and the other column from B . Thirdly, the CA-based model is evaluated for the N parameter sets in A , C_1 , and C_2 by constructing the burn frequency map with 48 repeated simulations, as described in Section 6.2. As such, we also account for the intrinsic stochasticity of the model. We used the parameter set resulting from the case-dependent calibration of CA1 (Table 6.1). The resulting outputs are vectors of length N , denoted as \mathbf{y}_A , \mathbf{y}_{C_1} , and \mathbf{y}_{C_2} , for every cell of the grid. Hence, for every cell c_i , the j th element of \mathbf{y}_M , denoted as $y_M^{(j)}$, corresponds with its burn frequency value f_i in burn frequency map resulting from the j th input set in matrix M .

In the fourth and final step, the so-called first-order sensitivity indices are estimated as

$$\hat{S}_i = \frac{\frac{1}{N} \sum_{j=1}^N y_A^{(j)} y_{C_i}^{(j)} - \left(\frac{1}{N} \sum_{j=1}^N y_A^{(j)} \right)^2}{\frac{1}{N} \sum_{j=1}^N \left(y_A^{(j)} \right)^2 - \left(\frac{1}{N} \sum_{j=1}^N y_A^{(j)} \right)^2}. \quad (6.4)$$

Following Ligmann-Zielinska (2013) we only calculated \hat{S}_i for cells where f_i varies considerably across the N evaluations of matrix A , since Eq. (6.4) becomes unstable at low variances due to values near zero in the denominator. As such, only cells for which the variance in \mathbf{y}_A exceeds 0.01 are considered in the GSA.

6.4.2 Results and discussion

Figure 6.9(a) illustrates the burn frequency map, obtained with the original wind data, along with the burn frequency variance map, calculated from \mathbf{y}_A . The latter indicates that the highest variances are located in areas where the burn frequencies are approximately 0.5, which is expected when most of the uncertainty in the model output results from the model's intrinsic variability. However, also some regions with high variances correspond to low burn frequency values, mainly in the north(-western) corner of the observed perimeter. This suggests that still some part of the variance can be related to uncertainty in the wind data. The sensitivity maps in Figure 6.9(b) indicate that the model is mostly sensitive to variations in the wind direction and largely insensitive to those in the wind speed.

It should be noted that the S_i values of some cells dropped below zero or exceeded unity, which is, according to the theory, impossible, as the S_i s are fractions of the total variance (Sobol', 1993). These values were set to 0 and 1, respectively, in making the maps in Figure 6.9(b). There are two complementary explanations for this. Firstly, we did not calculate S_i directly, but rather the estimator \hat{S}_i , thus leaving the possibility of numerical errors. Secondly, as the intrinsic variability of the stochastic simulations cannot be fully grasped with 48 simulations, it is expected that this might jeopardise the calculations of the \hat{S}_i . Yet, this issue should not undermine the conclusions drawn.

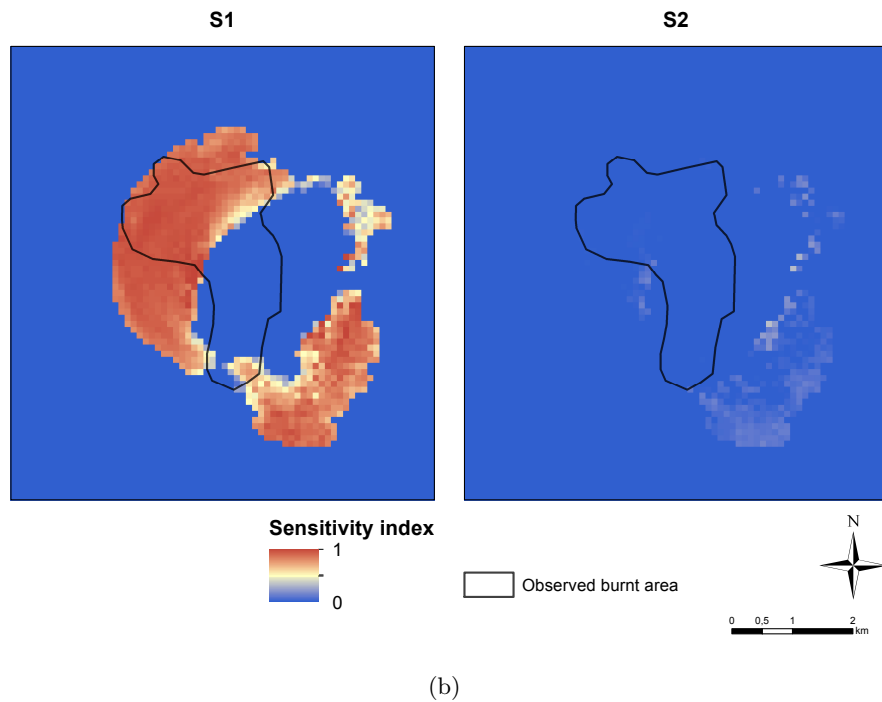
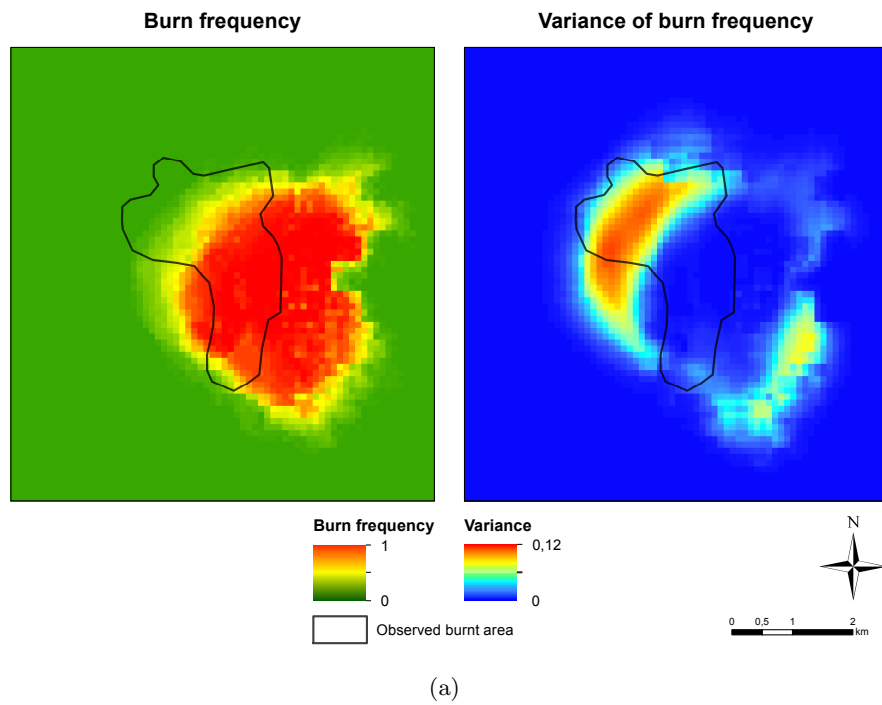


Figure 6.9: Burn frequency map and burn frequency variance map (a) and the sensitivity maps (b) of Case 2. S1 and S2 are the estimated first-order sensitivities of the wind direction and wind speed, respectively.

6.5 Conclusions

Two main conclusions can be drawn from the calibration results of the CA-based model. The first is that it is no easy task, even for the case-dependent calibrations. We may state that this is partly due to the model structure, causing the Ω to have a lot of local optima. Evidence hereof is the (very) rapidly converging optimisation algorithm—especially considering that there are 5 to 6 parameters to be optimised—the intrinsic variability of Ω due to the model’s stochastic nature, and the equifinality of different parameter sets. The latter is caused by non-linear interactions between the different parameters (see Eqs. (4.4)–(4.6)). Hence, introducing an additional parameter α only makes the optimisation problem more difficult to solve, without a significant effect on the resulting (accuracy of the) simulation.

Moreover, the high uncertainty of the data used also burdens the model calibration. This mainly applies to the data on the progression of the wildfires, since these are expected to have a great impact on the simulated fire dynamics. For example it was mentioned that the used wildfire durations are worst-case scenario’s, and thus overestimations of the real durations (Section 4.1.6). Calibrating with such data leads to parameter sets which underestimate the actual ROS. Moreover, as the wind data vary over time, longer wildfire durations also imply that new wind data are used in the simulations. If these new data strongly differ from the old ones, the wind dependency of the calibrated model will also differ.

This is indeed what we observed for Case 2—which had the longest reported fire duration of all cases (Table 4.3). The burn frequency variance and sensitivity maps (Figure 6.9) indicate that the case-dependent calibrated CA1 for this case is only slightly sensitive to variations in the wind direction and largely insensitive to those in the wind speed. This is also consistent with the results discussed in Section 6.2.2, as the high calibrated values of parameters $\psi_{1,2}$ (Table 6.3) result in a practically binary response of the model to the wind vector. Even very small wind components in the fire spread direction result in p_j values near unity. Hence, the model is—with the calibrated parameter set—only sensitive to perturbations of very low wind speeds. A possible way to quantitatively assess the effect of the estimated wildfire duration on the calibration would be to calibrate the CA-based model for different durations (possibly combined with a GSA such as the one in Section 6.4). Yet, this would require many simulations.

As was discussed in Section 4.2.3, the CA-based model has some fundamental shortcomings. These include its empirical nature, the fixed Δt , and the fact that n_{burn} is fixed for all cells and calibrated separately from the vegetation data. However, despite these issues the resulting burn frequency maps are of a similar quality with respect to the perimeters obtained with the two publicly available simulators that were tested in Chapter 5. This adds evidence to the second main conclusion, namely that, for the studied dataset, complex models do not lead to significantly better results.

CHAPTER 7

Conclusions and perspectives

In this dissertation, we have evaluated three real-time dynamic wildfire simulators regarding their operational usability in a Belgian context. The models comprised two (nearly) operational deterministic wildfire simulators, namely FARSITE and ForeFire, and one stochastic CA-based model in early research phase. For the evaluation of these models, a dataset, consisting of seven recent wildfire cases in Belgium and the Netherlands, was used.

In Chapter 5, we evaluated the simulation results obtained with both FARSITE and ForeFire for all wildfire cases. We concluded that neither of them simulated the considered wildfires with a sufficient level of accuracy to be useful in an operational setting. Although FARSITE is generally considered to be the standard reference model, it performed considerably worse than ForeFire for the presented dataset. FARSITE mostly underestimated the wildfire spread, which is inconsistent with findings in literature, where it generally (grossly) overestimates the ROS. We concluded that this may be due to FARSITE's high data demand in combination with the poor quality of the available (fuel) data. Both simulators did simulate the wildfires faster than real-time, yet, their cumbersome (and time-consuming) application requires expert knowledge and again limits their operational usability.

In Chapter 6, the CA-based wildfire model developed by Depicker et al. (2016) was calibrated and evaluated by means of simulations and a global sensitivity analysis. Although this model is much simpler than FARSITE and ForeFire, it proved to be very hard to calibrate. The latter was attributed to the model's stochastic nature, the equifinality of different parameter sets and, last but not least, the poor quality of the calibration data. Mainly the limited information on the progression of the wildfires seemed troublesome in this respect. The parameter sets that were found through calibration resulted in simulated wildfires that depend little on the wind data, as illustrated in both the simulated burn frequency maps and the global sensitivity maps of the wind speed and direction. Yet, accuracies of these burn frequency maps were not significantly lower than those obtained with FARSITE and ForeFire.

Finally, we may conclude that, given the available input data, none of the evaluated wildfire simulators are applicable in a Belgian context. Moreover, without detailed data on the progression of wildfires in a Belgian environmental context, no relevant calibration and validation of these models are possible. Hence, future wildfire events should be monitored in more detail, e.g. based on airborne thermal infra-red imagery (Valero et al., 2017), so that time-stamped snapshots of the fire progression are available for model testing and development.

Bibliography

- Adalsteinsson, D. and Sethian, J. A. (1995). A fast level set method for propagating interfaces. *Journal of Computational Physics*, 118:269–277.
- Albini, F. A. (1976). Estimating wildfire behavior and effects. Technical Report INT-30, USDA Forest Service, Intermountain Research Station, Ogden, USA.
- Alexander, M., Lawson, B., Stocks, B., and Van Wagner, C. (1992). Development and structure of the Canadian forest fire behavior prediction system. Technical Report ST-X-3, Forestry Canada Fire Danger Group, Ottawa, Canada.
- Alexander, M. E. (1985). Estimating the length-to-breadth ratio of elliptical forest fire patterns. In *Proceedings of the Eighth Conference on Fire and Forest Meteorology*, pages 287–304, Detroit, USA. Society of American Foresters.
- Alexandridis, A., Russo, L., Vakalis, D., Bafas, G. V., and Siettos, C. I. (2011). Wildland fire spread modelling using cellular automata: Evolution in large-scale spatially heterogeneous environments under fire suppression tactics. *International Journal of Wildland Fire*, 20:633–647.
- Alexandridis, A., Vakalis, D., Siettos, C. I., and Bafas, G. V. (2008). A cellular automata model for forest fire spread prediction: The case of the wildfire that swept through Spetses Island in 1990. *Applied Mathematics and Computation*, 204:191–201.
- Alexandrov, O. (2004). Illustration of Level set method. Retrieved March 05, 2017, from https://commons.wikimedia.org/wiki/File:Level_set_method.jpg.
- Anderson, D. H., Catchpole, E. A., De Mestre, N. J., and Parkes, T. (1982). Modelling the spread of grass fires. *Journal of Australian Mathematics Society, Series B*, 23:451–466.
- Anderson, H. E. (1969). Heat transfer and fire spread. Technical Report INT-RP-69, USDA Forest Service, Intermountain Forest and Ranger Experiment Station, Ogden, USA.

- Anderson, H. E. (1982). Aids to Determining Fuel Models for Estimating Fire Behavior. Technical Report INT-122, USDA Forests Service, Intermountain Forest and Range Experiment Station, Ogden, USA.
- Andrews, P. L. (1986). Behave: fire behaviour prediction and fuel modelling system - BURN subsystem, Part 1. Technical Report INT- 194, USDA Forest Service, Intermountain Forest and Range Experiment Station, Ogden, USA.
- Arca, B., Duce, P., Laconi, M., Pellizzaro, G., Salis, M., and Spano, D. (2007). Evaluation of FARSITE simulator in Mediterranean maquis. *International Journal of Wildland Fire*, 16:563.
- Baines, P. G. (1990). Physical mechanisms for the propagation of surface fires. *Mathematical and Computer Modelling*, 13:83–94.
- Balbi, J. H., Morandini, F., Silvani, X., Filippi, J. B., and Rinieri, F. (2009). A physical model for wildland fires. *Combustion and Flame*, 156:2217–2230.
- Balbi, J.-H., Rossi, J.-L., Marcelli, T. P., and Santoni, A. (2007). A 3D physical real-time model of surface fires across fuel beds. *Combustion Science and Technology*, 179:2511–2537.
- Ball, G. and Guertin, D. (1992). Improved fire growth modeling. *International Journal of Wildland Fire*, 2:47–54.
- Ballabio, C., Panagos, P., and Monatanarella, L. (2016). Mapping topsoil physical properties at European scale using the LUCAS database. *Geoderma*, 261:110–123.
- Beer, T. (1991). The interaction of wind and fire. *Boundary-Layer Meteorology*, 54:287–308.
- Bowman, D., Balch, J., Artaxo, P., Bond, W., Carlson, J., Cochrane, M., D’Antonio, C., DeFries, R., Doyle, J., Harrison, S., Johnston, F., Keeley, J., Krawchuk, M., Kull, C., Marston, J. B., Moritz, M., Prentice, I. C., Roos, C., Scott, A. C., Swetnam, T. W., van der Werf, G., and Pyne, S. (2009). Fire in the Earth System. *Science*, 324:481–484.
- Byram, G. (1959). Combustion of forest fuels. In: Davis, K.P., ed. Forest fire: control and use. In Davis, K., editor, *Forest fire: control and use*, pages 90–123. McGraw-Hill, New York, USA.
- Byram, G., Clements, H., Elliott, E., and George, P. (1964). An Experimental Study of Model Fires. Technical report, USDA Forest Service, Southeastern Forest Experiment Station, Southern Forest Fire Laboratory, Macon, USA.
- Cheney, P. N., Gould, J. S., and Catchpole, W. (1993). The influence of fuel, weather and fire shape variables on fire-spread in grasslands. *International Journal of Wildland Fire*, 3:34–44.

- Cheney, P. N., Gould, J. S., and Catchpole, W. (1998). Prediction of Fire Spread in Grasslands. *International Journal of Wildland Fire*, 8:1–13.
- Cheney, P. N. and Sullivan, A. L. (2008). *Grassfires : Fuel, Weather and Fire Behaviour*. CSIRO Publishing, Melbourne, Australia, 2nd edition.
- Clark, T. L., Coen, J. L., and Latham, D. (2004). Description of a coupled atmosphere fire model. *International Journal Of Wildland Fire*, 13:49–63.
- Coen, J. L., Cameron, M., Michalakos, J., Patton, E. G., Riggan, P. J., and Yedinak, K. M. (2013). WRF-Fire: coupled weather/wildland fire modeling with the Weather Research and Forecasting Model. *Journal of Applied Meteorology and Climatology*, 52:16–38.
- Cruz, M. G. (2010). Monte Carlo-based ensemble method for prediction of grassland fire spread. *International Journal of Wildland Fire*, 19:521–530.
- Cruz, M. G. and Alexander, M. E. (2013). Uncertainty associated with model predictions of surface and crown fire rates of spread. *Environmental Modelling and Software*, 47:16–28.
- Cruz, M. G., Gould, J. S., Alexander, M. E., Sullivan, A. L., McCaw, W. L., and Matthews, S. (2015). Empirical-based models for predicting head-fire rate of spread in Australian fuel types. *Australian Forestry*, 78:118–158.
- de Mestre, N. J., Catchpole, E. A., Anderson, D. H., and Rothermel, R. C. (1989). Uniform propagation of a planar fire front without wind. *Combustion Science and Technology*, 65:231–244.
- De Smith, M., J. G., M F, L., and P, A. (2007). *Geospatial analysis: a Comprehensive Guide to Principles, Techniques and Software Tools*, volume 1. Troubador Publishing Ltd.
- Depicker, A., Baetens, J. M., and De Baets, B. (2016). *Risk Analysis and Spatio-temporal modeling of Wildfires in Belgium*. Master’s thesis, Ghent University, Ghent, Belgium.
- Di Blasi, C. (1998). Comparison of semi-global mechanisms for primary pyrolysis of lignocellulosic fuels. *Journal of Analytical and Applied Pyrolysis*, 47:43–64.
- Doerr, S. H. and Santín, C. (2016). Global trends in wildfire and its impacts: perceptions versus realities in a changing world. *Philosophical transactions of the Royal Society of London. Series B, Biological sciences*, 371:281–329.
- Donovan, G. H. and Brown, T. C. (2007). Be careful what you wish for: The legacy of Smokey Bear. *Frontiers in Ecology and the Environment*, 5:73–79.
- Drysdale, D. (2011). *An Introduction to Fire Dynamics*. John Wiley & Sons, Ltd, Chichester, UK, 3rd edition.

- Duka, I. and Ioannilli, M. (2016). Fuel Type Classification in the Mediterranean Basin Context : State of the Art and Future Research. *International Journal of Environmental Science and Development*, 7:546–552.
- ESRI (2011). *ArcGIS Desktop*. Environmental Systems Research Institute, Redlands, USA. Version 10.2.2.
- Falk, D. A., Miller, C., McKenzie, D., and Black, A. E. (2007). Cross-scale analysis of fire regimes. *Ecosystems*, 10:809–823.
- Fendell, F. E. and Wolff, M. F. (2001). Wind-Aided Fire Spread. In Johnson, E. A. and Miyanishi, K., editors, *Forest Fires*, chapter 6, pages 171–223. Academic Press, San Diego, USA.
- Filippi, J. B., Bosseur, F., and Grandi, D. (2014a). ForeFire: open-source code for wildland fire spread models. In Viegas, D. X., editor, *Advances in forest fire research*, volume 4, chapter 1st, pages 275–282. Imprensa da Universidade de Coimbra, Coimbra, Portugal.
- Filippi, J. B., Bosseur, F., Mari, C., Lac, C., Le Moigne, P., Cuenot, B., Veynante, D., Cariolle, D., and Balbi, J.-H. (2009a). Coupled atmosphere-wildland fire modelling. *Journal of Advances in Modeling Earth Systems*, 1:9.
- Filippi, J. B., Bosseur, F., Pialat, X., Santoni, P.-A., Strada, S., and Mari, C. (2011). Simulation of coupled fire/atmosphere interaction with the MesoNH-ForeFire Models. *Journal of Combustion*, 2011:1–13.
- Filippi, J. B., Mallet, V., and Nader, B. (2014b). Evaluation of forest fire models on a large observation database. *Natural Hazards and Earth System Sciences*, 14:3077–3091.
- Filippi, J. B., Morandini, F., Balbi, J. H., and Hill, D. R. (2009b). Discrete Event Front-tracking Simulation of a Physical Fire-spread Model. *Simulation*, 86:629–644.
- Finney, M. A. (2002). Fire growth using minimum travel time methods. *Canadian Journal of Forest Research*, 32:1420–1424.
- Finney, M. A. (2004). FARSITE : Fire Area Simulator : model development and evaluation. Technical Report RMRS-RP-4 Revised, USDA Forest Service, Rocky Mountain Research Station, Ogden, USA.
- Finney, M. A., Cohen, J. D., Forthofer, J. M., McAllister, S. S., Gollner, M. J., Gorham, D. J., Saito, K., Akafuah, N. K., Adam, B. A., and English, J. D. (2015). Role of buoyant flame dynamics in wildfire spread. *Proceedings of the National Academy of Sciences*, 112:9833–9838.

- Finney, M. A., Cohen, J. D., McAllister, S. S., and Jolly, W. M. (2013). On the need for a theory of wildland fire spread. *International Journal of Wildland Fire*, 22:25–36.
- Finney, M. A., Grenfell, I. C., McHugh, C. W., Seli, R. C., Trethewey, D., Stratton, R. D., and Brittain, S. (2011). A Method for ensemble wildland fire simulation. *Environmental Modeling and Assessment*, 16:153–167.
- Flannigan, M., Cantin, A. S., De Groot, W. J., Wotton, M., Newbery, A., and Gowman, L. M. (2013). Global wildland fire season severity in the 21st century. *Forest Ecology and Management*, 294:54–61.
- Flannigan, M., Krawchuk, M. A., de Groot, W. J., Wotton, B. M., and Gowman, L. M. (2009). Implications of changing climate for global wildland fire. *International Journal of Wildland Fire*, 18:483–507.
- Fons, W. L. (1946). Analysis of fire spread in light forest fuels. *Journal of Agricultural Research*, 72:93–121.
- Forest Service Northern Region (2011). Crown fire. Retrieved March 07, 2017, from <https://www.flickr.com/photos/fsnorthernregion/5595403200/>.
- Forestry Canada Fire Danger Group (1992). Development and structure of the Canadian Forest Fire Behavior Prediction System. Technical Report ST-X-3, Forestry Canada Science and Sustainable Development Directorate, Ottawa, Canada.
- Frandsen, W. H. (1971). Fire spread through porous fuels from the conservation of energy. *Combustion and Flame*, 16:9–16.
- French, I. (1992). *Visualisation techniques for computer simulation of bushfires in two dimensions*. Master’s thesis, University of South Wales, Australian Defence Force Academy.
- Frigg, R. and Hartmann, S. (2012). Models in science. In *Stanford Encyclopedia of Philosophy*. Stanford University, Stanford, USA.
- Ghisu, T., Arca, B., Pellizzaro, G., and Duce, P. (2015). An optimal cellular automata algorithm for simulating wildfire spread. *Environmental Modelling and Software*, 71:1–14.
- Giglio, L., Randerson, J. T., and Van Der Werf, G. R. (2013). Analysis of daily, monthly, and annual burned area using the fourth-generation global fire emissions database (GFED4). *Journal of Geophysical Research: Biogeosciences*, 118:317–328.
- Gollner, M., Trouve, A., Altintas, I., Block, J., de Callafon, R., Clements, C., Cortes, A., Ellicott, E., Filippi, J. B., Finney, M. A., Ide, K., Jenkins, M. A., Jimenez, D., Lautenberger, C., Mandel, J., Rochoux, M., and Simeoni, A. (2015). Towards Data-Driven Operational

- Wildfire Spread Modeling: A Report of the NSF-Funded WIFIRE Workshop. Technical report, University of Maryland, College Park, USA.
- Green, D. G. (1983). Shapes of simulated fires in discrete fuels. *Ecological Modelling*, 20:21–32.
- Green, D. G., Tridgell, A., and Gill, A. M. (1990). Interactive simulation of bushfires in heterogeneous fuels. *Mathematical and Computer Modelling*, 13:57–66.
- Grishin, A. M. (1997). *Mathematical modeling of forest fires and new methods of fighting them*. Publishing house of the Tomsk state university, Tomsk, Russia, english edition.
- Hajian, M., Melachrinoudis, E., and Kubat, P. (2016). Modeling wildfire propagation with the stochastic shortest path: A fast simulation approach. *Environmental Modelling and Software*, 82:73–88.
- Hargrove, W., Gardner, R., Turner, M., Romme, W., and Despain, D. (2000). Simulating fire patterns in heterogeneous landscapes. *Ecological Modelling*, 135:243–263.
- Hartford, R. A. and Frandsen, W. H. (1992). When it’s hot, it’s hot... or maybe it’s not! (Surface flaming may not portend extensive soil heating). *International Journal of Wildland Fire*, 2:139–144.
- Hilton, J. E., Miller, C., Sullivan, A. L., and Rucinski, C. (2015). Effects of spatial and temporal variation in environmental conditions on simulation of wildfire spread. *Environmental Modelling and Software*, 67:118–127.
- Houben, G. (2011). Na het brandend konijn, nu de knoeiende Houthalenaar. *Het Belang Van Limburg*. Retrieved March 04, 2017, from <http://www.hbvl.be/cnt/aid1044783/na-het-brandend-konijn-nu-de-knoeiende-houthalenaar>.
- Jacquemyn, H., Brys, R., and Neubert, M. G. (2005). Fire increases invasive spread of *Molinia Caerulea* mainly through changes in demographic parameters. *Ecological Applications*, 15:2097–2108.
- Jahdi, R., Salis, M., Darvishsefat, A. A., Mostafavi, M. A., Alcasena, F., Etemad, V., Lozano, O., and Spano, D. (2015). Calibration of FARSITE simulator in northern Iranian forests. *Natural Hazards and Earth System Sciences*, 15:443–459.
- Johnston, P., Milne, G., and Kelso, J. (2006). A heat transfer simulation model for wildfire spread. *Forest Ecology and Management*, 234:S78.
- Joint Research Centre (2011). FUELMAP project: Final Classification and Mapping of EU Fuel Complexes. Deliverable2. JRC-ITT/RFQ Reference 2008/S 116-153998.

- Joint Research Centre (2015). Rapid Damage Assessment. Retrieved May 12, 2017, from <http://forest.jrc.ec.europa.eu/effis/about-effis/technical-background/rapid-damage-assessment/>.
- Keane, R. E. (2015). *Wildland Fuel Fundamentals and Applications*. Springer International Publishing, Cham, Switzerland.
- Keane, R. E., Burgan, R., and van Wagtenonk, J. (2001). Mapping wildland fuels for fire management across multiple scales: integrating remote sensing, GIS, and biophysical modeling. *International Journal of Wildland Fire*, 10:301.
- Keane, R. E., Loehman, R. a., and Holsinger, L. M. (2011). The FireBGCv2 landscape fire and succession model: a research simulation platform for exploring fire and vegetation dynamics. Technical Report RMRS-GTR-255, USDA Forest Service, Rocky Mountain Research Station, Fort Collins, USA.
- Keeley, J. E. (2009). Fire intensity, fire severity and burn severity: A brief review and suggested usage. *International Journal of Wildland Fire*, 18:116–126.
- KMI (2017). De maandnormalen te Ukkel. Retrieved May 14, 2017, from https://www.meteo.be/meteo/view/nl/360955-Maandelijkse+normalen.html#ppt_16230357.
- Knapp, E. (2002). Moderate intensity surface fire on a steep slope in Unit 4. Retrieved March 07, 2017, from <https://www.werc.usgs.gov/OLDsitedata/fire/seki/ffs/photos.htm>.
- Knight, I. and Coleman, J. (1993). A fire perimeter expansion algorithm based on Huygens' wavelet propagation. *International Journal of Wildland Fire*, 3:73–84.
- Kourtz, P. and O'Regan, W. (1971). A model for a small forest fire...to simulate burned and burning areas for use in a detection model. *Forest Science*, 17:163–169.
- Krawchuk, M. A., Moritz, M. A., Parisien, M.-A., Van Dorn, J., and Hayhoe, K. (2009). Global pyrogeography: the current and future distribution of wildfire. *PLoS ONE*, 4:e5102.
- Ligmann-Zielinska, A. (2013). Spatially-explicit sensitivity analysis of an agent-based model of land use change. *International Journal of Geographical Information Science*, 27:1764–1781.
- Lilburne, L. and Tarantola, S. (2009). Sensitivity analysis of spatial models. *International Journal of Geographical Information Science*, 23:151–168.
- Linn, R. (1997). *A transport model for prediction of wildfire behavior*. Reissue of phd thesis, Los Alamos National Laboratory (LANL), Los Alamos, USA.

- Lopes, A., Cruz, M., and Viegas, D. (2002). FireStation – an integrated software system for the numerical simulation of fire spread on complex topography. *Environmental Modelling & Software*, 17:269–285.
- Mallet, V., Keyes, D., and Fendell, F. (2009). Modeling wildland fire propagation with level set methods. *Computers & Mathematics with Applications*, 57:1089–1101.
- Mandel, J., Amram, S., Beezley, J. D., Kelman, G., Kochanski, a. K., Kondratenko, V. Y., Lynn, B. H., Regev, B., and Vejmelka, M. (2014). Recent advances and applications of WRF-SFIRE. *Natural Hazards and Earth System Science*, 14:2829–2845.
- Mandel, J., Beezley, J. D., Coen, J. L., and Minjeong, K. (2009). Data assimilation for wildland fires: Ensemble Kalman filters in coupled atmosphere-surface models. *IEEE Control Systems Magazine*, 29:47–65.
- Mandel, J., Beezley, J. D., and Kochanski, A. K. (2011). Coupled atmosphere-wildland fire modeling with WRF 3.3 and SFIRE 2011. *Geoscientific Model Development*, 4:591–610.
- Marrs, R. H., Phillips, J. D. P., Todd, P. A., Ghorbani, J., and Le Duc, M. G. (2004). Control of *Molinia caerulea* on upland moors. *Journal of Applied Ecology*, 41:398–411.
- McArthur, A. G. (1965). Weather and grassland fire behaviour. Technical Report Leaflet 107, Commonwealth Department of National Development, Forestry and Timber Bureau, Canberra, Australia.
- McArthur, A. G. (1967). Fire behaviour in eucalypt forests. Technical Report Leaflet 107, Commonwealth Department of National Development, Forestry and Timber Bureau, Canberra, Australia.
- McCarter, R. and Broido, A. (1965). Radiative and convective energy from wood crib fires. *Pyrodynamics*, 2:65–68.
- McKenzie, D., Miller, C., and Falk, D. A. (2011). Toward a Theory of Landscape Fire. In McKenzie, D., Miller, C., and Falk, D. A., editors, *The Landscape Ecology of Fire*, chapter 1, pages 3–25. Springer, Dordrecht, The Netherlands.
- McKenzie, D. and Perera, A. H. (2015). Modeling wildfire regimes in forest landscapes: abstracting a complex reality. In Perera, A. H., Sturtevant, B. R., and Buse, L. J., editors, *Simulation modeling of forest landscape disturbances*, chapter 4, pages 1–321. Springer, New York, USA.
- McRae, R. H. D., Sharples, J. J., Wilkes, S. R., and Walker, A. (2013). An Australian pyro-tornadogenesis event. *Natural Hazards*, 65:1801–1811.

- Mell, W., Jenkins, M. A., Gould, J., and Cheney, P. N. (2007). A physics-based approach to modelling grassland fires. *International Journal of Wildland Fire*, 16:1–22.
- Morandini, F. and Silvani, X. (2010). Experimental investigation of the physical mechanisms governing the spread of wildfires. *International Journal of Wildland Fire*, 19:570–582.
- Moritz, M. A., Batllori, E., Bradstock, R. A., Gill, A. M., Handmer, J., Hessburg, P. F., Leonard, J., McCaffrey, S., Odion, D. C., Schoennagel, T., and Syphard, A. D. (2014). Learning to coexist with wildfire. *Nature*, 515:58–66.
- Morvan, D. (2011). Physical phenomena and length scales governing the behaviour of wildfires: a case for physical modelling. *Fire Technology*, 47:437–460.
- Morvan, D. and Dupuy, J. L. (2001). Modeling of fire spread through a forest fuel bed using a multiphase formulation. *Combustion and Flame*, 127:1981–1994.
- Nelder, J. A. and Mead, R. (1965). A Simplex Method for Function Minimization. *The Computer Journal*, 7:308–313.
- Nelson, R. M. J. (2001). Water Relations of Forest Fuels. In Johnson, E. A. and Miyanishi, K., editors, *Forest Fires*, chapter 4, pages 79–149. Academic Press, San Diego, USA.
- Noble, I. R., Gill, A. M., and Bary, G. A. V. (1980). McArthur’s fire-danger meters expressed as equations. *Australian Journal of Ecology*, 5:201–203.
- North, M. P., Stephens, S. L., Collins, B. M., Agee, J. K., Aplet, G., Franklin, J. F., and Fule, P. Z. (2015). Reform forest fire management. *Science*, 349:1280–1281.
- Osher, S. and Fedkiw, R. (2003). *Level Set Methods and Dynamic Implicit Surfaces*, volume 153 of *Applied Mathematical Sciences*. Springer, New York, USA.
- Papadopoulos, G. D. and Pavlidou, F.-n. (2011). A comparative review on wild fire simulators. *IEEE Systems Journal*, 5:233–243.
- Pastor, E., Zàrate, L., Planas, E., and Arnaldos, J. (2003). Mathematical models and calculation systems for the study of wildland fire behaviour. *Progress in Energy and Combustion Science*, 29:139–153.
- Pechony, O. and Shindell, D. T. (2010). Driving forces of global wildfires over the past millennium and the forthcoming century. *Proceedings of the National Academy of Sciences of the United States of America*, 107:19167–19170.
- Peterson, S. H., Morais, M. E., Carlson, J. M., Dennison, P. E., Roberts, D. A., Moritz, M. A., and Weise, D. R. (2009). Using HFire for spatial modeling of fire in shrublands. Technical Report PSW-RP-259, USDA Forest Service, Pacific Southwest Research Station, Riverside, USA.

- Philpot, C. W. (1969). Seasonal changes in heat content and ether extractive content of chamise. Technical Report INT-61, USDA Forest Service, Intermountain Research Station, Ogden, USA.
- Philpot, C. W. (1970). Influence of mineral content on the pyrolysis of plant material. *Forest Science*, 16:461–471.
- Pyne, S. J. (2016). Fire in the mind: changing understandings of fire in Western civilization. *Philosophical Transactions of the Royal Society B: Biological Sciences*, 371:20150166.
- Raftoyannis, Y., Nocentini, S., Marchi, E., Sainz, R. C., Guemes, C. G., Pilas, I., Peric, S., Paulo, J. A., Moreira-Marcelino, A. C., Costa-Ferreira, M., Kakouris, E., and Lindner, M. (2014). Perceptions of forest experts on climate change and fire management in European Mediterranean forests. *IForest*, 7:33–41.
- Randerson, J. T., Chen, Y., Van Der Werf, G. R., Rogers, B. M., and Morton, D. C. (2012). Global burned area and biomass burning emissions from small fires. *Journal of Geophysical Research: Biogeosciences*, 117.
- Rein, G. (2009). Smouldering Combustion Phenomena in Science and Technology. *International Review of Chemical Engineering*, 1:3–18.
- Richards, G. D. (1990). An elliptical growth model of forest fire fronts and its numerical solution. *International Journal for Numerical Methods in Engineering*, 30:1163–1179.
- Richards, G. D. (1995). A general mathematical framework for modeling two-dimensional wildland fire spread. *International Journal of Wildland Fire*, 5:63–72.
- Rigolot, E., Fernandes, P., and Rego, F. (2009). Managing wildfire risk: prevention, suppression. In Birot, Y., editor, *Living with wildfires: what science can tell us. A contribution of the science-policy dialogue*, pages 49–52. European Forest Institute, Joensuu, Finland.
- Rothermel, R. C. (1972). A mathematical model for predicting fire spread in wildland fuels. Technical Report INT-115, USDA Forests Service, Intermountain Forest and Range Experiment Station, Ogden, USA.
- Rothermel, R. C. (1991). Predicting behavior and size of crown fires in the northern Rocky Mountains. Technical Report INT-438, USDA Forest Service, Intermountain Research Station, Ogden, USA.
- Rothermel, R. C., Wilson, R. A., Morris, G. A., and Sackett, S. S. (1986). Modeling moisture content of fine dead wildland fuels: Input to the BEHAVE fire prediction system. Technical Report INT-359, USDA, Forest Service, Intermountain Research Station, Ogden, USA.

- Russell, S. J. and Norvig, P. (2010). *Artificial Intelligence: A Modern Approach*. Pearson Education, Inc., Upper Saddle River, New Jersey, 3rd edition.
- Saito, K. (2001). Flames. In Johnson, E. A. and Miyanishi, K., editors, *Forest Fires*, chapter 2, pages 11–54. Academic Press, San Diego, USA.
- Salis, M. (2008). *Fire Behaviour Simulation in Mediterranean Maquis Using FARSITE (Fire Area Simulator)*. Phd, University of Sassari, Sassari, Italy.
- Saltelli, A., Ratto, M., Andres, T., Campolongo, F., Cariboni, J., Gatelli, D., Saisana, M., and Tarantola, S. (2008). *Global Sensitivity Analysis. The Primer*. John Wiley & Sons, Ltd, Chichester, UK.
- San-Miguel-Ayanz, J., Durrant, T., Boca, R., Liberta, G., Boccacci, F., Di Leo, M., Lopez Perez, J., and Schulte, E. (2016). Forest Fires in Europe, Middle East and North Africa 2015. Technical Report EUR 28148 EN, European Commission, Joint Research Center, Ispra, Italy.
- San-Miguel-Ayanz, J., Schulte, E., Schmuck, G., Camia, A., Strobl, P., Liberta, G., Giovando, C., Boca, R., Sedano, F., Kempeneers, P., McInerney, D., Withmore, C., de Oliveira, S. S., Rodrigues, M., Houston Durrant, T., Corti, P., Oehler, F., Vilar, L., and Amatulli, G. (2012). Comprehensive monitoring of wildfires in Europe: the European Forest Fire Information System (EFFIS). In Tiefenbacher, J., editor, *Approaches to Managing Disaster - Assessing Hazards, Emergencies and Disaster Impacts*, chapter 5. In-Tech Publishers, Rijeka, Croatia.
- Schmuck, G., San-Miguel-Ayanz, J., Durrant, T., Boca, R., Libertà, G., Petroliaqkis, T., Di Leo, M., Rodrigues, D., Boccacci, F., and Schulte, E. (2015). Forest fires in Europe, Middle East and North Africa 2014. Technical Report EUR 27400 EN, European Commission, Joint Research Center, Ispra, Italy.
- Scott, A. C. and Glasspool, I. J. (2006). The diversification of Paleozoic fire systems and fluctuations in atmospheric oxygen concentration. *Proceedings of the National Academy of Sciences of the United States of America*, 103:10861–10865.
- Scott, J. H. and Reinhardt, E. D. (2001). Assessing Crown Fire Potential by Linking Models of Surface and Crown Fire Behavior. Technical Report RMRS-RP-29, USDA Forest Service, Rocky Mountain Research Station, Fort Collins, Colorado.
- Sethian, J. A. (1996). A fast marching level set method for monotonically advancing fronts. *Proceedings of the National Academy of Sciences*, 93:1591–1595.
- Sharples, J. J. (2008). Review of formal methodologies for windslope correction of wildfire rate of spread. *International Journal of Wildland Fire*, 17:179–193.

- Simard, A. J. (1968). The moisture content of forest fuels - I: a review of the basic concepts. Technical Report FF-X-14, Government of Canada, Department of Forestry and Rural Development, Forest Fire Research Institute, Information Report FF-X-14, Ottawa, Canada.
- Simeoni, A. (2016). Wildland Fires. In Hurley, M. J., Gottuk, D. T., Hall, J. R. J., Harada, K., Kuligowski, E. D., Puchovsky, M., Torero, J. L., Watts, J. M. J., and Wieczorek, C. J., editors, *SFPE Handbook of Fire Protection Engineering*, chapter 87, pages 3283–3302. Springer, New York, USA, 5th edition.
- Sivillo, J. K., Ahlquist, J. E., and Toth, Z. (1997). An Ensemble Forecasting Primer. *Weather and Forecasting*, 12:809–818.
- Sneeuwjagt, R. and Peet, G. (1985). *Forest Fire Behaviour Tables for Western Australia*. Department of Conservation and Land Management, Perth, Australia, 3rd edition.
- Sobol', I. (1993). Sensitivity Estimates for Nonlinear Mathematical Models.
- Srivas, T., Artés, T., de Callafon, R. A., and Altintas, I. (2016). Wildfire spread prediction and assimilation for FARSITE using Ensemble Kalman Filtering. *Procedia Computer Science*, 80:897–908.
- Sullivan, A. L. (2009a). Wildland surface fire spread modelling, 1990-2007. 1: Physical and quasi-physical models. *International Journal of Wildland Fire*, 18:349–368.
- Sullivan, A. L. (2009b). Wildland surface fire spread modelling, 1990-2007. 2: Empirical and quasi-empirical models. *International Journal of Wildland Fire*, 18:369–386.
- Sullivan, A. L. (2009c). Wildland surface fire spread modelling, 1990-2007. 3: Mathematical analogues and simulation models. *International Journal of Wildland Fire*, 18:387–403.
- The National Wildfire Coordinating Group (2015). Glossary of Wildland Fire Terminology. Retrieved December 20, 2016, from <http://www.nwcg.gov/glossary-of-wildland-fire-terminology>.
- Thompson, M. P. and Calkin, D. E. (2011). Uncertainty and risk in wildland fire management: A review. *Journal of Environmental Management*, 92:1895–1909.
- Tolhurst, K., Shields, B., and Chong, D. (2008). Phoenix: development and application of a bushfire risk management tool. *The Australian Journal of Emergency Management*, 23:47–54.
- Toukiloglou, P., Eftychidis, G., Gitas, I., and Tompoulidou, M. (2013). ArcFuel methodology for mapping forest fuels in Europe. In *Proceedings of SPIE - The International Society for Optical Engineering*, volume 8795, page 87951J.

- Trunfio, G. A., D'Ambrosio, D., Rongo, R., Spataro, W., and Di Gregorio, S. (2011). A new algorithm for simulating wildfire spread through Cellular Automata. *ACM Transactions on Modeling and Computer Simulation*, 22:1–26.
- Tymstra, C., Bryce, R. W., Wotton, B. M., Taylor, S. W., and Armitage, O. B. (2010). Development and structure of Prometheus: the Canadian Wildland Fire Growth Simulation Model. Technical Report NOR-X-417, Canadian Forest Service, Northern Forestry Centre, Edmonton, Canada.
- Valero, M. M., Verstockt, S., Rios, O., Pastor, E., Vandecasteele, F., and Planas, E. (2017). Flame filtering and perimeter localization of wildfires using aerial thermal imagery. In Bison, P. and Burleigh, D., editors, *SPIE 10214 -Thermosense: Thermal Infrared Applications*, page 1021404, Anaheim, USA. SPIE.
- Van Wagner, C. E. (1969). A simple fire-growth model. *The Forestry Chronicle*, 45:103–104.
- Van Wagner, C. E. (1977). Conditions for the start and spread of crown fire. *Canadian Journal of Forest Research*, 7:23–34.
- Viegas, D. X. and Simeoni, A. (2011). Eruptive Behaviour of Forest Fires. *Fire Technology*, 47:303–320.
- von Neumann, J. (1966). *Theory of Self-Reproducing Automata*. University of Illinois Press, Urbana, USA.
- Ward, D. (2001). Combustion Chemistry and Smoke. In Johnson, E. A. and Miyanishi, K., editors, *Forest Fires*, chapter 3, pages 55–77. Academic Press, San Diego, USA.
- Williams, F. (1982). Urban and wildland fire phenomenology. *Progress in Energy and Combustion Science*, 8:317–354.
- Williams, F. A. (1977). Mechanisms of fire spread. *Symposium (International) on Combustion*, 16:1281–1294.
- Willingham, A. (2016). Firefighter captures pic of terrifying ‘fire whirl’. Retrieved March 07, 2017, from <http://edition.cnn.com/2016/08/16/health/beaver-creek-fire-tornado-trnd/>.
- Wilson, R. O. (1980). Reformulation of forest fire spread equations in SI units. Technical Report INT-292, USDA Forests Service, Intermountain Forest and Range Experiment Station, Ogden, USA.
- Wolfram Research Inc. (2016). *Mathematica*. Wolfram Research Inc., Champaign, USA. Version 11.1.

Zhou, X. and Mahalingam, S. (2001). Evaluation of reduced mechanism for modeling combustion of pyrolysis gas in wildland fire. *Combustion Science and Technology*, 171:39–70.

APPENDIX A

Fuel classifications

Table A.1: JRC fuel classification and corresponding NFFL classes.

JRC classification		NFFL classification	
ID	Class	ID	Class
1	Peat bogs	5	Brush
2	Wooded peatbogs	6	Dormant brush
3	Pastures	1	Short Grass
4	Sparse grasslands	1	Short Grass
5	Mediterranean grasslands and steppes	2	Grass and understory
6	Temperate, Alpine and Northern grasslands	1	Short Grass
7	Mediterranean moors and heathlands	5	Brush
8	Temperate, Alpine and Northern moors and heathlands	5	Brush
9	Mediterranean open shrublands (sclerophyllous)	2	Grass and understory
10	Mediterranean shrublands (sclerophyllous)	4	Chaparral
11	Deciduous broadleaved shrublands (thermophilous)	5	Brush
12	Alpine open shrublands (conifers)	6	Dormant brush
13	Shrublands in Mediterranean conifer forests	7	Southern rough
14	Shrublands in Mediterranean sclerophyllous forests	4	Chaparral
15	Shrublands in Mediterranean montane conifer forests	7	Southern rough
16	Shrublands in thermophilous broadleaved forests	5	Brush
17	Shrublands in beech and mesophytic broadleaved forests	5	Brush
18	Northern open shrublands in broadleaved forests	5	Brush
19	Shrublands in Alpine and Northern conifer forests	7	Southern rough
20	Mediterranean long needled conifer forest (Mediterranean pines)	10	Timber (litter and understory)

21	Mediterranean scale-needled open woodlands (juniperus, cupressus)	8	Closed timber litter
22	Mediterranean montane long needled conifer forest (black and scots pines)	10	Timber (litter and understory)
23	Mediterranean montane short needled conifer forest (firs, cedar)	8	Closed timber litter
24	Temperate conifer plantations	8	Closed timber litter
25	Alpine long needled conifer forest (pines)	10	Timber (litter and understory)
26	Alpine short needled conifer forest (fir, alpine spruce)	8	Closed timber litter
27	Northern long needled conifer forest (scots pine)	10	Timber (litter and understory)
28	Northern short needled conifer forest (spruce)	8	Closed timber litter
29	Mediterranean evergreen broadleaved forest	4	Chaparral
30	Thermophilous broadleaved forest	9	Hardwood litter
31	Mesophytic broadleaved forest	9	Hardwood litter
32	Beech forest	9	Hardwood litter
33	Montane beech forest	10	Timber (litter and understory)
34	White birch boreal forest	10	Timber (litter and understory)
35	Mixed mediterranean evergreen broadleaved with conifers forest	4	Chaparral
36	Mixed thermophylous broadleaved with conifers forest	9	Hardwood litter
37	Mixed mesophytic broadleaved with conifers forest	10	Timber (litter and understory)
38	Mixed beech with conifers forest	9	Hardwood litter
39	Riparian vegetation	5	Brush
40	Coastal and inland halophytic vegetation and dunes	1	Short Grass
41	Aquatic Marshes	3	Tall Grass
42	Agroforestry areas	2	Grass and understory
50	Agriculture unburnable	0	Not fuel
51	Agriculture	0	Not fuel
52	Agriculture with natural vegetation	0	Not fuel
53	Urban and barren	0	Not fuel
54	Urban discontinuous	0	Not fuel
55	Water bodies	0	Not fuel